Geomorphic Response to Catastrophic Flooding on the Umatilla River, Oregon.

by

Nicole Kathleen Merrill

A thesis accepted and approved in partial fulfillment of the

requirements for the degree of

Master of Science

in Geography

Thesis Committee:

Patricia McDowell, Chair

Mark Fonstad, Member

University of Oregon

Fall 2024

THESIS ABSTRACT

Nicole Kathleen Merrill

Master of Science in Geography

Title: Geomorphic Response to Catastrophic Flooding on the Umatilla River, Oregon.

Using aerial imagery and digitization, this thesis studied changes to geomorphology and vegetation on the Umatilla River after catastrophic flooding in 2020 and 1996-7, compared geomorphic effectiveness of the two floods, and tested potential control variables. On average, the channel widened, shifted laterally, built bars, and stripped vegetation, though changes were slightly less pronounced in 1996-7 than in 2020. Internal thresholds that maintain channel width and sinuosity as well as the lower discharge in 1996 contributed to this difference. Active channel widening and lateral movement were the most sensitive to the control variables in 2020 and in 1996-7. Channel sinuosity played the largest part in controlling shear stress and, therefore, planimetric changes. However, bar accretion, which was influenced the most by sediment availability, was more depended on tributary input. Comparison of lateral activity and channel widening in 1996-7 and 2020 showed the downstream reaches that had not been channelized underwent the most change from both floods, which reflects previous flood effects on this river. Climate change and uncertain future flood risk make understanding river response to flooding extremely important for river planners managing community safety and ecological restoration.

CURRICULUM VITAE

NAME OF AUTHOR: Nicole Kathleen Merrill

GRADUATE AND UNDERGRADUATE SCHOOLS ATTENDED:

University of Oregon, Eugene
Northeastern University, Boston

DEGREES AWARDED:

Master of Science, Geography, 2024, University of Oregon
Bachelor of Science, Environmental Science, 2017, Northeastern University

AREAS OF SPECIAL INTEREST:

Fluvial Geomorphology
Hydrology
Remote Sensing
Cartography

PROFESSIONAL EXPERIENCE:

Graduate Teaching Fellow, University of Oregon, October 2019 – December 2021

Research Assistant, Harvard University, June 2016 – December 2016

Laboratory Technician, Cambridge Water Department, January 2015 – June 2015

GRANTS, AWARDS, AND HONORS:

William G. Loy Award for Excellence in Cartography, "Surtsey: Born in Fire, Lost at Sea", University of Oregon, 2020

Magna Cum Laude, Northeastern University, 2017

PUBLICATIONS:

Merrill, N. K., García De Cortázar-Atauri, I., Parker, A. K., Walker, M. A., & Wolkovich, E. M. (2020). Exploring Grapevine Phenology and High Temperatures Response Under Controlled Conditions. *Frontiers in Environmental Science*, *8*, 516527. https://doi.org/10.3389/fenvs.2020.516527

ACKNOWLEDGMENTS

This thesis would not have been possible without the support of so many people. First, I would like to thank my advisor, Dr. Patricia McDowell, for helping me to think critically about the natural world and develop as a geomorphologist. Her guidance, patience, and encouragement were invaluable throughout my time at the University of Oregon. I would also like to thank Dr. Mark Fonstad for serving on my committee, offering his insight into conducting research, and helping me problem-solve when I encountered obstacles. Furthermore, I am very grateful to have been a part of the Department of Geography and to have received advice, assistance, and comradery from the other students, faculty, and staff there.

Thank you to my family and friends for believing in me and helping me make it through this thesis project without losing sight of my goals beyond graduate school. Finally, I would like to offer my sincerest gratitude to my partner, Sabrina Castaneda, for her unconditional support and understanding. She has been a continual source of positivity and love and has never failed to offer help in whatever way she could.

TABLE OF CONTENTS

Chapter Page

Chapter Page

LIST OF FIGURES

Figure Page

LIST OF TABLES

Table Page

CHAPTER I

INTRODUCTION

1. Introduction

Floods, from the rare and catastrophic to the more frequent and less extreme, serve as agents of change for rivers. For many communities that live near rivers, this change means destruction of property, livelihood, or life, but for the ecosystem, the change is natural and maintains important river processes. Understanding what drives these effects is paramount for managing rivers both for the health of the ecosystem and the reduction of risk for people living around them.

Research has shown that large magnitude floods tend to cause channel widening, increased lateral movement, development of meander cutoffs and avulsions, bar building, and vegetation removal (Dean & Schmidt, 2013; Fuller, 2007; Huckleberry, 1994; Magilligan et al., 2015; Nelson & Dubé, 2016; Righini et al., 2017; Sholtes et al., 2018; Sloan et al., 2001; Surian et al., 2016; Thompson & Croke, 2013; Wicherski et al., 2017). However, the change wrought by a particular flood can vary a great deal depending on the characteristics of the flood, the climate and geology of the basin, and channel pattern and geometry (Knighton, 1998). Multi-channel, gravel-bedded rivers pose a particular challenge to researchers and managers alike due to their dynamism, sometimes termed instability, and complexity. For this reason, the relationships between floods and river processes in these rivers are not as well understood.

Comparing the geomorphic effectiveness of floods to one another has helped researchers better understand how floods affect rivers across a variety of spatiotemporal scales (Lisenby et al., 2018). Geomorphic effectiveness was initially conceptualized as the relationship between the magnitude of a disturbance (such as the peak discharge of a flood or its return interval) and the sediment it transported (Wolman & Miller, 1960). The definition has evolved to more broadly describe how a disturbance changes a landscape both in the short and long term, but it remains a useful framework for building hypotheses about the ways in which floods and river processes interact. The applicability of geomorphic effectiveness is broadened when concepts of recovery, sensitivity, connectivity, and thresholds are incorporated into such comparisons and provide a more holistic explanation of flood response (Costa & O'Connor, 1995; Dean & Schmidt, 2013; Fryirs, 2017; Newson, 1980; Sloan et al., 2001; Wolman & Gerson, 1978).

Aerial and satellite imagery are useful tools for comparing a river before and after a disturbance, like a flood, and they have been used to track changes in both morphology (e.g.

Fuller, 2007) and vegetation (e.g. Smith, 2013). They can cover a variety of spatial and temporal scales, and while researchers may choose to collect this imagery as part of a specific project, there also exists a large record of contemporary and historical imagery. Because flooding is nearly impossible to predict, researchers comparing a basin before and after a flood are often reliant on aerial imagery records to determine the river's pre-flood condition, unless the basin is intensively monitored.

2. Research Goals

In February of 2020, the Umatilla River, a Columbia River tributary in northeastern Oregon, experienced a record-breaking flood after an atmospheric river (AR) brought heavy rains to the Umatilla and nearby Walla-Walla basins, which fell on snowpack, triggering snowmelt and intense runoff. The purpose of this study was to explore changes to the Umatilla River from this flood. To accomplish that goal, this study compared imagery of the river in 2017 with imagery captured in the summer of 2020. Channel features and surface cover were digitized from the imagery to track changes in morphology and vegetation. Morphological changes were then compared with changes observed after the flooding in 1996 and 1997, for which digitizing products had already been created by McDowell et al. (2003). Regression analysis was used to investigate the role of possible causal variables in controlling the intensity and spatial distribution of the flood responses. Specifically, this research asked the following questions:

1. *What effects did the 2020 flood have on the geomorphology (active channel width, lateral movement, bar accretion, sinuosity) and vegetation of the Umatilla River?*

2. *What role did surface cover type, active channel width, channel slope, channel confinement, or sinuosity before the flood play in changes to active channel width, bar formation, lateral movement, sinuosity, and vegetation cover?*

3. *How do changes caused by the 2020 flood compare to changes from the 1996-7 floods?*

Much of the basis for this research comes from the work of Hughes (2008), who investigated flood effects and recovery on the Umatilla River between 1965 and 1975. In this study, that work is continued, building a richer temporal understanding of flooding on the Umatilla, addressing variable effects at multiple scales, and investigating vegetative as well as morphological controls

on change. The results provide further insight into how floods drive change, particularly for semi-arid, multi-threaded, gravel-bedded rivers, the flood responses of which have been less intensely studied. Potential future climate changes make this issue particularly important. Climate models for the region have suggested that, while summer flows will be slightly lower, winter flows will increase by around 30% by the end of the century (Hamlet et al., 2013). In addition, Queen et al. (2021) predicted an increase in flood magnitude for the entire Columbia River basin, which would make understanding flood response imperative to planners and managers in the coming decades. Conclusions drawn from this work could guide plans for future restoration and flood mitigation measures that do not hamper important and necessary rivers processes.

3. Study Site

The Umatilla River basin is located in northeast Oregon. The river is part of the larger Columbia River basin and flows from its headwaters in the Blue Mountains northwest across the Columbia River plateau to Umatilla, Oregon, where it joins the Columbia River. The basin has an area of around 6,475 km^2. Major tributaries include Meacham, Wildhorse, Tutuilla, McKay, Birch, and Butter Creeks. Elevation in the basin ranges from as low as 80 m above sea level (asl) at its junction with the Columbia River to 1676 m asl. Land uses within the watershed include national forest lands, the Umatilla Indian Reservation, ranching and agricultural land, the city of Pendleton, and several smaller towns. This study focuses on a segment of the Upper Umatilla River between the Meacham Creek confluence and the Pendleton stream gage which drains approximately 1,650 km^2 at the downstream end near Pendleton, Oregon (Figure 1).

The geology of the basin is dominated by Columbia River basalts dating to eruptions in the Miocene, which extend across nearly the entire basin and are overlain by Quaternary loess, alluvium, and glacial-fluvial deposits. The Umatilla River is a gravel-bedded river, and its sediment is mostly derived from the basaltic volcanic rocks found throughout the basin. Some sections are highly geomorphically active, forming multiple channels and weaving around bars and vegetated islands across the floodplain, while others are constrained by exposed sections of the Columbia River basalts and canyon walls and have only a single, main channel. The channel best fits descriptions of the wandering pattern described by Church (1983), though it is similar to the Type 5 anabranching channel described by Nanson and Knighton (1996) and the island-braided pattern described by Beechie et al. (2006).

In general, the Umatilla River basin has a semi-arid climate. The majority of the basin receives less than 305 mm of precipitation a year, most of which falls between November and

January. Historically, the plateau vegetation was a diverse sage-and-juniper shrub ecosystem supported by high river-floodplain connectivity in the braided sections. Stands of willow and cottonwood also grew there, especially near the river in the bedrock confined sections where flooding was less frequent. Today, the uplands are mostly used for forestry and dryland farming, while the floodplain and terraces are used for ranching, irrigated farming, and residential development.

3.1 The Floods

On February 4th and 5th, 2020, an atmospheric river (AR) brought heavy snow (250 – 500 mm) and then rain (75 – 150 mm) to the Blue Mountains. The combination of rain and snowmelt led to record high peak discharge at all three stream gages on the main stem Umatilla River (Figure 2) and around $50 million in damages to homes, roads, bridges, and other structures in northeast Oregon and southeast Washington (Oregon – Severe Storms, Flooding Landslides, and Mudslides – FEMA-4519-DR, 2020; Wittwer, 2022). In the media, this flood was often compared to the 1996 flood, which was the most recent catastrophic flood in the basin (Table 1). Like the 2020 flood, the 1996 flood occurred in early February when an AR delivered a great deal of snow and then rain to the area between February 5th and 9th. The winter had already been unusually wet, leaving soils saturated, and heavy snowfall in January greatly increased snowpack across the region. The warm, moist air melted snow, which joined runoff from the heavy rains and caused flooding across the Pacific Northwest which caused between $500 million and $1 billion in damages (McAllister, 1996).

Between 1996 and 1997, the Umatilla River experienced several floods, including the major flood mentioned above (Figure 3). While many of these floods were minor, the continued saturation of soils may have increased runoff and amplified flood effects. Saturated soils may have also increased the likelihood of mass wasting events, several of which are known to have occurred in the mountains of the Umatilla River headwaters between 1996 and 1997 (Hofmeister, 2000). Conditions surrounding the 2020 flood were not as wet, but there was flooding in April of 2019 (Figure 3), which likely played a part in changes to the river between imagery captured in 2017 and 2020. The 2019 flooding was most intense in the lower Umatilla River and registered as only minor flooding at the Gibbon stream gage. However, this flooding did last longer than the February floods in either 1996 or 2020 which may have increased its impact.

Figure 1. This is a map of the study site and its subbasin within the larger Umatilla River Basin. Tributaries that join the Umatilla River in this segment as well as nearby communities are labeled, and the upstream (Gibbon) and downstream (Pendleton) stream gages are also shown. The inset map in the top right shows the study site subbasin and the entire Umatilla Basin's location in the state of Oregon.

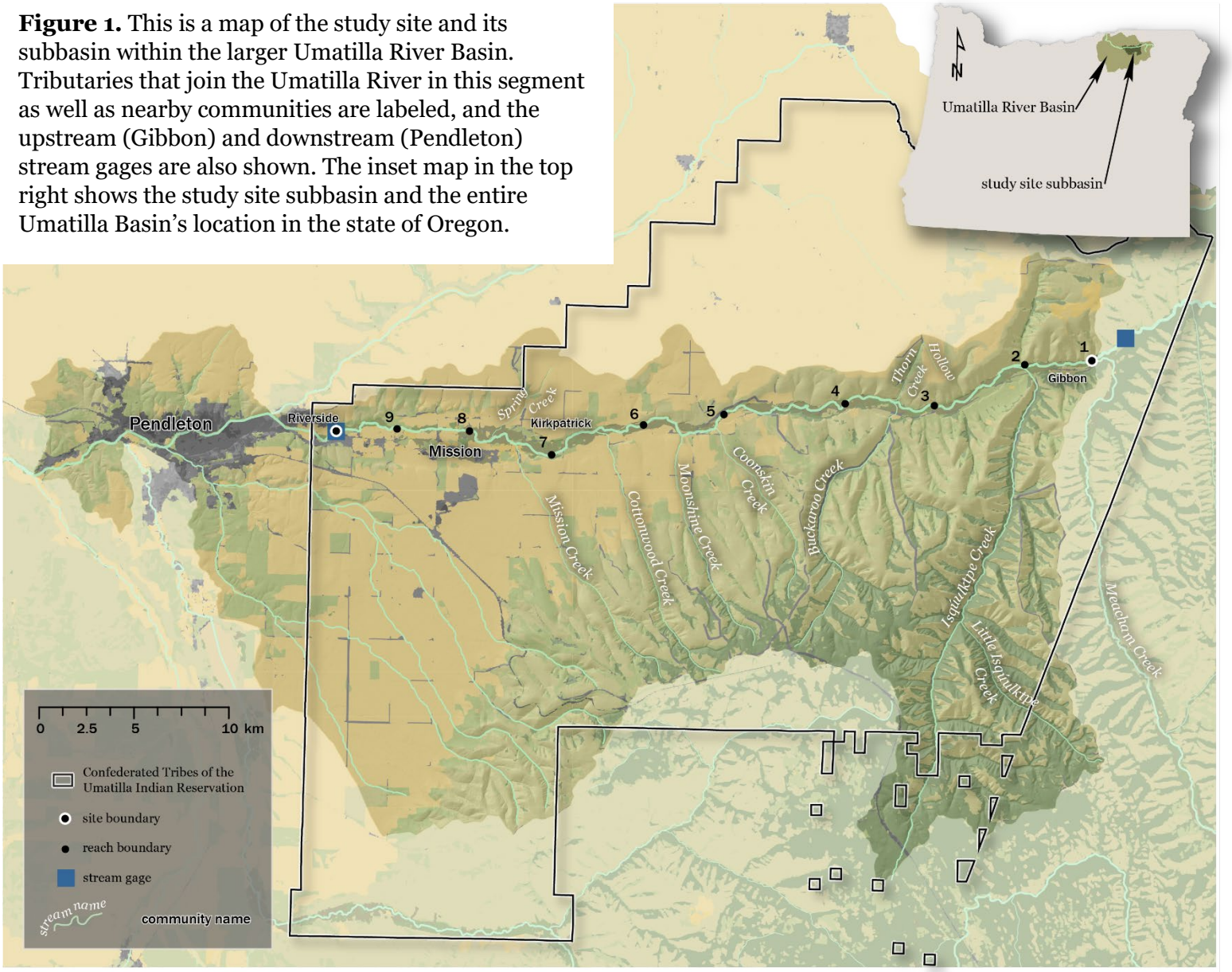

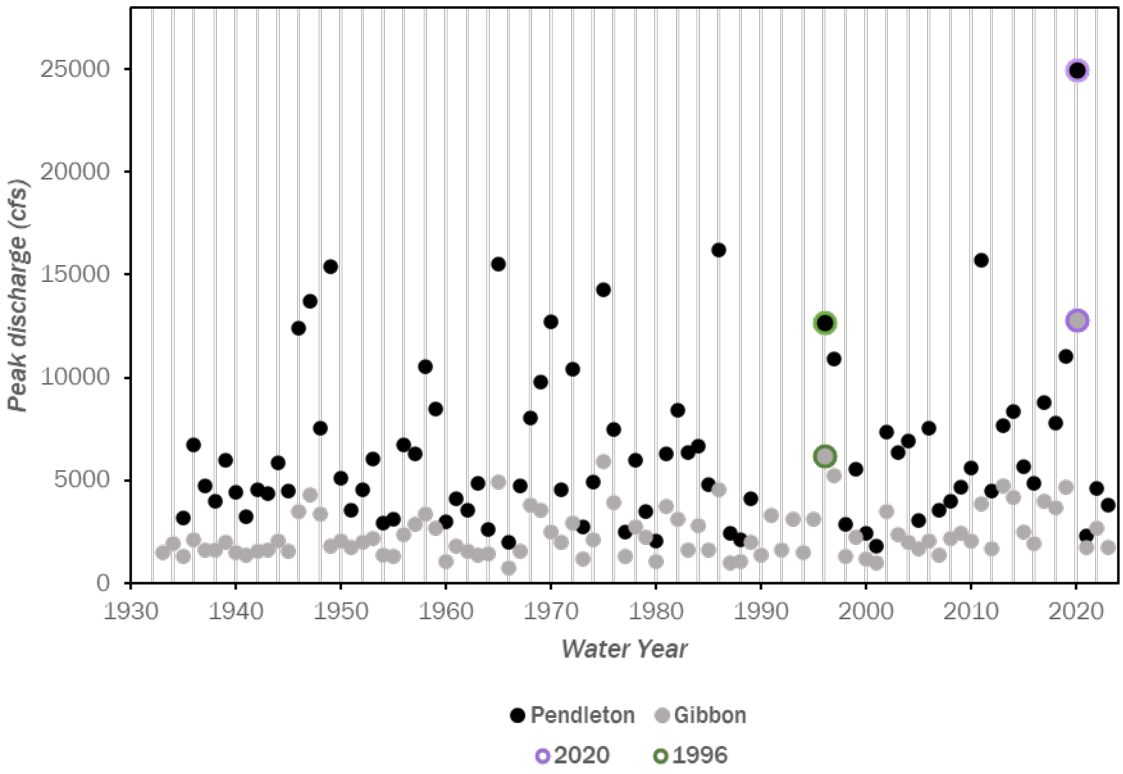

Figure 2. Annual peak flow (by water year) at both the Gibbon (upstream) and Pendleton (downstream) gages. See Figure 1 for their location. Peak discharge for the 1996 flood is highlighted in green, and peak discharge in 2020 is highlighted in purple. Between 1989 and 1996 the gage at Pendleton was taken offline and replaced, so there is no data there during that time.

Table 1. Flood characteristics for the two main floods analyzed in this study. Time to peak duration is the time between the river reaching flood stage and its peak discharge for that flood. Total duration is the time spent above flood stage at that stream gage. *In 1996, discharge reached a near-peak discharge (in both cases, about 1,000 cfs below peak discharge at that gage) quickly and then slowly increased to peak discharge over a longer period.

Water Year	*Gage*	*Peak discharge (cfs)*	*Time to peak discharge (hours)*	*Total duration (hours)*	*Last major flood*
1996	Gibbon	6,220	13.5*/43.5	64.5	1964
	Pendleton	12,800	7.25*/39.75	51.5	
2020	Gibbon	12,700	13.5	79	1996
	Pendleton	25,000	10.5	42.75	

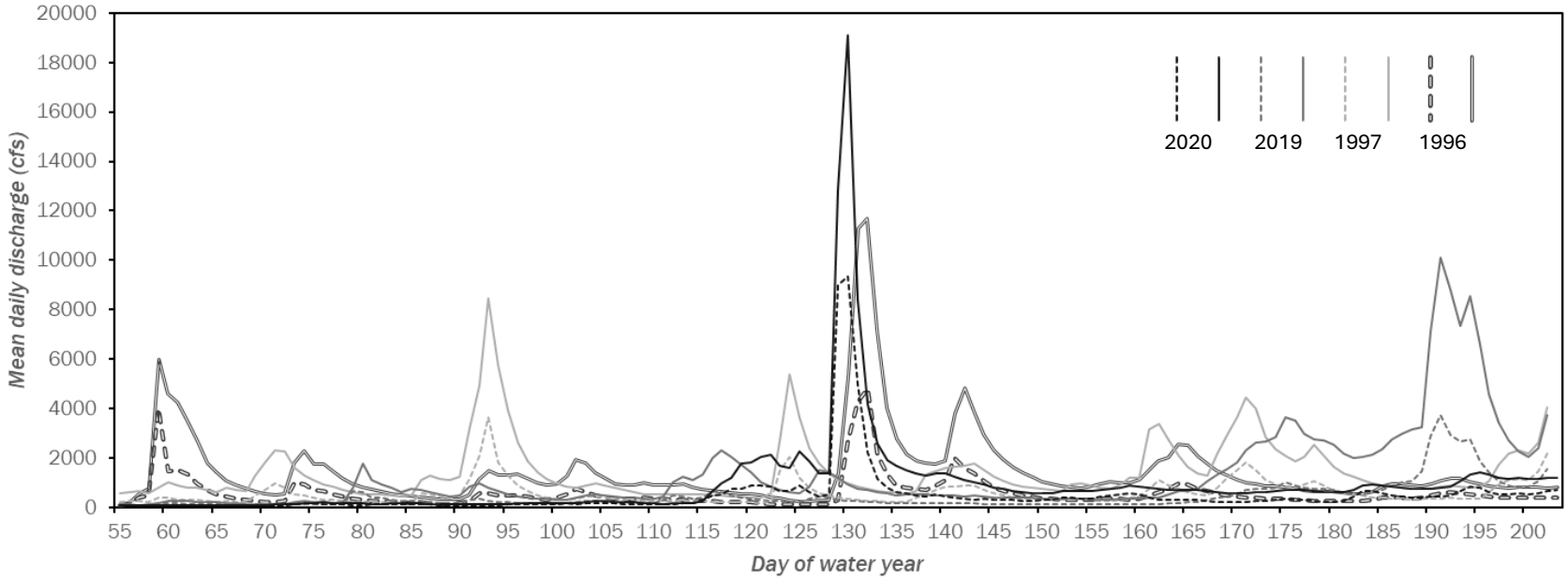

Figure 3. Hydrographs of flooding at the Pendleton (solid line) and Gibbon (dashed line) gages in 1996, 1997, 2019, and 2020. Data cover November 20 through April 20 of each given water year over which most notable flood events occurred.

CHAPTER II

BACKGROUND

1. Catastrophic Floods

Catastrophic floods are rare and have flows far greater than normal, sometimes defined as discharge ten times that of the mean annual flood ($Q_{2.33}$), with the potential to greatly alter the landscape, disrupt channel equilibrium, and even alter channel pattern (Baker, 1977; W. Erskine, 1993; W. D. Erskine & Saynor, 1996; Kochel et al., 2016). Catastrophic floods are particularly effective at altering the landscape in arid and semi-arid climates, as well as in smaller basins with flashier hydrology and gravel- or cobble-bedded channels (Baker, 1977; Graf, 1988; Wolman & Gerson, 1978). Commonly, large floods widen the channel (Dean & Schmidt, 2013; Fuller, 2007; Huckleberry, 1994; Nelson & Dubé, 2016; Sholtes et al., 2018; Sloan et al., 2001; Surian et al., 2016; Tamminga et al., 2015; Thompson & Croke, 2013; Wicherski et al., 2017), increase lateral movement and trigger avulsions or meander cutoffs (Dean & Schmidt, 2013; Magilligan et al., 2015; Nelson & Dubé, 2016; Wicherski et al., 2017), build bars (Dean & Schmidt, 2013; Fuller, 2007; Nelson & Dubé, 2016), and strip vegetation from islands and banks (Dean & Schmidt, 2013; Righini et al., 2017). Most research that tracks flood changes has focused on single-channel rivers, so flood response on rivers with multi-threaded channels are not as well understood. However, these types of rivers may be more strongly affected by floods (Nardi & Rinaldi, 2015), making further study of their flood response across a diverse range of basins all the more necessary.

2. Geomorphic Effectiveness

Geomorphic effectiveness is the ability of a disturbance event, in this case a flood, to alter the landscape and the persistence of those changes (Wolman & Gerson, 1978). When this concept was first theorized, Wolman & Miller (1960) proposed that the geomorphic work accomplished by a flood, a measure of its effectiveness, could be quantified, at least in part, by measuring the sediment it transported. By comparing floods of varying magnitude and frequency with records of sediment transport, they concluded that more frequent, moderate flows are most effective, and rare, high flows accomplish comparatively little geomorphic work.

However, floods of similar magnitude may affect basins very differently, and magnitude and frequency, alone, are poor determinants of flood effectiveness (Baker & Costa, 1987; Costa & O'Connor, 1995; Fuller, 2007; Huckleberry, 1994; Miller, 1990). Miller (1990) compared 1985 flooding in the Appalachians, USA to historic flooding in the area and found that, although the

peak discharge for the 1985 flood was neither unique nor the largest on record, the geomorphic work accomplished far exceeded any previous floods. In a comparison of two floods on the Gila River in Arizona, USA, Huckleberry (1994) found that the much higher discharge event was not nearly as effective as the longer-lasting, lower-flow event, indicating that duration should be accounted for in studies of effectiveness. In both cases, flood magnitude did not accurately predict the geomorphic work of the flood, which suggests there were other variables more important than discharge that played a part in the channels' flood responses.

Many researchers have since opted to use stream power over flood magnitude to gauge flood effectiveness. In order to entrain and transport sediment, stream power and shear stress along banks and beds must surpass the resistance threshold determined by the shear strength of the channel banks (Baker & Costa, 1987; Magilligan, 1992). Therefore, where stream power is greater, more geomorphic work should be accomplished. Magilligan (1992) suggested that, in a humid basin, significant geomorphic change would occur when stream power had exceeded a threshold of 300 W/m^2, a benchmark against which researchers could gauge the relative effectiveness of a particular flood. Stream power varies with changes to channel geometry, slope, and velocity, along a river, which provides higher spatial resolution for analysis of change than discharge. However, this strategy requires more data collected before a flood for calculations and analysis, which is not always possible.

Furthermore, in many cases stream power alone cannot fully explain flood response (Heritage et al., 2004; Tamminga et al., 2015; Thompson & Croke, 2013). Heritage et al. (2004) found no strong correlation between channel change and any of the hydraulic variables they tested, including stream power, in the bedrock-influenced Sabie River in South Africa after it underwent extreme flooding. Furthermore, although stream power was strongly correlated with patterns of erosion and deposition in Lockyer Basin in Queensland, Australia, a flood chute formed in one of the unconfined reaches where stream power was much lower (Thompson & Croke, 2013). In this case, the formation of the flood chute was triggered by a logjam, which illustrates the unpredictable nature of flood response and the need to understand the relationship between flood effects and variables besides stream power.

Researchers have attempted to find additional or alternative parameters to include in analysis to better explain flood response and compare geomorphic effectiveness of different floods. Some of the most common variables that may be included are flood duration (e.g. Bertoldi et al., 2010; Costa & O'Connor, 1995), bend stress (e.g. Buraas et al., 2014) or sinuosity (e.g. Dean & Schmidt, 2013; Fuller, 2007), slope (e.g. Surian et al., 2016), confinement (e.g.

Sholtes et al., 2018; Thompson & Croke, 2013), channel width (e.g. Nardi & Rinaldi, 2015), or proportion of woody vegetation cover (e.g. Righini et al., 2017). Costa & O'Connor (1995) found that the duration of a flood was very important for determining the geomorphic work it could accomplish, as Huckleberry (1994) had proposed. To take this into account they calculated the total energy of a flood to compare the effectiveness of floods across a diverse range of spatiotemporal scales, a method which has since grown in popularity and has exhibited better explanatory power for geomorphic work than stream power (e.g. Fuller, 2007; Wicherski et al., 2017).

To explain differences in flood response along a river during a single flood, researchers have considered morphological controls, such as differences in bend stress. Meander bends are known to be hotspots of erosion, and modeling shows that some bends may exert shear stress similar to that of a narrow, steep canyon, where stream power is often at its highest (Miller, 1995). By incorporating a bend curvature parameter into their framework, Buraas et al. (2014) improved predictions of resistance to erosion during flooding caused by Tropical Storm Irene in 2011 on the White and Saxtons Rivers in Vermont, USA. However, its inclusion did not improve identification of areas that were more likely to erode. The complexity of the relationships between cause and response, variations in the spatiotemporal scales these relationships operate on, and the difficulty of obtaining data during a flood complicate these efforts (Nardi & Rinaldi, 2015; Tamminga et al., 2015).

In 1978, Wolman and Gerson proposed an alternative definition of geomorphic work: landscape change and recovery time, or how long it takes for the system to return to pre-disturbance equilibrium. This understanding of geomorphic effectiveness is slightly harder to quantify and compare across basins and floods than sediment flux, but it does improve understanding of how different environments are affected. In humid climates, for example, rapid vegetation growth may quickly, over one or two years, return a channel to its pre-flood width (Patton, 1988), while semi-arid and arid rivers usually recover over much longer periods, decades or more (Wolman & Gerson, 1978). However, many other factors influence recovery besides climate and vegetation, such as sediment loads, flow regimes, and geologic setting (Bertoldi et al., 2011; Knighton, 1998; Sloan et al., 2001).

Reframing geomorphic effectiveness with landscape recovery in mind opens the door for other non-linear relationships of geomorphology (e.g. sensitivity, connectivity, and thresholds) to be incorporated into the concept, which was initially framed as a linear relationship between cause and effect. Floods push rivers out of equilibrium, and, in the time it takes for rivers to

recover from that disturbance, the system may be less sensitive to further disturbance, like another large flood (Fryirs, 2017; Fuller, 2007; Hughes, 2008). This decreased sensitivity could make the next flood less geomorphically effective, even if the flood is otherwise very similar to the first. Some studies combine analysis of erosion and deposition with landscape change and recovery to provide a more holistic account of flood effectiveness (e.g. Kochel et al., 2016).

3. Flood Processes and Landform Change

Floods raise erosion and deposition rates, because stream power and stream power gradients tend to increase. Stream power tends to be greater in highly confined channels, which promotes erosion, and once the valley begins to widen and confinement decreases, stream power tends to decrease quickly, which promotes deposition (Nelson & Dubé, 2016; Sholtes et al., 2018; Thompson & Croke, 2013). On the other hand, modeling has shown that stream power remains high as a channel first emerges from a narrow, confined canyon to a wider valley, particularly if the channel is not straight (Miller, 1995). Many researchers categorize a channel as either confined or unconfined for analysis, which may obscure downstream effects of channel confinement.

Channel widening is the most common geomorphic response studied, because it is often the most responsive to even moderate floods (Knighton, 1998; Yochum et al., 2017), and it is not unusual for widening to be the only response researchers measure. A large range of widening values has been reported, usually as percent change in width or a ratio of pre- and post-flood widths to facilitate inter-basin comparison. A major 2011 flood in central-north Italy on the Magra River caused the channel to widen between 3% and 90% (Nardi & Rinaldi, 2015). Fuller (2007) reported an average 171%, 57%, and 25% increase in channel width for each of three tributaries studied after a catastrophic, “150-year” flood event in the mountains of the North Island of New Zealand. Where widening is investigated at cross-sections or scales smaller than a reach, widening greater than 500% has been reported (Dean & Schmidt, 2013; Fuller, 2007; Surian et al., 2016). One reach of a tributary of the Magra River widened by over 1800% after catastrophic flooding in 2011 (Surian et al., 2016).

Widening is usually accomplished by a combination of bank erosion and scour or stripping of overbank surfaces as the channel adjusts to the greater volume of water and sediment being transported during a flood. When testing their combined framework of bend curvature and stream power for identifying zones of erosion, Buraas et al. (2014) noted that when both variables were high, channel widening was due mostly to bank erosion, while areas where only one of the two were high widened mostly by stripping vegetation from islands and floodplain.

Channel pattern may also determine which process is more likely to widen a channel during a flood. In multi-threaded channels, channel widening is often accomplished through overbank scour, deposition of sediment, and vegetation stripping more so than bank erosion (Nardi & Rinaldi, 2015; Righini et al., 2017).

Because they tend to increase sediment transport and, therefore rates of erosion and deposition, floods are often accompanied by increased rates of lateral movement. Lateral movement here is used generally to refer to changes in channel location, either gradual, in the case of lateral migration, or sudden, in the case of cutoffs and avulsions. Although many studies report increased channel movement caused by large floods, very few report measurements of these changes, and it is difficult to find a metric that facilitates comparison between different rivers. Nelson & Dubé (2016) found rates of lateral movement increased in flood periods. In one reach, lateral migration occurred at a rate of around 1 m per year between 1990 and 2006 but increased to nearly 10 m per year between 2006 and 2009, likely because of the major flooding that occurred in 2007. On the Umatilla River, Hughes (2008) found that reach-average lateral movement ranged from just under 20 m to over 80 m during periods characterized by at least one large flood. In the time between these floods, reach-average lateral movement was generally less and had a much smaller range.

Increased deposition during floods raises the chance of triggering avulsions, in which the channel abruptly shifts location, especially in braided channels. Channel aggradation as well as blocking or constriction (by sediment or other obstacles, like large woody debris) may divert the flow onto an alternative path around bars and islands within the active channel or else outside the active channel, perhaps capturing new parts of the floodplain within the active channel (Leddy et al., 1993; Osterkamp, 1998). In contrast to cutoffs, which straighten the channel by bypassing a single meander, avulsions do not always decrease sinuosity and tend to occur on a larger scale that affects multiple meanders. Avulsions commonly reactivate formerly abandoned channels and play an important role in the complex processes that govern island, bar, and floodplain connectivity characteristic of braided or wandering channels (Gurnell et al., 2001; Marcinkowski et al., 2017; Nanson & Knighton, 1996; O'Connor et al., 2003; Osterkamp, 1998).

Increased sediment transport during a flood also affects bar accretion, usually leading to larger and more numerous bars, and during catastrophic floods bars may be completely reworked (Knighton, 1998; Nelson & Dubé, 2016; Reid et al., 2019; Surian et al., 2009). Bars generally form when channel widening (and bank erosion) increases the sediment load of the river, where obstacles slow or redirect flow, or where increased roughness, often from

vegetation, encourages deposition (Wohl, 2000). In their study of sediment slug evolution following 2007 flooding in the Chehalis Basin in western Washington, USA, Nelson & Dubé (2016) saw increases in bar area in all reaches after flooding, with bar area in some reaches growing by 500%. The most geomorphically active tributary in Fuller's 2007 study of wandering channels in New Zealand exhibited a 600% increase in bar area, while bar area in the other two tributaries increased by 127% and 65%.

The erosive effects of floods strip vegetation from islands and other near-channel surfaces, sometimes in conjunction with channel widening. Catastrophic floods often have enough energy to uproot trees and other woody vegetation that resist erosion during more moderate floods (Baker, 1977). Righini et al. (2017) found that more than 50% of the woody vegetation around two tributaries in the Posada Basin in north Sardinia, Italy was removed after a high magnitude flash flood in 2013. However, vegetation-flood dynamics are not always straightforward. Vegetation increases surface roughness, decreasing flow velocity, which can decrease local erosion or cause deposition (Huang & Nanson, 1997). Furthermore, root systems can greatly increase shear strength of channel banks, although most catastrophic floods exert enough force to overcome this added resistance (Beechie et al., 2006; Eaton & Giles, 2009). When floodplain is captured by avulsion or other lateral movement and becomes an island within the channel, this increases vegetation within the channel, which may outweigh vegetation loss from stripping and scouring (Hughes, 2008).

CHAPTER III

METHODS

1. Methodological Approach

Aerial imagery is a common tool used by geomorphologists to assess change in rivers, because it can provide data on channel morphology and vegetation cover through time and at a variety of scales. Traditional field-based methods would not have been able to address the research questions of this study, because no recent field observations or measurements had been collected before the flood. Without this baseline data, detecting change or determining pre-flood characteristics would not have been possible. The imagery captured a snapshot of the river at a single point in time, and by comparing imagery of the same location at different times, I explored patterns of change and causal relationships. The methods for digitizing landforms and many of the channel characteristics were the same used by Hughes (2008) for ease of comparison.

2. Aerial Imagery

This study used imagery from Oregon Statewide Imagery Program (OSIP) and the National Agriculture Imagery Program (NAIP) to investigate planimetric changes on the Umatilla River after a catastrophic flood in February of 2020 in answer to the first two research questions. The 2017 OSIP imagery, taken about two and a half years before the February 2020 flood, was the most recent imagery available before the 2020 flood, and the imagery collected the closest to the flood after it occurred, taken between five and six months after the flood, was the 2020 NAIP imagery (Table 2). In both cases, imagery was captured in parts across three days over a period of nearly four weeks. I downloaded the two sets of aerial imagery from United States Geologic Survey (USGS) Earth Explorer and projected them in NAD 1983 UTM Zone 11. Because of the difference in resolution, I resampled the OSIP imagery to a resolution of 1x1 m using cubic convolution. To investigate the third research question, I compared changes from the 2020 flood to changes from the 1996-7 floods using orthophotos collected by USGS and Umatilla County (Table 2). These orthophotos were initially orthorectified and digitized by McDowell et al. (2003) following the methods described in Hughes (2008). This imagery was taken in 1994, a little less than two years before the first major flood in the 1996-7 flood cluster, and in 1998, slightly less than three years after the February 1996 flood.

Table 2. Imagery used for this study. All 1994 imagery was captured 05-06-1994, while the Pendleton gage was replaced, so the discharge reading is only available from the Gibbon gage. All other discharge values are an average between the Gibbon and Pendleton gages. The exact dates the 1998 imagery was captured are unknown, although they were collected between July and September. Discharge values are an average of values within that time frame. The 2017 imagery was collected 07-14-2017, 08-01-2017, and 08-15-2017. The 2020 imagery was collected 07-18-2020, 07-21-2020, and 08-13-2020.

Flood water year	*Imagery year*	*Month*	*Source*	*Discharge (cfs)*	*Resolution*
1996-7	1994	May	USGS DOQ	285.8	1-meter
	1998	unspecified - summer	Umatilla County Orthophotos	52.3	1-meter
2020	2017	July and August	OSIP	43.8	1-foot
	2020	July and August	NAIP	61.4	1-meter

3. Division of the Floodplain

For his research, Hughes (2008) delineated the boundary of the Umatilla River floodplain based on soil maps and topography. Next, he split the Umatilla River and its floodplain into 9 reaches at tributary junctions or variations in channel morphology (i.e. valley width, sinuosity, channel pattern; Figure 1, Table 3). He then broke those reaches down into 156 boxes (lengths ranging from 189 m to 267 m, median = 199 m; areas ranging from 38,204 m^2 to 335,566 m^2, median = 96,083 m^2; Figure 4). This study makes use of those same levels of division.

Additionally, I grouped together between 2 and 6 boxes (median of 3 boxes) with similar water surface slope and confinement index (CI) to create 46 subreaches (Figure 4). Finally, based on visual assessment of the imagery and identification of bedrock by Hughes (2008), I sorted the subreaches into one of three categories of increasing bedrock influence: alluvial, semialluvial, and bedrock (Figure 4). Alluvial channels were those with no visible bedrock in or along the channel. Semialluvial channels were those with some visible bedrock within or along the channel, but which affected less than 50% of the subreach channel length. Bedrock channels were those where more than 50% of the channel length was visibly influenced by bedrock. In addition to the reach analysis, similar to that performed by Hughes (2008), I analyzed change at subreach and, for some variables, box level for the 2020 flood to expand understanding of the relationships between variables at multiple scales. Because there were no elevation data to determine slope in 1994, the reaches were not subdivided into subreaches for analysis of causal variables. However, I sometimes used the 2017 subreach boundaries for comparison between the floods.

Table 3. Reach-average and channel-type-average morphological characteristics before the 1996-7 (1994 imagery) and 2020 (2017 imagery) floods for the study site. At the bottom, the median, minimum, and maximum values across all boxes are given. CI median, minimum, and maximum exclude values from Reach 8.

*Slope values were not available before the 1996-7 floods, and subreach-level-analysis was not performed for that flood.

	Sinuosity Index (SI)		*Slope** *(mm^{-1})*	*Confinement Index (CI)*		*Average active channel width (m)*		*Average bar area (m^2) – Average proportion of box area designated bar (%)*		*Floodplain width (m)*
Reach	*2017*	*1994*	*2017*	*2017*	*1994*	*2017*	*1994*	*2017*	*1994*	
1	1.171	1.096	0.0065	9.5	5.1	57.2	97.7	4,707.8 – 5.7	1,576.8 – 2.0	423.4
2	1.201	1.151	0.0058	10.0	6.9	48.1	73.7	2,984.3 – 3.2	4,946.1 – 5.2	470.3
3	1.169	1.092	0.0051	12.1	8.0	42.7	65.5	3,116.0 – 3.4	862.4 – 0.8	486.8
4	1.199	1.181	0.0050	8.3	5.9	53.1	72.1	4,208.1 – 5.7	4,079.2 – 5.0	388.9
5	1.142	1.099	0.0050	8.7	6.5	51.8	60.3	2,544.7 – 3.9	2,746.6 – 4.5	381.3
6	1.186	1.132	0.0048	8.0	5.9	73.9	104.4	4,242.0 – 4.2	3,167.7 – 3.3	540.5
7	1.243	1.207	0.0049	16.6	14.2	87.5	109.9	7,203.5 – 3.6	6,155.6 – 2.6	1,153.7
8	1.043	1.038	0.0064	32.2	32.5	42.6	43.8	2,483.8 – 0.9	739.0 – 0.3	1,421.8
9	1.179	1.075	0.0045	17.0	8.8	45.5	93.2	3,251.2 – 2.2	3,815.7 – 2.2	792.2
Channel type										
Alluvial	1.171	-	0.0047	9.6	-	78.8	-	4,846.2 – 4.3	-	655.0
Semialluvial	1.187	-	0.0049	11.6	-	47.9	-	3,502.9 – 3.5	-	628.0
Bedrock	1.160	-	0.0060	10.6	-	52.5	-	3,702.8 – 4.2	-	641.8
Box median	1.170	1.107	0.0051	9.7	6.6	46.9	65.9	2,349.4 – 3.4	1,860.0 – 1.6	482.1
Box minimum	1.028	1.006	0.00002	2.8	1.8	21.7	27.7	0.0	0.0	192.8
Box maximum	1.598	1.532	0.011	31.6	30.1	235.3	487.9	10,461.8 – 16.0	18,472.8 – 28.2	1,698.0

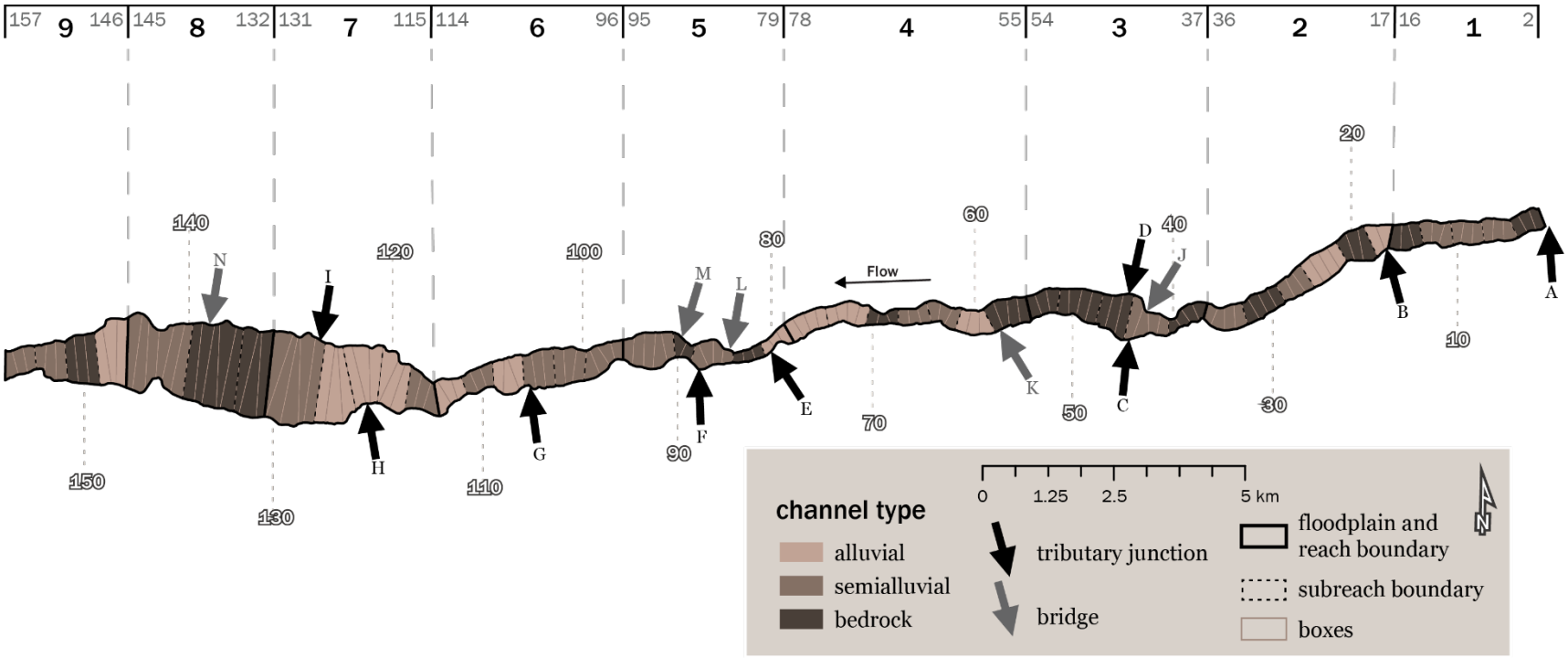

Figure 4. Reference map of all floodplain division (box, subreach, reach). Bridges and tributary junctions are indicated by arrows and letters, and subreach channel types are indicated by fill color. Reach numbers are shown at the top in black alongside the first and last box number of each reach in gray, and the number of every 10th box is shown connected to its corresponding box by a dotted line. Tributaries: A – Meacham Creek, B – Isqúulktpe Creek, C – Buckaroo Creek, D – Thorn Hollow Creek, E – Coonskin Creek, F – Moonshine Creek, G – Cottonwood Creek, H – Mission Creek, I – Spring Creek. Bridges: J – Thorn Hollow Road Bridge, K – unnamed railway bridge, L – N. Cayuse Road Bridge, M – unnamed railway bridge, N – S. Market Road (OR-331) Bridge).

4. Digitization

I used heads-up digitization of the aerial imagery in ArcGIS Pro 2.4.2 to gather data before and after the floods. First, I digitized the landforms and extracted channel characteristics, which allowed me to answer the first and third research questions, as well as parts of the second research question. Then, I digitized the landcover, which allowed me to answer the rest of the second research question. The minimum polygon area I used for digitization was 25 square meters, and I performed digitization at or near a scale of 1:1,000, the same parameters Hughes used for his 2008 study of the river.

4.1 Landforms

The first step of digitization was to delineate the active channel within the river floodplain, following the methods and definitions used by Hughes (2008). The active channel was defined as the wetted channel plus all side channels, recently disturbed bars, and enclosed vegetated islands. Within the active channel, Hughes divided the surfaces into four landform types: low-flow channels, bars, scoured surfaces, and vegetated surfaces. Low-flow channels (or wetted channels) were the areas where water was present in the channel when the imagery was collected. Areas of unvegetated or thinly vegetated sediment along and within the channel with typical barform (i.e. point, diagonal, mid-channel) were classified as bars. Scoured surfaces were defined as unvegetated or thinly vegetated areas further from the wetted channel or which lacked typical barform. Scoured surfaces were generally irregular in shape and often included abandoned or dry secondary channels. Vegetated surfaces were defined as those with at least 50% vegetation cover completely surrounded by low-flow channels or channel-like scoured surfaces. Then, I digitized the channel centerline along the main branch of the wetted channel, following the thalweg wherever visible.

4.1.1 Correcting for Differences in Discharge

According the USGS stream gages at Gibbon and Pendleton, the Umatilla River discharge was slightly greater in 2020 than it was in 2017 when imagery was captured (Table 2). At a lower discharge, more bare sediment along the channel would be exposed, leading to an artificially larger bar area in 2017. To correct for this difference, I found the relationship between gage height and channel width based on stream gage data for low flow conditions from the last 30 years, and then I developed a correction factor based on that relationship. Gage height and channel width were measured on August 3, 2020, just before the final NAIP flight collecting imagery for the study site (covering Reaches 8 and 9). Because of the overlap between field

measurement and imagery collection, this date was used as the standard to which measurements were corrected. The correction factor was used to decrease bar area in 2017 (increasing wetted width) and increase bar area in the first seven reaches of the study site in 2020 (decreasing wetted width) so that they would reflect discharge conditions in early August 2020 and could be directly compared.

The disparity between discharge in 1994 and 1998 was even greater (Table 2), so I also corrected those values by increasing bar area in 1994 and reducing wetted area by a correction factor. The correction factor for this data was based on historical data with a wider range of flow conditions, but otherwise I developed it as I had for the 2017 and 2020 imagery. Because imagery in 1998 was captured during discharge conditions similar to summer 2020 (to which it would be compared), the correction factor was only used to adjust the measurements from the 1994 imagery.

4.2 Landcover Classification

In order to answer the second research question, the landcover of the floodplain also had to be classified and digitized. I classified landcover in the same area both before and after the 2020 flood, which included the combined active channels in 2017 and 2020 as well as a buffer of 2 m. Surfaces were categorized as either trees, grass and scrub (sometimes referred to as grass), mixed grasses and trees, bare ground, or developed areas. For more detailed descriptions and example images of the vegetation classifications see Table 4.

5. Analysis

Once digitization was complete, I used ArcGIS Pro tools to measure width, length, area, and elevation of the features in each box (details below; all box-level data can be found in the Appendix). Using the elevation data from a DEM, I calculated water surface slope in R version 4.4.0 (details below). Then, I exported the data to Microsoft Excel where I cleaned them, performed analysis (both univariate statistics and linear regression at various scales), and created charts, plots, and tables. Using ArcGIS Pro and Adobe Illustrator 2024, I created other visual elements including maps and sample images of vegetation classification types.

5.1 Measuring Control Variables

First, I established the floodplain dimensions and channel length within each box (see Appendix). I calculated *active channel width* by first taking the area of the active channel in each box. Then, I divided that area by the length of channel in the box, because the boxes were

irregular in area and channel length due to variability in floodplain width and river orientation (Figure 4). To find the percent cover of each *landcover type*, I separated the polygons of each type of landcover into the separate boxes and then divided the area of each different landcover type by the box area.

I used the *confinement index (CI)* of the channel, which I calculated by dividing the average floodplain width by the average active channel width for the box and the two boxes adjacent to it (widths averaged over three boxes), to express lateral channel confinement of the channel before the flood for each box (Fuller, 2007; Righini et al., 2017; Rinaldi et al., 2016; Surian et al., 2016; Yochum et al., 2017). Higher CI values indicate less confinement. Very few boxes met the accepted definition for confined channels (generally CI < 4; Beechie et al., 2006; Sholtes et al., 2018), and the range of values, especially of reach averages, is limited (Table 3).

Sinuosity generally needs to be measured over distances greater than the length of a single floodplain box in order to generate meaningful measurements. Following methods similar to those used by Dean & Schmidt (2013), I calculated the local *sinuosity index (SI)* for each box. I generated points every 10 m along the channel centerline, found the straight-line distance between the points 600 m upstream and 600 m downstream (following the channel centerline) of the central point in each box, and then divided 1200 m (the total distance along the centerline) by the straight-line distance between those two points (see Appendix for straight-line distances used in calculation). This distance (1200 m) was appropriate because it far exceeded both half a meander wavelength and the active channel width before the flood. The range in reach-average SI was especially limited in 2017 (Table 3), though at the subreach and box level there was greater variation.

I followed the methods outlined by Vocal Ferencevic & Ashmore (2012) to calculate *slope*. The Oregon Department of Geology and Mineral Industries (DOGAMI) used LiDAR collected in 2016 to create a 5-m resolution DEM, from which I extracted elevation values along the channel centerline. I calculated water surface slope over 200 m, 400 m, 600 m, 800 m, 1000 m, and 1500 m in R to determine an appropriate distance for determining slope that neither exhibited small, local differences nor obscured differences all together. Based on that analysis, I used a window of 800 m to find the slope for each box based on the trend between elevation data extracted from the DEM over the 800 m window (400 m upstream and downstream from the center of the channel centerline of each box).

Subreach- and reach-average values were calculated as an average of all box values that fell within that larger subset. See the Appendix for all box-level control variable values.

Table 4. Key for vegetation classification. Bars, the main landform with bare surface cover, were generally smaller in 2017, so the bare cover example shows three slivers of bare ground taken from three different locations.

2017 example imagery	*Landcover type and description*	*2020 example imagery*
	**Bare** Surfaces categorized as bare were identified by their minimal vegetation or complete lack of vegetation. Generally, these surfaces ranged in color from grey to white, and most bare surfaces were located near the wetted channel where recent inundation and reworking prevented vegetative growth.	
	**Grass and scrub** Surfaces categorized as grass and scrub were brown or light green. Sometimes there were small tufts of darker green, but this vegetation did not cast large shadows, allowing it to be distinguished from trees. Trees make up less than 10% of the area of this cover type.	
	**Mixed grasses and trees** Surfaces categorized as mixed grasses and trees had the same brown or green look as grass and scrub, but with darker green trees scattered throughout, which cast large shadows. Trees make up between 10 and 75% of the area of this cover type. This was the least common cover type.	
	**Trees** Surfaces categorized as trees were dark green with a rough, uneven texture created by variation in height at the crown of the canopy. In some areas, the lighter green or brown of understory or grass was visible between patches of trees. Trees make up more than 75% of the area of this cover type.	

5.2 Measuring Response Variables

I measured the area of the different landform types I delineated earlier for each box. Like *active channel width*, I calculated *wetted channel width* by dividing the area of low-flow

channels in each box by the pre-flood length of channel in the box and then applying the correction factor. *Bar area* was corrected before calculations were performed. I calculated the percent change of active channel width, wetted width, and bar area to gauge change after the floods. To illustrate the *change in sinuosity*, I found the difference between SI before and after the flood.

I determined the average distance of *lateral movement* in each box by first overlaying the centerlines from before and after the flood and extracting the polygon between the centerlines (see Appendix for polygon areas). I then classified this polygon as either extension, translation, straightening, or avulsion, using the same definitions as Hughes (2008). Polygons with areas less than 200 m^2 were too small to accurately classify, and so they were left unclassified. Finally, I split the polygons into the separate boxes and divided the total polygon area in each box by the pre-flood channel length in that box. This distance represented the average lateral distance the channel moved (without cancelling out movement in either direction) within each box.

5.3 Scales of Effectiveness

Although each variable was measured at the box level, and change was studied at all three scales (box, subreach, reach), most causal relationships were only analyzed at the subreach or reach level, depending on the scale on which they are known to operate as well as data availability and resolution. The relationships between the response variables and either pre-flood channel width, SI, or CI in 2020 were all analyzed at the subreach and reach level. Vegetation effects were analyzed at the box, subreach, and reach level. Because the floodplain reaches were not divided into subreaches for the 1996-7 flood analysis, the relationships between control and response variables for that flood were only investigated at the reach level.

Therefore, research question 1 has been explored at all three scales (box, subreach, and reach), while most of the relationships in research question 2 have been investigated on the subreach and reach level (except where vegetation cover effects are analyzed in finer detail). Research question 3 has been answered at both the box level, where planimetric change observations were noted, and the reach level, where causal relationships were investigated.

CHAPTER IV

RESULTS

1. Overview

This section describes the results of each of the three research questions separately. For each research question, I restated the question and my hypotheses, explained the sections that make up the results, and then described the results themselves. The results were divided by response variable (active channel width change, lateral migration and sinuosity change, bar area change, and vegetation loss).

2. Planimetric Changes in 2020

Question 1 – *What effects did the 2020 flood have on the geomorphology (active channel width, lateral movement, sinuosity, bar accretion) and vegetation of the Umatilla River?*

a. Hypothesis 1 – *The active channel will widen and bar area will increase.*
b. Hypothesis 2 – *Sinuosity will decrease, and lateral migration will be dominated by movement that decreases sinuosity (cutoffs, straightening, avulsions).*
c. Hypothesis 3 – *More herbaceous vegetation than woody vegetation will be removed.*

To answer this question, I analyzed both reach-average patterns (presented in Table 5) as well as box-level trends (based on Figure 5) in the response variables. I then described areas where variations in control variables (Table 3) or additional factors, such as tributary junctions or bedrock prevalence (Figure 4), may have been responsible for some of the changes observed. Relationships between causal and response variables were also explored, and those results can be found in 3. Causal Relationships with further explanation in the Discussion. In 4. Historical Comparison, these changes were compared with the changes caused by the 1996-7 floods.

The river widened, increased in bar area, shifted laterally, and lost sinuosity and vegetation, similar to other rivers where flood effects have been studied (Figure 5). In general, patterns of change in channel width, lateral migration, and sinuosity were geographically similar, while changes in bar area were not. Vegetation removal shared some geographical patterns with all morphological change response variables. Because it has been channelized and its banks have been artificially strengthened, Reach 8 exhibited much less change than all other reaches and was often an outlier

Table 5. Reach-average and channel-type average change in response variables after the 1996-7 and 2020 floods with univariate statistics for each variable at the bottom.

*Boxes that had no bars before the flood excluded from calculation. †Six outlier boxes with greater than 4,000% change excluded from calculation.

	Change in average active channel width (%)		*Change in bar area (%)*		*Average lateral movement (m)*		*Change in average wetted channel width (%)*		*Change in sinuosity*		*Tree area lost (%)*	*Grass area lost (%)*
Reach	2020	1996-7	2020	1996-7	2020	1996-7	2020	1996-7	2020	1996-7	2020	2020
1	31	-6	97	398	19.4	18.4	-29	-24	-0.013	0.073	59	62
2	50	8	275	458	25.4	24.9	-20	-9	-0.021	-0.010	61	63
3	20	5	230	360	11.6	13.9	-13	-22	0.015	0.031	55	65
4	45	22	183	341	18.9	36.0	-30	-28	-0.005	0.013	49	53
5	29	3	529	297	18.3	10.6	-24	-29	0.003	0.015	55	64
6	63	37	260	224	36.1	29.9	-28	-40	-0.046	-0.048	42	59
7	66	40	150	210	51.5	67.1	-31	-36	-0.018	0.086	61	73
8	15	9	33	-47	7.1	4.8	-8	-24	-0.010	0.005	36	39
9	44	-21	215	172	14.3	27.4	-16	-39	-0.044	0.030	43	64
Channel type												
Alluvial	48	-	315	-	32.0	-	-13	-	-0.010	-	46	65
Semialluvial	44	-	200	-	21.3	-	-25	-	-0.015	-	55	59
Bedrock	32	-	175	-	18.9	-	-20	-	-0.017	-	51	58
Box median	30	6	142*	107*†	16.5	13.4	-25	-28	-0.008	0.011	54	66
Box minimum	-26	-69	-91*	-100*	1.1	0.9	-65	-72	-0.216	-0.168	2	0
Box maximum	305	274	2,411	2,905†	131.7	363.0	69	48	0.220	0.398	97	100

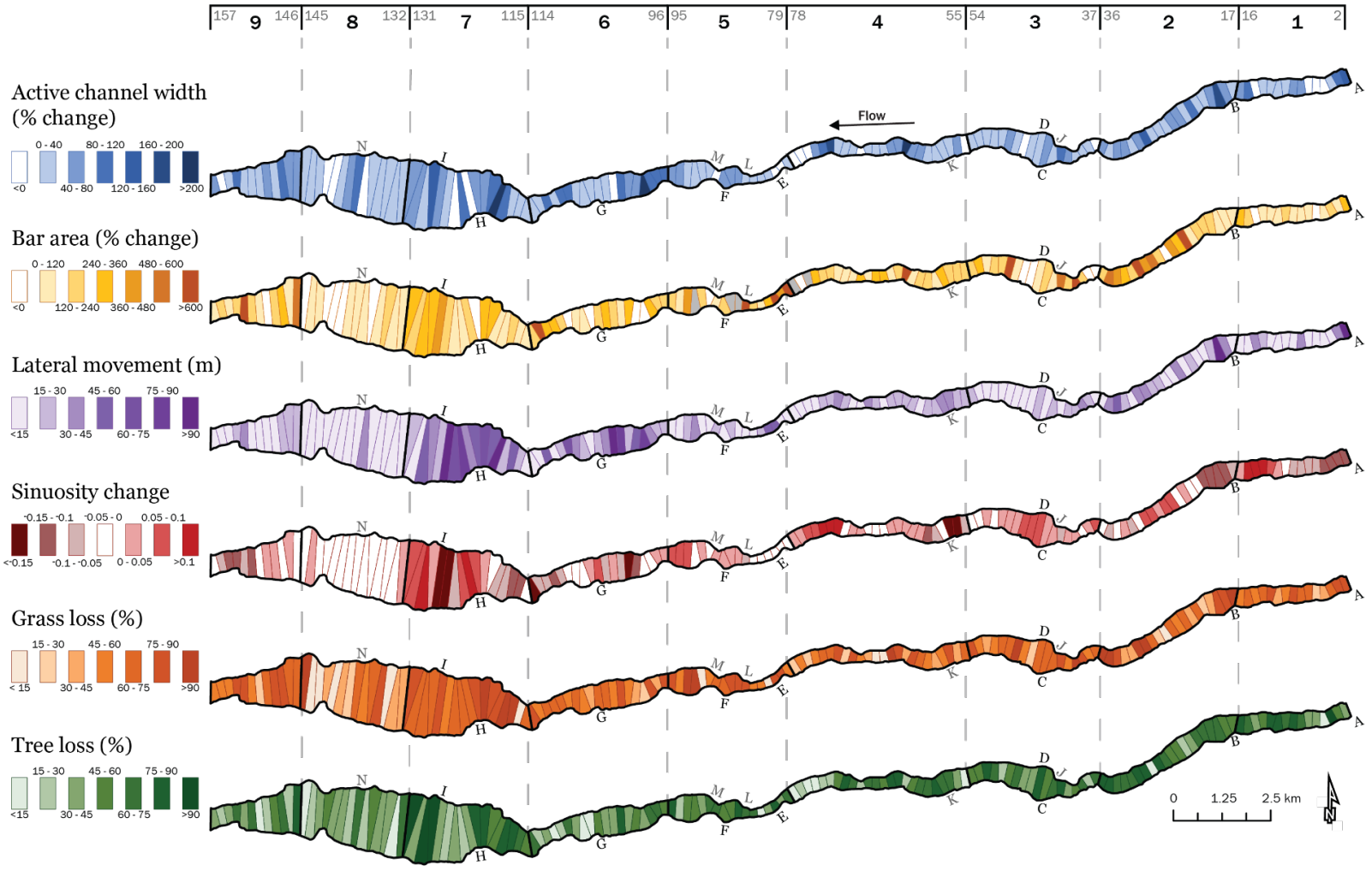

Figure 5. Response variable change map after the 2020 flood by box. Reaches are outlined and numbered on the top in black alongside the first and last box number of each reach in gray, and bridges and tributary junctions are indicated by the letters along the boxes. Boxes excluded from averages are gray. Tributaries: A – Meacham Creek, B – Isqúulktpe Creek, C – Buckaroo Creek, D – Thorn Hollow Creek, E – Coonskin Creek, F – Moonshine Creek, G – Cottonwood Creek, H – Mission Creek, I – Spring Creek. Bridges: J – Thorn Hollow Road Bridge, K – unnamed railway bridge, L – N. Cayuse Road Bridge, M – unnamed railway bridge, N – S. Market Road (OR-331) Bridge).

2.1 Channel Width Change

The wetted channel generally narrowed, though to a lesser extent in Reaches 3 and 8, likely because channel bed scour during the flood increased channel depth (Table 5). High bedrock influence in Reaches 3 and 8 may have limited channel bed scour, so depths and widths changed less. The active channel, in contrast, was wider in the 2020 imagery. All reaches except Reach 8 saw an increase of at least 20% in active channel width, and in Reaches 2, 4, 6, 7, and 9 reach-average active channel width increased more than 40%. In some boxes in Reaches 2, 4, 6, and 7, the active channel width increased by more than 160% (Figure 5).

Despite widening overall, there were a few instances of slight channel narrowing. Of the 156 boxes, only 21 underwent a decrease in active channel width (Figure 5). This seemed to be caused by vegetation encroachment between the collection of imagery in 2017 and the 2020 flood. In some cases, this encroachment was preceded by the aggradation of small side channels which had marked the boundary of the active channel. The boxes that lost active channel width did not have a geographical trend, and all reaches had at least one box where active channel width decreased except for Reach 2. The greatest widening happened in Reaches 6 and 7, where the channel widened, on average, over 30 m, but Reach 7, which had the greatest concentration of small side channels, also had some of the greatest narrowing of the channel in boxes 123 and 125. However, this narrowing was still minimal in comparison to the degree of widening elsewhere.

Channel and valley width before the flood seemed to have some control of channel widening. Downstream of Reach 5, the valley begins to widen, and the channel is less confined. This may account for some of the major channel widening that occurred in the downstream portion of the study site. The channel was also wider in this area, and grass tended to dominate the surface cover. All of these factors may have contributed to the increase in widening in Reaches 6 and 7 (Table 5, e.g. Figure 24 on p. 36). Widening also appeared to be greatest in areas where sinuosity was higher before the flood (e.g. Figure 6, Figure 7).

Bedrock limited channel widening. For example, widening in Reach 4 was greatest where bedrock became less plentiful in and around the channel, such as boxes 63 or 73, which fell in a semialluvial and alluvial subreach, respectively (Figure 5, see the channel type reference map: Figure 4). Channels in alluvial and semialluvial subreaches widened, on average, much more than those in bedrock subreaches (Table 5).

Figure 6. Active channel widening and lateral movement for the 2020 flood (shown on2017 imagery) in Reach 1 – boxes 14 through 16 and Reach 2 – boxes 17 through 20.

Another factor influencing widening is tributary junctions. Where Isqúulktpe, Mission, and Spring Creek join the Umatilla (Reach 2 – box 17, see Figure 6, and Reach 7 – boxes 122 and 127, respectively) significant widening occurred both upstream and downstream (B, H, and I in Figure 5). Tributaries increase discharge, introduce sediment, and lower slope, all of which may contribute to channel widening.

Many of these factors are illustrated in Figure 6, which shows where Isqúulktpe Creek joins the mainstem Umatilla River in Reach 2 – box 17 and the widening that occurred in the area. The meander bends in boxes 14 and 17 through 19 increased local sinuosity in those locations. Boxes 17, 18, and 19 did not have any visible bedrock, whereas the other boxes all had some bedrock in or alongside the channel and, in many cases, were constrained by the valley walls, preventing more widening and lateral migration. There is a great deal of contrast in widening and lateral movement in box 16 compared with box 19 because of these factors.

2.2 Lateral Movement

As is often seen in multi-threaded gravel-bedded rivers, there was a great deal of geomorphic work that went towards shifting the channel location (Table 5). Like channel widening, lateral

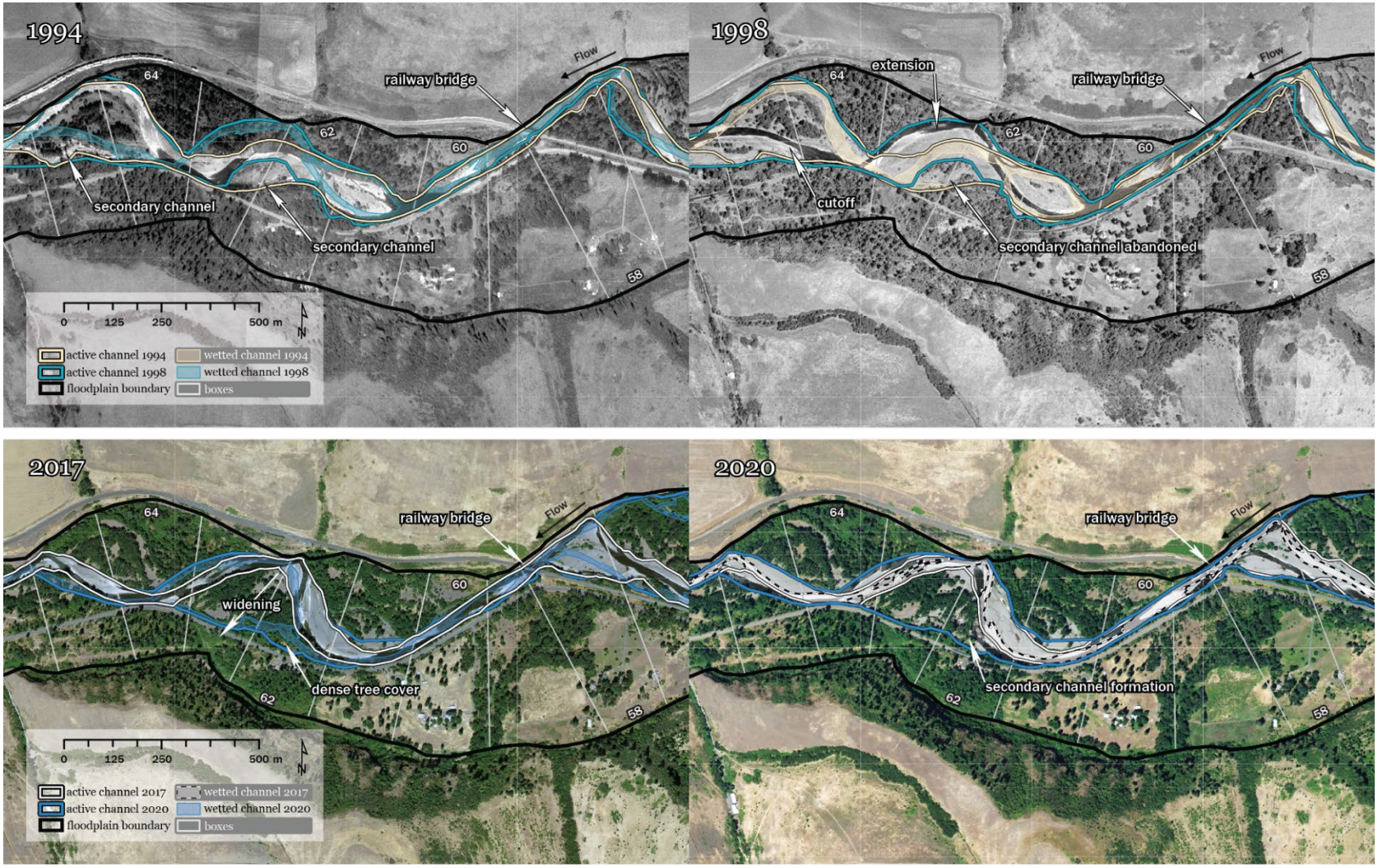

Figure 7. Active channel widening and lateral movement for both the 1996-7 and 2020 floods in Reach 4 – boxes 58 through 65. Before both floods, the channel was narrower and less sinuous in boxes 59 and 60, where little change occurred. However, in boxes 61 through 65, greater sinuosity and a wider active channel may explain some of the lateral movement (extension and cutoff) and widening (secondary channel formation). The railway bridge in box 58 also constrained the channel and created a bottleneck, which may have driven some of the lateral movement and widening upstream, as well.

movement was most extreme in Reaches 6 and 7, though there were also peaks of lateral movement at the upstream end of both Reaches 1 and 2, near tributary junctions (Figure 5, e.g. Figure 6 explained in 2.1 Channel Width Change). Again, Reach 8 saw the least lateral activity, though Reaches 3 and 9 also exhibited much less movement, on average. There were no continuous geographical trends in the distance the channel shifted or in the classification of the movement across the entire study site (Table 6).

Like channel widening, lateral movement was generally greater in areas with high sinuosity, a wide active channel, or proximity to tributary junctions, but it was limited by lateral constraints (e.g. Figure 7). It is not surprising that lateral activity was greatly reduced in bedrock subreaches, but even semialluvial reaches experienced much less lateral activity than alluvial subreaches, on average (Table 5). Reaches 6 and 7 provided favorable conditions for lateral activity because the channel was wide, sinuous, and unconfined with several tributary junctions, and so lateral activity was high there. Reach 8, in contrast, had been straightened and channelized and was highly influenced by bedrock, and the limited lateral activity there reflected that.

In reaches where there was a mix of characteristics both favorable and unfavorable for lateral movement, there did not appear to be a single dominant control. The channel in Reach 4 was more sinuous and wider than average, characteristics that generally coincided with greater lateral movement, but this reach was also more confined (lower CI) than most other reaches, which may have prevented more lateral movement (Table 3). In addition, there were no tributary junctions in Reach 4, which might otherwise have driven lateral movement (Figure 5). In contrast, despite multiple tributary junctions, the narrow active channel in Reach 3 likely limited lateral movement there during the flood (Table 3). Some of the greatest lateral shifts occurred around tributaries (e.g. the 120.7 m moved in Reach 7 – box 126, one box upstream of Spring Creek's junction, labeled I in Figure 5), even in bedrock reaches (e.g. the 104.9 m of lateral movement in Reach 2 – box 19, two boxes downstream of Isqúulktpe Creek's junction seen in Figure 6), but there were also several tributary junctions where the channel only shifted slightly (C and D in Figure 5).

Channel widening and lateral movement often coincided. For example, the peak in active channel widening in Reach 2 – box 19 was accompanied by a great deal of lateral movement due to a cutoff which significantly straightened the channel (Figure 6). Here, the channel was less

Table 6. Reach-average meters of movement per box attributed to each movement classification. At the bottom, the sum total lateral movement caused by each type of lateral movement is given, along with the box mean and maximum values (the minimum and median values for all classifications were 0), and the total number of distinct occurrences of each type.

	Extension (m)		*Translation (m)*		*Avulsion (m)*		*Straightening (m)*		*Unclassified (m)*	
Reach	2020	1996-7	2020	1996-7	2020	1996-7	2020	1996-7	2020	1996-7
1	5.2	14.8	0.9	0.0	10.1	0.0	2.7	3.5	0.5	0.4
2	8.9	5.0	5.9	0.5	0.0	12.3	10.3	6.2	0.3	0.4
3	3.7	11.8	5.0	0.0	0.0	0.0	2.4	0.3	0.6	1.1
4	7.4	22.0	2.3	0.3	0.0	6.3	8.7	7.3	0.5	0.3
5	7.9	4.7	1.6	0.0	7.3	0.0	0.4	3.7	1.1	1.8
6	7.0	5.0	0.0	0.0	8.8	0.0	20.2	24.0	0.2	0.1
7	5.8	13.7	24.2	0.0	14.4	60.8	7.0	0.1	0.1	0.3
8	0.4	0.5	0.0	1.4	0.0	0.0	5.6	0.0	1.1	2.9
9	6.9	12.7	0.0	8.3	0.0	0.0	6.9	5.3	0.5	0.1
Total	954.5	1,632.2	714.4	135.7	687.7	1,430.4	1,167.9	941.5	80.5	118.1
Box mean	5.9	10.0	4.4	1.2	4.5	8.8	7.1	5.6	0.5	0.8
Box maximum	54.4	99.8	131.6	57.2	120.7	490.5	104.9	97.9	7.4	7
Total # occurrences	52	51	19	4	9	10	44	18	114	107

constrained by bedrock and valley walls than it was upstream or downstream, and several meanders increased local sinuosity, all of which contributed to lateral activity and widening.

Lateral migration was due mostly to shifts which straightened the channel (i.e. cutoffs, avulsions, and general straightening by channel migration). There were 18 more occurrences of extension and translation than straightening (including cutoffs) and avulsions, but the latter processes were responsible for larger lateral shifts, as hypothesized (Table 6). Avulsions generally resulted in much larger lateral shifts per event, but they were also the rarest type of lateral movement. Straightening accomplished greater lateral change than extension overall and was responsible for some lateral movement in all reaches.

2.2.1 Sinuosity Change

As was expected, sinuosity across the entire site decreased (Table 5), though in Reaches 4, 5, and 7 the loss of sinuosity was minimal. Sinuosity only increased in Reach 3, where extension accounted for more movement than straightening and avulsions combined (Table 6). Reach 5 was the only reach where more lateral movement was classified as extension than any other type, which likely limited sinuosity loss there. In Reaches 2, 4, 6, and 8, straightening was responsible for the most movement, while translation caused the most movement in Reaches 3 and 7. Straightening and extension each accounted for the same distance of channel movement in Reach 9. Sinuosity declined the most in this reach because the straightening occurred at major meander bends which were responsible for much of the pre-flood sinuosity within the reach, while the extension occurred in smaller pockets throughout, and so had less of an impact on reach-average sinuosity (Figure 8). Reach 1 was the only reach where avulsion was the largest source of the lateral movement, though there was also a great deal of extension in that reach, which limited sinuosity loss.

Channel characteristics did not exert much control on sinuosity change, but lateral migration and sinuosity change did appear connected. Tributary junctions and bedrock dominance did little to influence sinuosity changes, either. Some boxes with large decreases in sinuosity (Figure 5) were located in bedrock-influenced subreaches (e.g. Reach 4 – boxes 56 and 57), while others were in semialluvial subreaches (e.g. Reach 6 – boxes 100 and 101) or alluvial subreaches (e.g. Reach 6 – box 114; see the channel type reference map: Figure 4). Boxes where extreme channel migration occurred tended to see greater drops in sinuosity (e.g. Reach 1 – box 2, Reach 2 – box 19, Reach 6 – box 100, or Reach 7 – box 126 in Figure 5), which reflected the dominance of straightening and avulsions among the lateral movement classifications.

Figure 8. Two types of lateral movement with different impacts on sinuosity in the 2020 flood (shown on 2017 imagery) in Reach 9 – boxes 150 through 154. The slight extension in box 150 had much less of an impact on channel sinuosity than the straightening in boxes 153 and 154, despite both types of lateral movement being responsible for a similar distance of shifting (Table 6).

2.3 Bar Area Change

Bar area more than tripled after the 2020 flood (Table 5). While there were 5 boxes without any bars in 2017 (marked by gray fill in Figure 5, excluded from the analysis of bar accretion), all boxes in 2020 had either in-channel or latitudinal bars. There was a subtle trend of bar area change decreasing further downstream. However, the trend was discontinuous, because it was interrupted at Reaches 2, 5 and 9, where bar area increased more than the previous reach. The two reaches with the fewest bars in 2017 (Reaches 2 and 5; Table 3), excluding Reach 8, saw the largest increases in bar area. Bar accretion was most extreme in Reach 5, where several boxes' bar area increased by more than 1,500% (boxes 79, 81, and 85; Figure 5). In contrast, Reach 8 bar area increased much less and even decreased by as much as 61% in box 141.

Bar area increased less where bedrock was prevalent and the channel was steeper. Reach 8 had some bedrock in all boxes and was also the steepest reach. The bedrock likely limited sediment input from within the reach, while the steeper slope facilitated transport of sediment through the reach without being deposited in bars there. Almost all of the boxes where bar area

increased by over 800% had no bedrock visible on the imagery in 2020 or 2017 (though some fell within bedrock subreaches), and bar area increased the least, on average, in bedrock subreaches (Table 5). However, semialluvial subreaches had only a slightly greater increase in bar area than bedrock subreaches. The only two subreaches where bar area increased more than 1,000%, Reach 5 – subreaches 24 (boxes 79 through 81) and 26 (boxes 85 through 88), were an alluvial and semialluvial subreach, respectively (Figure 5, see the channel type reference map: Figure 4).

Tributary junctions were also very important in determining patterns of bar accretion. Tributaries were likely major sources of sediment during the 2020 flood, a necessary component of bar building, and may have contributed to the extreme levels of bar formation seen in and around those junctions, particularly in Reach 5. Both Coonskin and Moonshine Creek joined the Umatilla in Reach 5, providing ample sediment supply (E and F in Figure 5). Other tributary junctions also appeared to have an outsized effect on bar accretion, as was seen at Reach 3 – box 49, where bar area increased 1,438% only a few boxes downstream of both the Buckaroo and Thorn Hollow Creek junctions (C and D in Figure 5).

Higher slopes negatively influenced bar building. For example, in Reach 3 – subreaches 13 and 14, Buckaroo and Thorn Hollow Creeks, respectively, join the Umatilla River. These were likely large sources of sediment during the floods, and so, would be expected to have undergone much more bar accretion, like the peaks seen in Reach 5 – subreaches 24 and 26 (Figure 9). However, the higher slope in those subreaches may have limited deposition and bar formation, instead transporting sediment downstream to less steep areas (like subreach 15). This may also account for the less active bar building in Reach 1 and upstream parts of Reach 2, two of the steepest reaches in the study site (Figure 5, Table 3).

2.4 Vegetation Loss

All vegetation in and around the active channel decreased from 2017 to 2020, and bare, unvegetated surfaces increased by 78%. There were several instances of sizeable tree removal that occurred at the downstream, outside end of meanders (Figure 10). Both grass loss and tree loss seemed to be greater where sinuosity was highest. Unlike the geomorphic changes, changes in vegetation cover did not seem to be related to either tributary junctions or bedrock influence.

Non-woody vegetation was more-easily stripped from surfaces. Grass and scrub lost nearly half their surface area to vegetation removal, and mixed grasses and trees lost just over 40% of their surface area (Table 7). Because the herbaceous vegetation was so easily stripped, surfaces

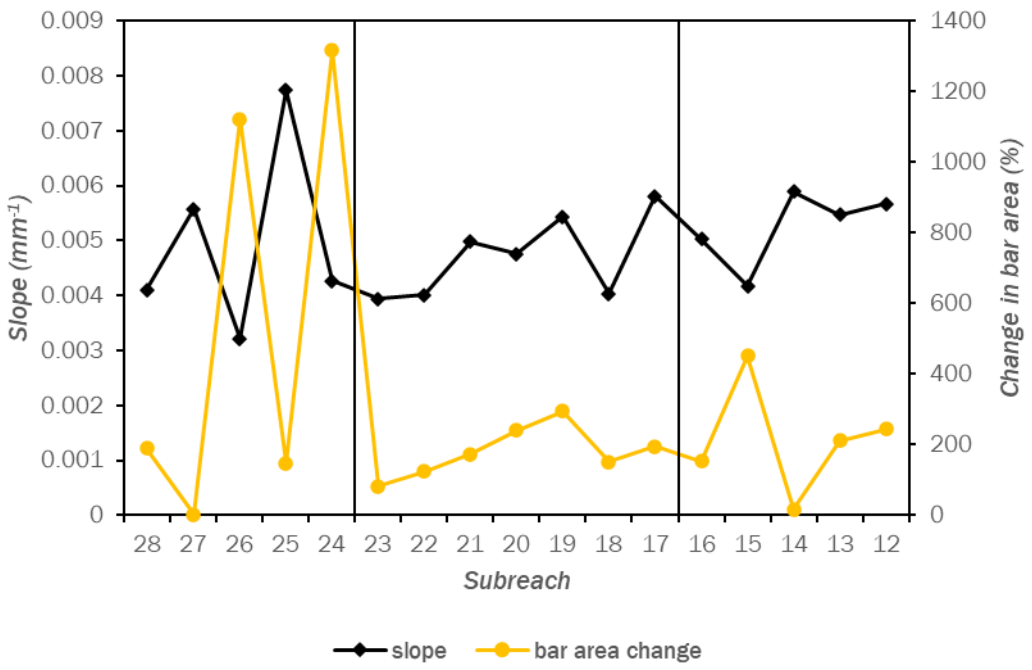

Figure 9. Subreach-average slope and bar area change in Reaches 3, 4, and 5 where steep sloped limited bar accretion near some tributary junctions in the 2020 flood. The vertical black lines show reach boundaries. Tributaries join the Umatilla in subreaches 13, 14, 24, and 26.

categorized as grass in 2017 accounted for just under a quarter of the bare surface area mapped in 2020 (Table 8). However, water was the most common 2017 surface cover type to be converted to bare surface by 2020 (Table 8), mostly due to shifts in channel location, which underscored the extent of the lateral activity during the flood. Though trees covered a similar proportion of the area around the channel as grass before the flood, only about 29% were lost (Table 7), and only 13% of bare surface area in 2020 had been tree cover in 2017 (Table 8).

However, both grass and trees lost around 20% of their pre-flood area to erosion by the wetted channel (Table 7). This was expected, because surfaces that are dry during low flow likely experience less shear stress, even when covered by flood waters, while the thalweg and main channel would have the greatest stream power, so the increased rooting depth of trees would not have been sufficient to prevent their removal.

Unsurprisingly, grass was the vegetation type that saw the greatest decline in abundance overall (-57%), though mixed grasses and trees declined by nearly as much (-54%), and trees were the vegetation type most resistant to change (-44%). As a result, trees, which were the dominant vegetation type in only four reaches before the flood, were the most common vegetation in six out of nine reaches after.

Table 7. Fate of each surface cover type from 2017. The percentage here indicates the ratio of each surface cover type in 2017 (on the left) that was later classified as each surface cover type in 2020 (along the top), where darker fill colors correspond to greater proportions. The diagonal line of boxes with a thick black outline indicates the percentage of each surface cover type that did not change between 2017 and 2020. The total area of each surface cover type in 2017 is listed on the right side of the table. For example, 47% of the 665,865 m² classified as grass and scrub in 2017 was removed between 2017 and 2020, and so was classified as bare in 2020.

		2020						
		Water	*Bare*	*Grass and scrub*	*Mixed grasses and trees*	*Trees*	*Developed*	*2017 area (m²)*
2017	*Water*	48%	49%	3%	0%	0%	0%	770,300
	Bare	23%	72%	5%	0%	0%	0%	775,137
	Grass and scrub	19%	47%	29%	1%	4%	0%	665,865
	Mixed grasses and trees	18%	41%	24%	6%	12%	0%	32,213
	Trees	20%	29%	8%	1%	43%	0%	636,168
	Developed	39%	38%	5%	0%	0%	17%	6,865

Table 8. Source of each surface cover type in 2020. The percentage here indicates the ratio of each surface cover type in 2020 (along the top row) that was initially classified as each surface cover type in 2017 (on the left), where darker fill colors correspond to greater proportions. The diagonal line of boxes with a thick black outline indicates the percentage of each surface cover type that did not change between 2017 and 2020. The total area of each surface cover type in 2020 is listed at the bottom of the table. For example, 26% of the 1,446,697 m² of bare surface classified in 2020 had been previously classified as water in 2017.

		2020					
		Water	*Bare*	*Grass and scrub*	*Mixed grasses and trees*	*Trees*	*Developed*
2017	*Water*	46%	26%	7%	14%	0%	17%
	Bare	22%	38%	13%	0%	0%	1%
	Grass and scrub	16%	22%	62%	45%	8%	13%
	Mixed grasses and trees	1%	1%	2%	12%	1%	0%
	Trees	15%	13%	16%	29%	91%	8%
	Developed	0%	0%	0%	0%	0%	62%
	2020 area (m²)	806,402	1,446,697	314,866	15,556	301,100	1,926

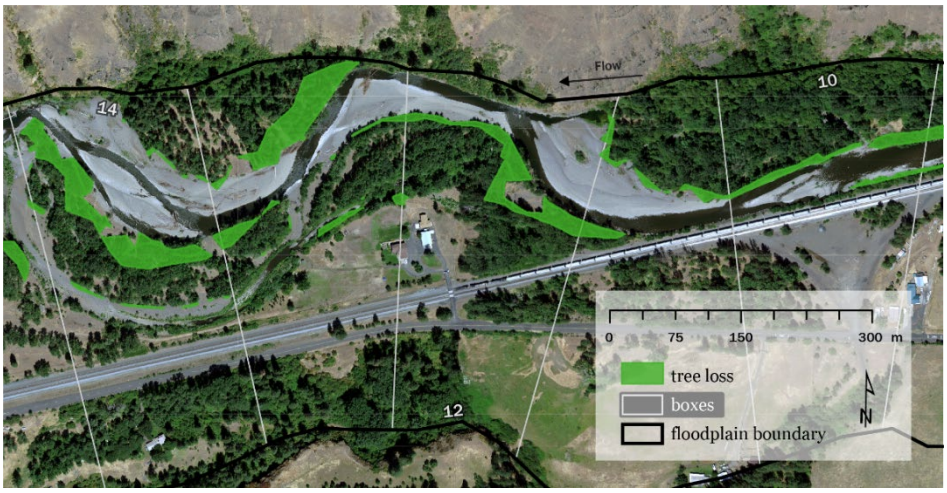

Figure 10. Removal of trees in the 2020 flood (shown on 2017 imagery) in Reach 1 – boxes 10 through 14. In the more sinuous section (boxes 11 through 14), flood waters removed larger portions of the tree cover in and around the active channel than in the straighter area upstream (box 10), particularly at the downstream end of several meander bends.

3. Causal Relationships

Question 2 – *What role did surface cover type, active channel width, channel slope, channel confinement, or sinuosity before the flood play in changes to active channel width, bar formation, lateral movement, sinuosity, and vegetation cover?*

a. Hypothesis 1 – *Increases in channel width are likely to be related to high sinuosity, low confinement, low active channel widths, and greater proportion of grass surface cover.*
b. Hypothesis 2 – *Lateral activity is likely to be related to increased sinuosity, low confinement, high active channel widths, and greater proportion of grass cover*
c. Hypothesis 3 – *Increases in bar area are likely to be related to low slopes and a greater proportion of grass cover.*
d. Hypothesis 4 – *Greater losses of grass and trees are likely to be related to high sinuosity, high confinement, and lower proportion of bare surface cover.*
e. Hypothesis 5 – *Increases in sinuosity are likely to be related to low sinuosity and high slopes.*

To address the second research question, I analyzed the results of simple regression analysis for each response variable at the reach (Table 9) and subreach levels (Table 10). I described the direction and significance of the relationships between the response variable and control variables as well as any differences that arose from channel type at the subreach level. Bar and

line charts were used to illustrate significant relationships at the reach level. I also created scatter plots to demonstrate significant relationship between vegetation cover and the response variables at the box level as well as the results of the box-level regression analysis, which was performed for all 156 boxes together and separately for each reach's boxes (12 to 24 boxes depending on the reach).

I posited possible explanations for some of the relationships, though a more detailed summary of the relationships and their implications is provided in the Discussion. Furthermore, the results of this analysis were compared with the observations from the 1996-7 floods in 4. Historical Comparison.

Generally, correlations found in this analysis were not very strong, and very few relationships proved significant. This may be due to both the complex nature of these relationships as well as limited variability in some control variables (as discussed in the Methods; Table 3). However, those relationships which are significant as well as the direction of the relationships both significant and insignificant provide insight into how these variables interact and influence change. At both the reach (Table 9) and subreach level (Table 10), the only control variables to exert significant control of any of the response variables were grass and scrub area, sinuosity, and active channel width.

3.1 Channel Width Change

At the reach level, change in active channel width had a positive, significant relationship with SI, channel width, and grass cover (Table 9, Figure 11). Although not significant, tree cover, bare cover, and CI all had a positive relationship with this response variable, while slope had a negative relationship with it.

However, at the subreach level, the only significant relationship between change in active channel width and the control variables was with grass cover (Table 10). As was seen at the reach level, tree cover, SI, and CI had positive relationships with this response variable, while slope had a negative relationship with it. Despite the positive relationship between change in active channel width and active channel width at the reach level, at the subreach level, that relationship was negative.

When regression analysis was performed on each grouping of subreach channel type separately, only semialluvial channels exhibited a significant relationship between change in active channel width and grass cover ($R^2 = 0.31$, p-value = 0.01). Although they did not demonstrate the same correlation between channel width change and grass cover, bedrock

Table 9. Reach-average regression analysis results for the 2020 flood. Possible control variables are on the vertical axis, and response variables are at the top on the horizontal axis (morphological changes to the left and vegetative changes to the right). Significant relationships are in bold and negative relationships are in italics. Reach 8 was excluded from the analysis of CI because it has been channelized, so the CI value does not accurately reflect confinement of the channel.

	Active channel width change		*Bar area change*		*Lateral migration*		*Sinuosity change*		*Loss of grass cover*		*Loss of tree cover*	
Control variables	R^2	p-value	R^2	p-value	R^2	p-value	R^2	p-value	R^2	p-value	R^2	p-value
	n = 9								*n = 9*			
Bare (%)	0.14	0.33	*0.39*	*0.07*	0.11	0.39	*0.08*	*0.46*	0.08	0.47	0.02	0.71
Grasses and scrub (%)	**0.45**	**0.05**	0.27	0.16	**0.45**	**0.05**	*0.16*	*0.29*	0.40	0.07	0.01	0.80
Tree (%)	0.13	0.35	*0.04*	*0.63*	0.12	0.36	0.00	0.95	0.01	0.78	0.31	0.12
Active channel width (m)	**0.93**	**<0.001**	*0.00*	*0.93*	**0.93**	**<0.001**	*0.17*	*0.27*	0.20	0.23	0.04	0.60
Sinuosity Index (SI)	**0.62**	**0.01**	0.03	0.65	**0.50**	**0.03**	*0.06*	*0.54*	**0.65**	**0.01**	0.40	0.07
Slope (mm^{-1})	*0.1*	*0.41*	*0.26*	*0.16*	*0.10*	*0.41*	0.06	0.53	*0.22*	*0.20*	0.00	0.90
	n = 8								n = 8			
Confinement Index (CI)	0.02	0.74	*0.1*	*0.45*	0.01	0.81	*0.07*	*0.54*	0.43	0.08	*0.00*	*0.95*

Table 10. Subreach-average regression analysis results for the 2020 flood. Possible control variables are on the vertical axis, and response variables are at the top on the horizontal axis (morphological changes to the left and vegetative changes to the right). Significant relationships are in bold and negative relationships are in italics. Subreaches from Reach 8 were excluded from the analysis of CI because that reach has been channelized, so the CI value does not accurately reflect confinement of the channel.

	Active channel width change		*Bar area change*		*Lateral migration*		*Sinuosity change*		*Loss of grass cover*		*Loss of tree cover*	
Control variables	R^2	p-value	R^2	p-value	R^2	p-value	R^2	p-value	R^2	p-value	R^2	p-value
	n = 46								*n = 46*			
Bare (%)	*0.04*	*0.21*	*0.03*	*0.22*	0.04	0.19	*0.06*	*0.09*	0.05	0.14	0.02	0.34
Grasses and scrub (%)	**0.19**	**0.002**	**0.11**	**0.02**	**0.19**	**0.002**	*0.00*	*0.99*	**0.16**	**0.01**	*0.01*	*0.56*
Tree (%)	0.07	0.09	*0.03*	*0.29*	0.07	0.08	*0.00*	*0.97*	0.01	0.65	0.03	0.30
Active channel width (m)	*0.01*	*0.56*	0.00	0.80	**0.32**	**<0.001**	*0.01*	*0.44*	0.03	0.22	*0.06*	*0.11*
Sinuosity Index (SI)	0.06	0.11	*0.00*	*0.85*	**0.12**	**0.02**	*0.07*	*0.07*	0.04	0.19	0.07	0.08
Slope (mm^{-1})	*0.01*	*0.58*	*0.06*	*0.09*	0.01	0.53	*0.01*	*0.56*	*0.06*	*0.11*	*0.00*	*0.75*
	n = 43								*n = 43*			
Confinement Index (CI)	0.05	0.15	*0.03*	*0.26*	*0.01*	*0.54*	0.03	0.60	0.01	0.53	0.01	0.55

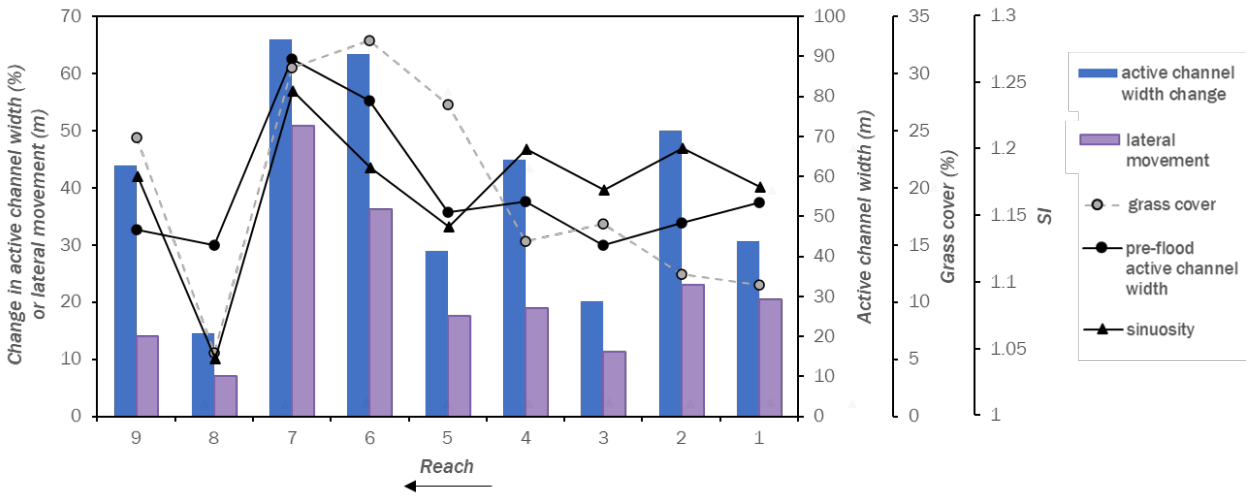

Figure 11. Bar and line graph of reach-average change in active channel width, lateral movement, active channel width, grass cover, and SI for the 2020 flood. Response variables are colored bars with their vertical axis on the left, while control variables are lines with their vertical axis on the right.

subreaches did show a positive and significant correlation between tree cover and change in active channel width (R^2 = 0.38, p-value = 0.01). In both cases, the significant relationship between vegetation cover and channel width change was positive. No other channel-type had significant relationships between change in active channel width and the control variables.

Box level analysis showed a significant relationship between all vegetation cover types and change in active channel width (Figure 12, Figure 13, Figure 14), though, as was seen at the subreach level, only grass and tree cover were positively correlated with change in active channel width. Bare cover had a negative relationship with this variable at the box level.

3.2 Lateral Movement

Like change in active channel width, grass cover, SI, and active channel width were the only control variables with significant relationships with lateral movement, all of which were positive relationships (Table 9, Figure 11). Similarly, bare cover, tree cover, and CI all had positive relationships with lateral movement distance, while slope had a negative relationship with this variable, and none of those relationships were significant.

At the subreach level, those same three control variables (grass cover, SI, and active channel width) still exhibited significant and positive relationships with lateral movement (Table 10). Bare and tree cover both maintain a positive relationship with lateral movement at the subreach

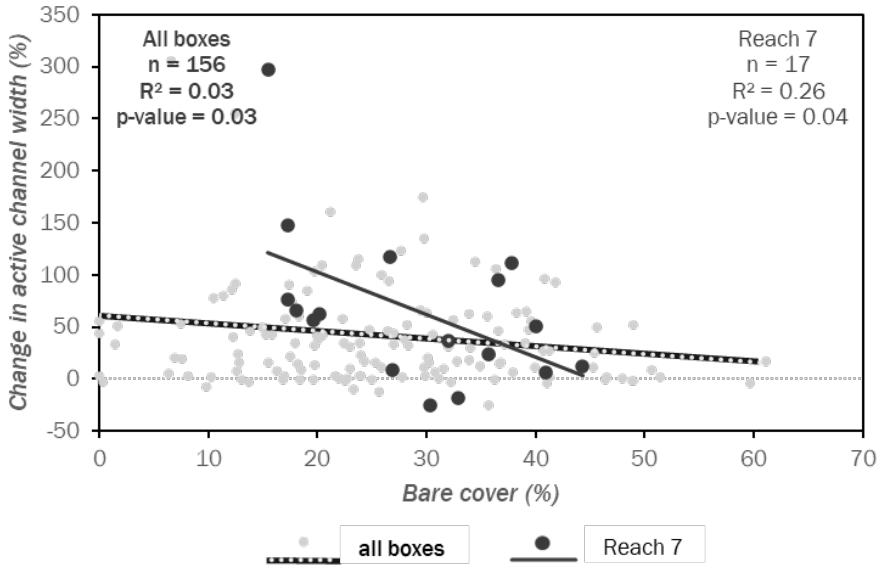

Figure 12. Scatter plot of box-level data showing the negative relationship between bare cover and change in active channel width. The R^2 and p-value of the regression of all 156 boxes is in the top left corner. On the right is the R^2 and p-value of the regression of the boxes in Reach 7, the only reach where the relationship between these variables was significant at the box-level.

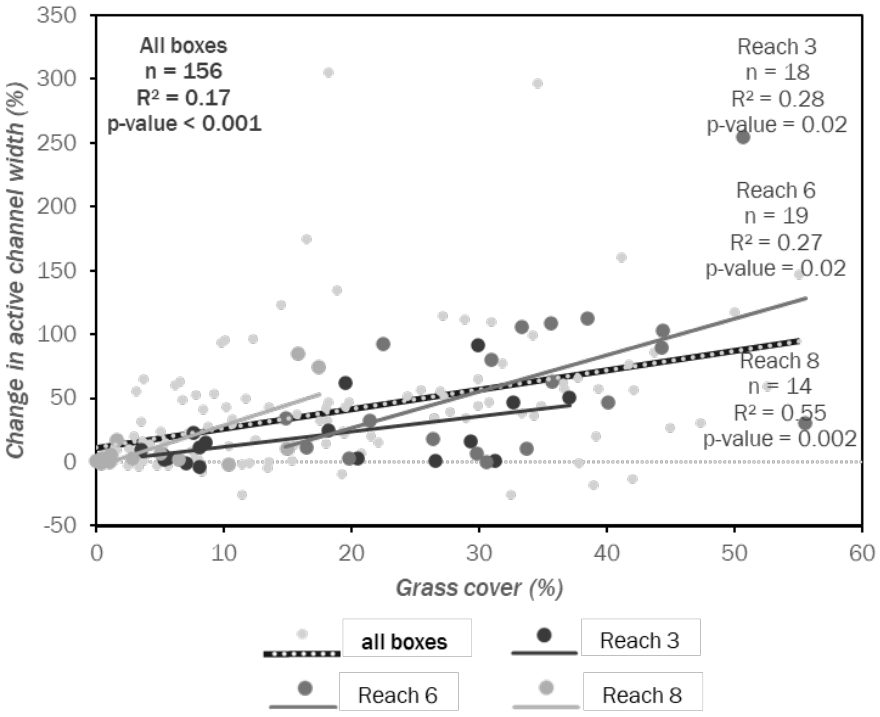

Figure 13. Scatter plot of box-level data showing the positive relationship between grass cover and change in active channel width. The R^2 and p-value of the regression of all 156 boxes is in the top left corner. On the right are the R^2 and p-values of the regression of the boxes in Reaches 3, 6, and 7, the only reaches where the relationship between these variables was significant at the box-level.

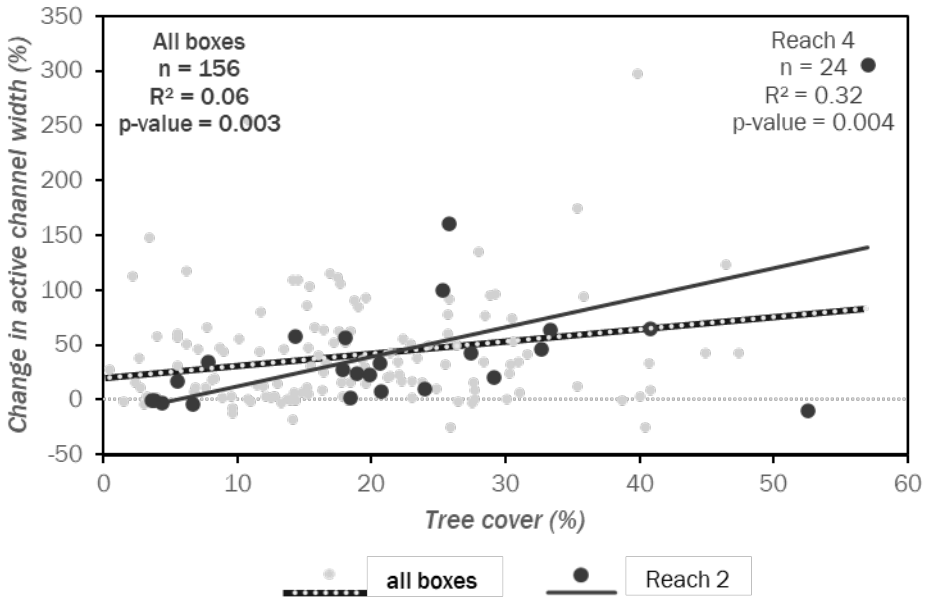

Figure 14. Scatter plot of box-level data showing the positive relationship between tree cover and change in active channel width. The R^2 and p-value of the regression of all 156 boxes is in the top left corner. On the right is the R^2 and p-value of the regression of the boxes in Reach 4, the only reach where the relationship between these variables was significant at the box-level.

level, but slope had a positive relationship with lateral movement and CI had a negative relationship with lateral movement, in contrast to those two relationships at the reach level.

Channel type regression analysis showed that these relationships were only significant for semialluvial subreaches (grass cover $R^2 = 0.38$, p-value = 0.005; SI $R^2 = 0.22$, p-value = 0.05; active channel width $R^2 = 0.43$, p-value = 0.002). Bedrock subreaches exhibited a significant, positive relationship between tree cover and lateral movement, as well ($R^2 = 0.66$, p-value < 0.001). In bedrock subreaches, because slopes were generally steeper (Table 3), tree cover likely played a more important role in lowering velocity and, therefore, increasing deposition. Downed trees may have also created logjams or otherwise increased the density of woody debris, which could help block and aggrade the channel and force it to shift position or avulse. No other channel-type had significant relationships between lateral movement and the control variables.

Lateral movement was significantly and positively correlated with both grass and tree cover at the box level (Figure 15, Figure 16). Bare cover, although not significantly correlated with lateral movement, did have a positive relationship with this response variable, as it did at the subreach and reach levels.

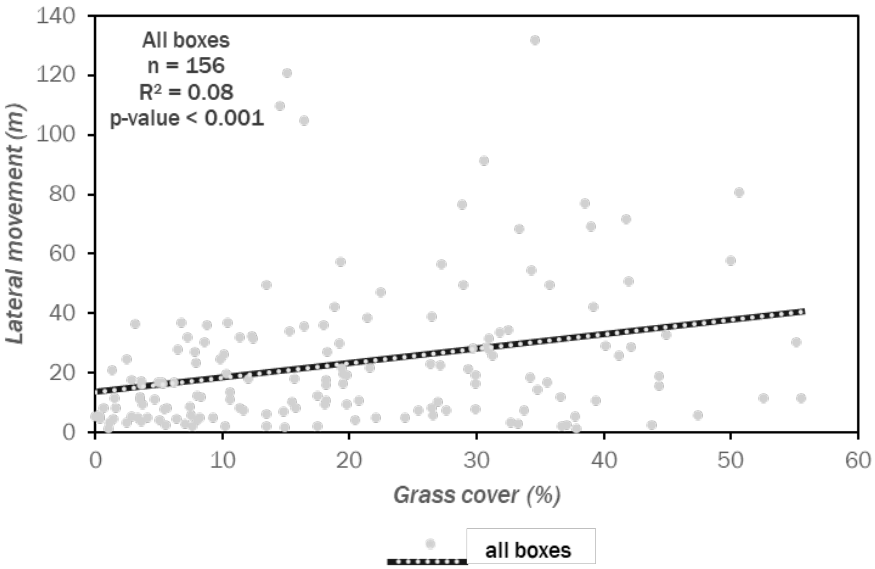

Figure 15. Scatter plot of box-level data showing the positive relationship between grass cover and lateral movement. The R^2 and p-value of the regression of all 156 boxes is in the top left corner. No single reach exhibited a significant relationship between these variables at this level of analysis.

3.2.1 Sinuosity Change

Change in sinuosity did not have a significant relationship with any of the control variables at reach, subreach, or box level (Table 9, Table 10). At the reach level, bare cover, grass cover, SI, CI, and active channel width all had negative relationships with change in sinuosity, while tree cover and slope had positive relationships with change in sinuosity. The relationships at the subreach level were much the same, although the direction of the relationship between tree cover and change in sinuosity was negative. Channel type did not affect the significance of any relationships between change in sinuosity and the control variables. Box level analysis exhibited another shift in the direction of these relationships. Bare cover and tree cover both had a negative relationship with change in sinuosity, while grass cover had a positive relationship with it.

3.3 Bar Area Change

At the reach level, none of the control variables had significant relationships with change in bar area (Table 9). Both grass cover and SI had positive relationships with this variable, while bare cover, tree cover, slope, CI, and channel width all had negative relationships with it.

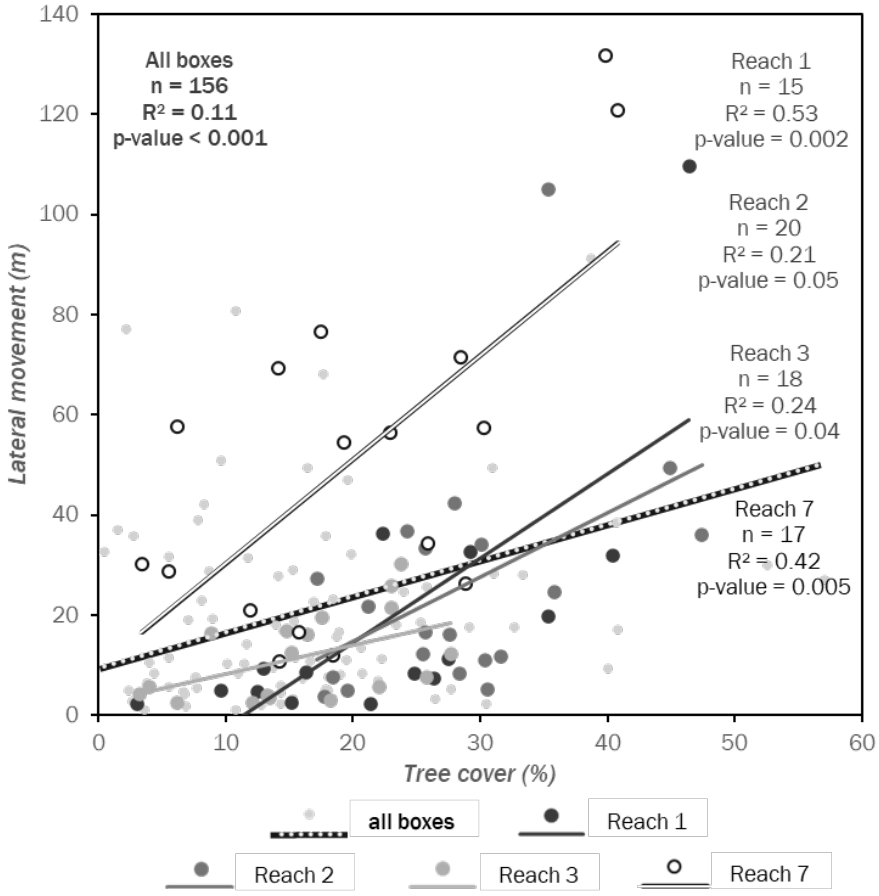

Figure 16. Scatter plot of box-level data showing the positive relationship between tree cover and lateral movement. The R^2 and p-value of the regression of all 156 boxes is in the top left corner. On the right are the R^2 and p-values of the regression of the boxes in Reaches 1, 2, 3, and 7, the only reaches where the relationship between these variables was significant at the box-level.

Subreach-level analysis showed that grass cover was significantly positively correlated with change in bar area (Table 10). As was shown by reach level analysis, bare cover, tree cover, slope, and CI all had negative relationships with change in bar area at this level. However, sinuosity had a negative relationship with this variable at the subreach level and channel width had a positive relationship with it, both the opposite of those relationships at the reach level.

For semialluvial subreaches, both bare cover and slope were significantly negatively correlated with change in bar area (bare cover $R^2 = 0.22$, p-value = 0.04; slope $R^2 = 0.25$, p-value = 0.03). No other channel-types had significant relationships between change in bar area and the control variables. Regression analysis of all boxes showed both bare cover and grass cover had a significant relationship with change in bar area, although the relationship with bare

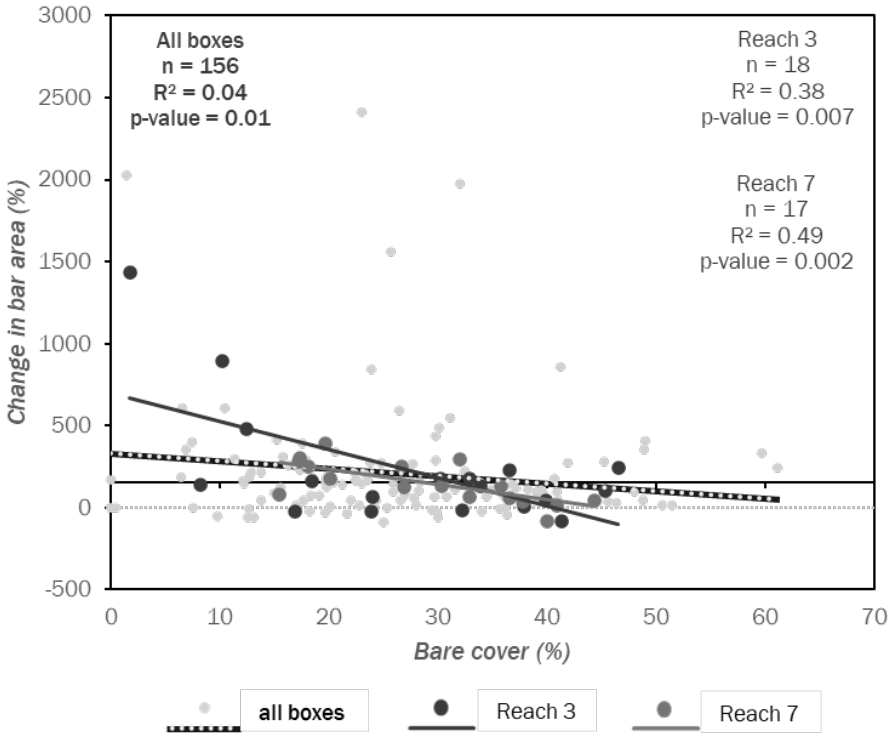

Figure 17. Scatter plot of box-level data showing the negative relationship between bare cover and change in bar area. The R^2 and p-value of the simple regression of all 156 boxes is in the top left corner. On the right are the R^2 and p-values of the regression of the boxes in Reaches 3 and 7, the only two reaches where the relationship between these variables was significant at the box-level.

cover was negative (Figure 17) and the relationship with grass cover was positive (Figure 18). As was seen in reach and subreach analysis, tree cover had a negative relationship with change in bar area.

3.4 Vegetation Loss

The only significant relationship between either vegetation response variable and a control variable at the reach level was between SI and grass loss, which was positively correlated (Table 9, Figure 19). Grass loss had a positive relationship with every other control variable except for slope. Tree loss, similarly, had a positive relationship with every control variable except for one at the reach level, which was CI.

Subreach-level analysis showed, again, only one significant relationship between either vegetative response variable and any of the control variables, which was grass cover's significant positive relationship with grass loss (Table 10). As it did at the reach level, grass loss had a

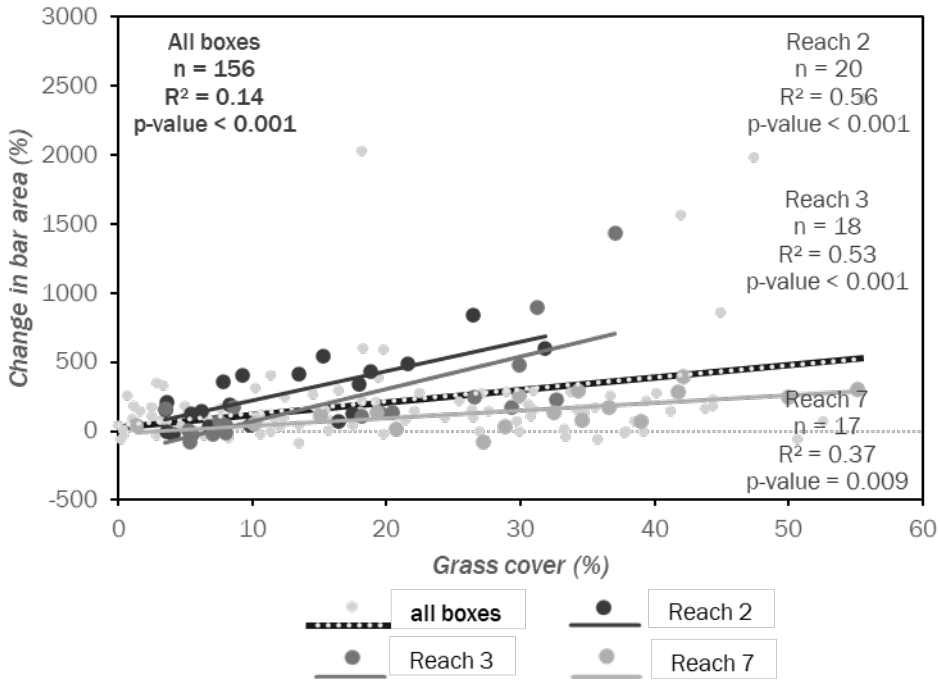

Figure 18. Scatter plot of box-level data showing the positive relationship between grass cover and change in bar area. The R^2 and p-value of the regression of all 156 boxes is in the top left corner. On the right are the R^2 and p-values of the regression of the boxes in Reaches 2, 3, and 7, the only reaches where the relationship between these variables was significant at the box-level.

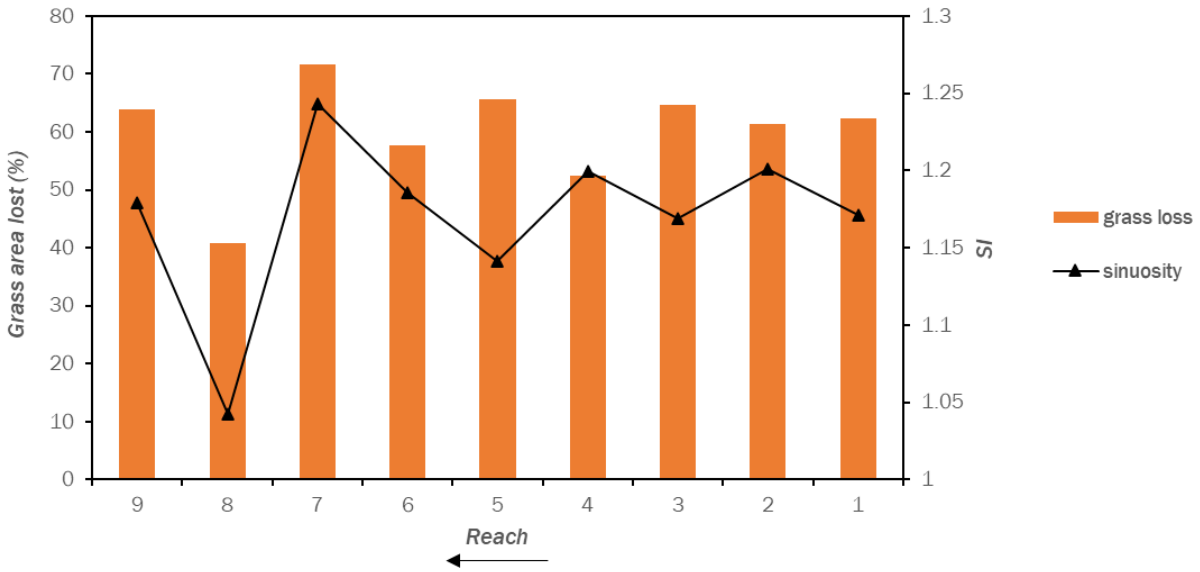

Figure 19. Bar and line graph of reach-average grass loss and SI. The response variable (grass loss) has its vertical axis on the left, while the control variable (sinuosity) has its vertical axis on the right.

positive relationship with all other variables except for slope. Tree loss had a negative relationship with slope, as well, but it also had a negative relationship with grass cover and active channel width, both of which were positive relationships at the reach level. The relationship between CI and tree loss, which was negative at the reach level, was positive at this level. Bare cover, tree cover, and SI similarly had positive relationships with tree loss.

When subreaches were analyzed by separate channel type, semialluvial channels were the only type to demonstrate a significant relationship between grass cover and grass loss (R^2 = 0.23, p-value = 0.04). Semialluvial subreaches also exhibited a significant relationship between SI and grass loss (R^2 = 0.34, p-value = 0.008). Additionally, in alluvial subreaches, bare cover was significantly correlated with grass loss (R^2 = 0.43, p-value = 0.02). Tree cover was significantly positively correlated with tree loss in bedrock channels (R^2 = 0.29, p-value = 0.04). These were no further significant relationships in channel-type subreach analysis.

At the box level, the only significant relationship involving the vegetative response variables was the positive relationship between grass cover and grass loss (Figure 20). All cover types had a positive relationship with grass loss, in analysis of all boxes. Bare cover and tree cover both had a positive relationship with tree loss, while grass cover had a negative relationship with that response variable.

4. Historical Comparison

Question 3 - *How do changes caused by the 2020 flood compare to changes from the 1996-7 floods?*

a. Hypothesis 1 – *Due to its greater discharge, the 2020 flood was the more geomorphically effective flood.*
b. Hypothesis 2 – *Highly geomorphically dynamic areas in 1996-7 will be similarly active in 2020.*

In this section, I compared the changes from the 1996-7 floods to those of 2020 flood (Figure 21, compare with Figure 5). Like the first two questions, I described changes for each of the response variables (change in active channel width, lateral movement, change in sinuosity, and change in bar area) separately. Reach-average change and univariate statistics were summarized in Table 5. I also performed simple regression analysis on the reach-average data for the 1996-7 flood (Table 11, compare with Table 9). For each response variable, I investigated differences in the magnitude of change and any geographical patterns in variable response and proposed

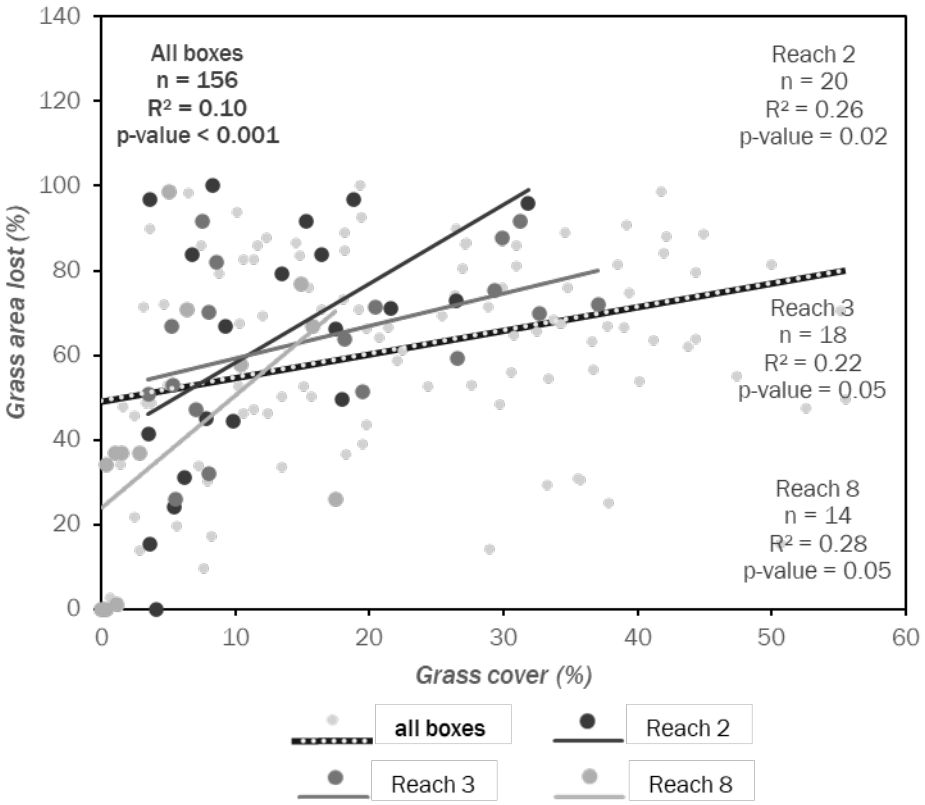

Figure 20. Scatter plot of box-level data showing the positive relationship between grass cover and grass loss. The R^2 and p-value of the regression of all 156 boxes is in the top left corner. On the right are the R^2 and p-values of the regression of the boxes in Reaches 2, 3, and -8, the only reaches where the relationship between these variables was significant at the box-level.

reasons for these patterns. I explored possible explanations for similarities and differences between the 1996-7 and 2020 floods, which are explained further in the Discussion.

The floods in February of 1996 and 2020 were often compared in the news, and both were considered catastrophic. However, peak discharge reached in the upper Umatilla River differed significantly between them. The Pendleton gage peaked at 25,000 cfs in 2020, but only around half as high in 1996 at 12,700 cfs (Figure 2, Figure 3). Like the 2020 flood, the floods in 1996 and 1997 increased channel widths and bar area and resulted in a great deal of lateral movement (Table 5, Figure 21). However, sinuosity increased, instead of decreasing as in 2020, which is unusual and more often seen in periods without major flooding.

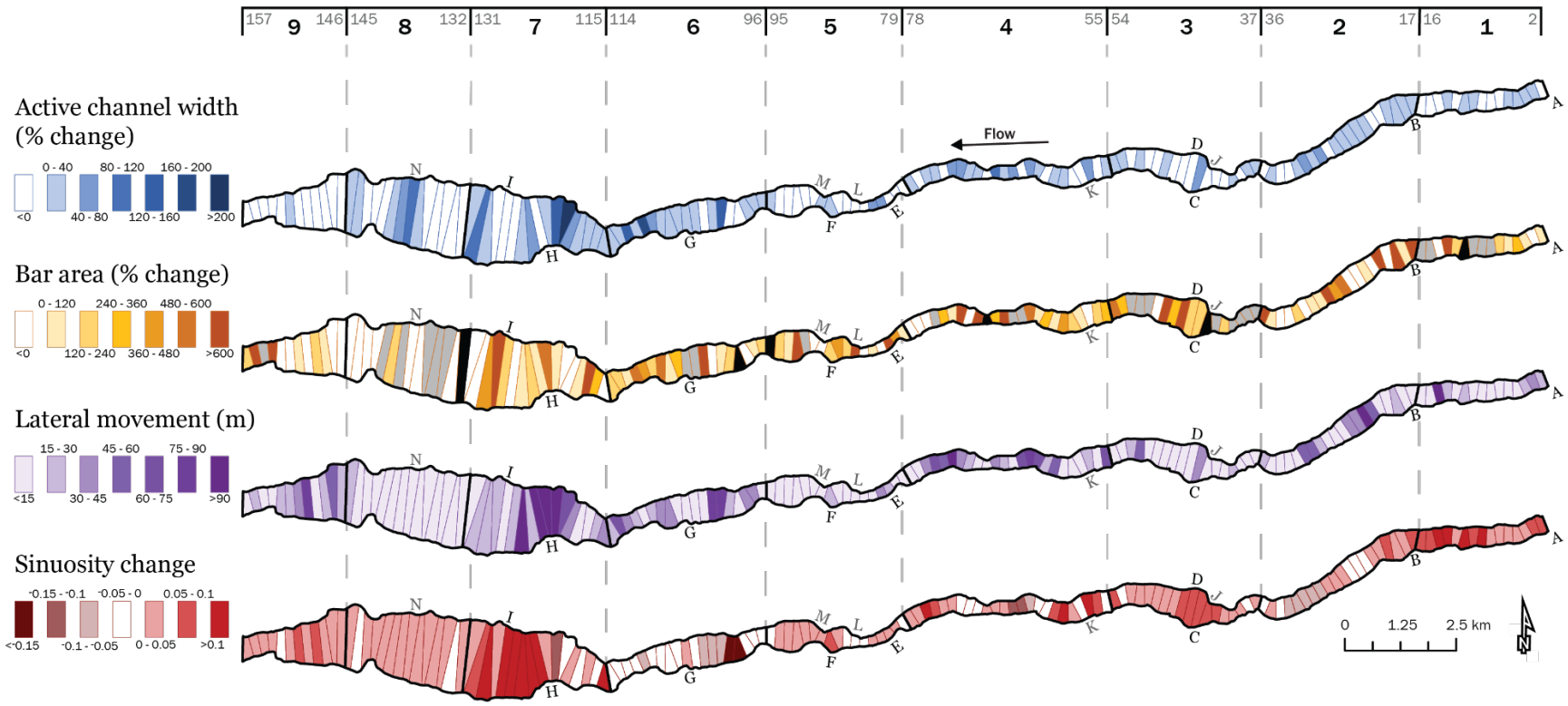

Figure 21. Response variable change map after the 1996-7 floods by box. Reaches are outlined and numbered on the top in black alongside the first and last box number of each reach in gray, and bridges and tributary junctions are indicated by the letters along the boxes. Boxes excluded from bar averages are gray (if the box did not have any bars in 1994) or black (if the bar area increased by greater than 4,000 %). Tributaries: A – Meacham Creek, B – Isqúulktpe Creek, C – Buckaroo Creek, D – Thorn Hollow Creek, E – Coonskin Creek, F – Moonshine Creek, G – Cottonwood Creek, H – Mission Creek, I – Spring Creek. Bridges: J – Thorn Hollow Road Bridge, K – unnamed railway bridge, L – N. Cayuse Road Bridge, M – unnamed railway bridge, N – S. Market Road (OR-331) Bridge). Compare with Figure 5.

Table 11. Reach-average regression analysis results for the 1996-7 floods. Possible control variables are on the vertical axis, and response variables are at the top on the horizontal axis. Significant relationships are in bold and negative relationships are in italics. Reach 8 was excluded from the analysis of CI because it has been channelized, so the CI value does not accurately reflect confinement of the channel. Compare with Table 9.

	Active channel width change		*Bar area change*		*Lateral migration*		*Sinuosity change*	
Control variables	R^2	p-value	R^2	p-value	R^2	p-value	R^2	p-value
	n = 9							
Active channel width (m)	0.09	0.43	0.20	0.23	**0.60**	**0.02**	0.08	0.46
Sinuosity Index (SI)	**0.47**	**0.04**	0.05	0.57	**0.73**	**0.003**	0.03	0.67
	n = 8							
Confinement Index (CI)	0.11	0.43	*0.25*	*0.20*	**0.53**	**0.04**	0.29	0.17

4.1 Channel Width Change

As it did in 2020, the wetted channel narrowed slightly after the 1996 flood, likely because of bed scour, which deepened the channel (Table 5). In all reaches except for Reaches 1, 2, and 4, the wetted channel narrowed slightly more in 1996-7.

Widening of the active channel from the 1996-7 floods was much less pronounced than it was in 2020, though the channel did get wider, on average, between 1994 and 1998 (Figure 21). There was less change in active channel width in all reaches in 1996-7 compared to 2020, and two reaches, Reaches 1 and 9, underwent narrowing of the active channel.

Simple regression analysis for the 1996-7 reach-average values showed that sinuosity had a significant positive relationship with change in active channel width, the same as was found in 2020 (Table 11, Figure 22). Neither CI nor active channel width were significantly correlated with change in active channel width, despite channel width having a significant relationship with active channel change in 2020. However, in 1996-7 both did have positive relationships with that response variable, as they did in 2020. The anomalous narrowing of the active channel in Reaches 1 and 9 likely affected the significance of the relationship between active channel width and active channel widening in 1996-7.

It is possible that the greater proportion of vegetated surfaces in the active channel in 1994 increased bank shear strength enough to limit erosion and widening, so that the river scoured

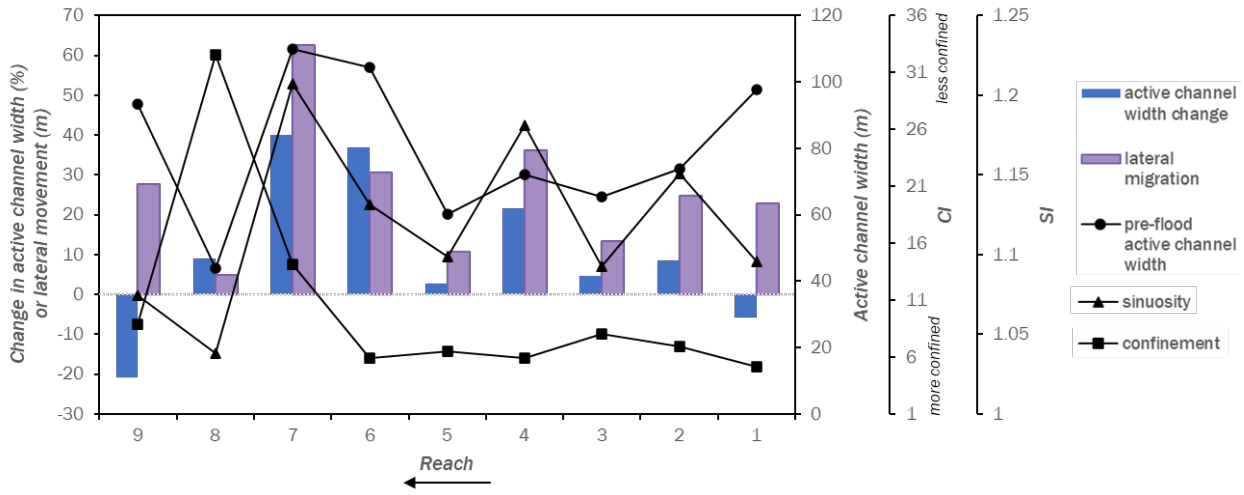

Figure 22. Bar and line graph of reach-average change in active channel width, lateral movement, active channel width, SI, and CI for the 1996-7 floods. Response variables are colored bars with their vertical axis on the left, while control variables are lines with their vertical axis on the right. Compare with Figure 11.

the channel bed instead (Table 12). The deeper channel would then need less width to accommodate low summer flows, thus the narrower wetted channel and less-extreme widening of the active channel. Also, the channel was generally less sinuous in 1994, so given the positive relationships between SI and channel widening, it makes sense that the more sinuous 2017 channel widened more during flooding (Table 3).

There were no downstream trends in active channel widening, however, reach-average channel width changes had similar relationships between reaches from upstream to downstream (i.e. Reach 2 widened more, on average, than Reach 1, Reach 3 widened less, on average, than Reach 2 etc.) to 2020, except for Reach 9 (Table 5). Lack of sinuosity and increased confinement of the channel in Reach 9 may have contributed to this difference (Table 3). Also, several secondary channels that were at least partially wetted and clearly lacking vegetation in 1994 appeared to have aggraded and been colonized by vegetation by 1998, particularly in Reach 9 – boxes 147 through 151 (Figure 23). This vegetation may have grown after the 1996-7 flood, after an influx of sediment from the flood filled the secondary channel.

Other similarities in channel widening between the floods were found in Reach 6 and 7, where several peaks in channel widening occurred in similar locations (Figure 5, Figure 21). For example, in Reach 6 – boxes 101 in 1996-7 and 102 in 2020, channel width increased 125% and 112%, respectively, (Figure 24). High sinuosity likely played a major part in the widening there both years (Table 9, Table 11). In both these boxes, sinuosity was much greater than the

Table 12. Reach-average and channel type-average percent of each active channel landform type in 1994 and 2017 (before each flood).

	Vegetated (%)		*Scoured (%)*		*Bar (%)*		*Water (%)*	
Reach	*2017*	*1994*	*2017*	*1994*	*2017*	*1994*	*2017*	*1994*
1	9	43	8	13	29	10	55	34
2	16	15	7	6	20	30	57	49
3	11	24	6	19	22	8	61	49
4	10	16	5	9	27	24	58	51
5	14	9	11	7	14	19	61	66
6	22	31	14	7	20	16	43	46
7	21	16	13	3	29	33	37	49
8	3	0	1	0	20	9	76	91
9	18	22	2	4	23	20	57	54
Channel type								
Alluvial	19	-	13	-	25	-	44	-
Semialluvial	12	-	5	-	22	-	61	-
Bedrock	12	-	8	-	22	-	57	-
Box median	6	7	0	0	20	13	56	45
Box minimum	0	0	0	0	0	0	7	7
Box maximum	68	93	67	62	59	81	100	100

average pre-flood sinuosity for their respective years. This was particularly clear in 2017-2020, where the large meander bend in boxes 100 through 103 greatly increased local sinuosity, in contrast with the straighter channel further downstream in boxes 104 through 106.

Similar areas of increased channel widening from both floods are found in Reach 7, such as boxes 120 in 1996-7 and 119 in 2020 where channel width increased 274% and 297%, respectively, and boxes 109 through 114, where the active channel widening peaked at 189% in 1996-7 and 106% in 2020 (Figure 25). Reach 7 – boxes 109 through 111, 119, and 120 had less confined channels because the valley widens, and the channel was relatively unconstrained by bedrock or valley walls. Both factors mean the channel had room to widen and that the banks were not as resistant to erosion as they were where bedrock was present. Because the active channel was slightly wider between boxes 109 and 113 in 2017, increasing confinement (lowering CI), it makes sense that there was less widening there than there was in 1996-7. The channel is wider and more constrained in boxes 106 through 108, and, therefore, there was relatively little widening. The active channel in boxes 112 through 114 was also wider than average in 2017 and very close to the median in 1994 (Table 3), but still underwent widening during both floods, so it

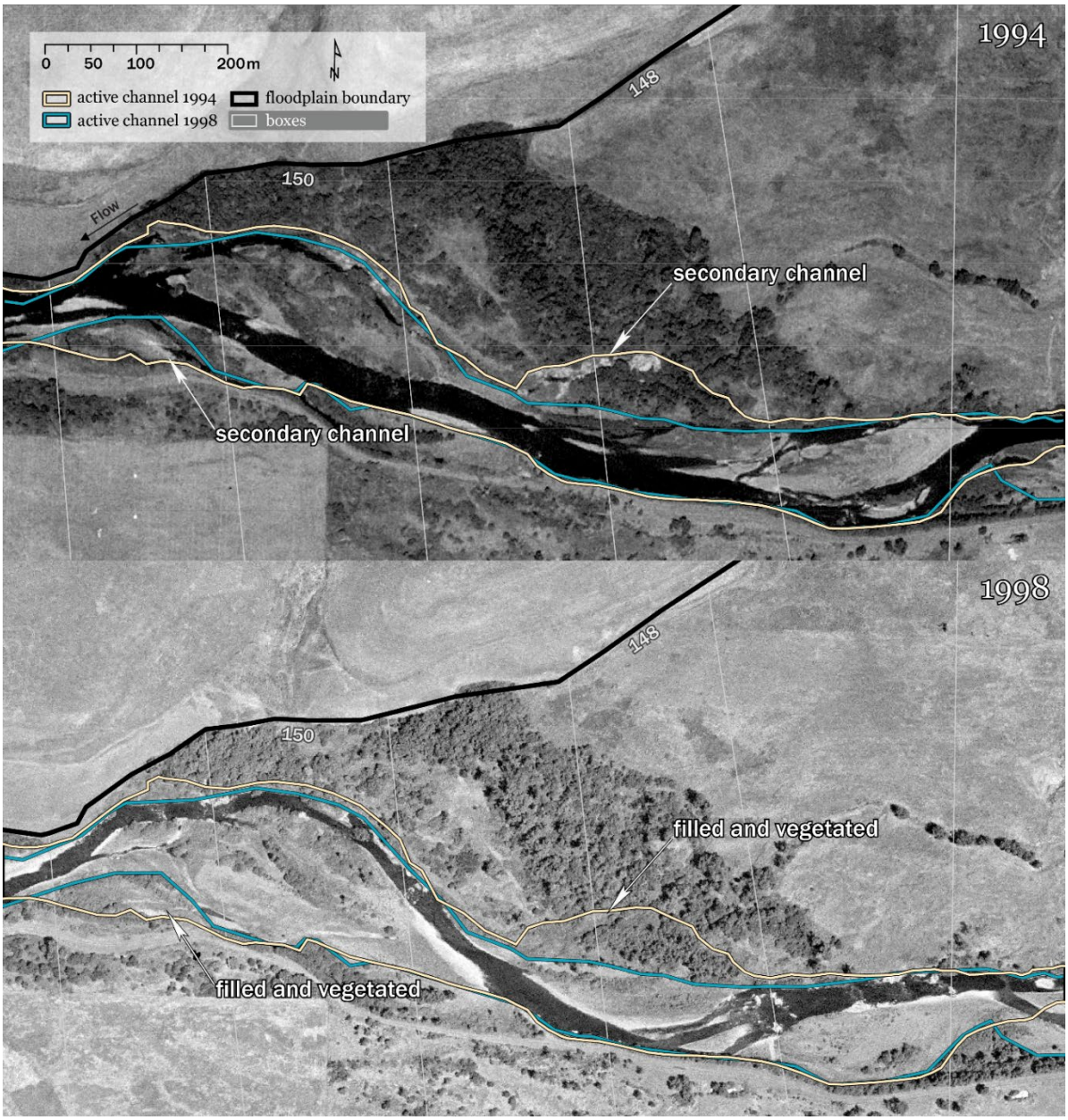

Figure 23. Active channel narrowing between 1994 and 1998 in Reach 9 – boxes 147 through 151, shown on 1994 and 1998 imagery. Side channels in boxes 148 and 151 visible on the 1994 imagery appear to have aggraded and been at least partially colonized by vegetation between 1994 and 1998. It is possible these channels aggraded during flooding with the introduction of large volumes of sediment and then grew vegetation between 1997 and 1998 before imagery was captured.

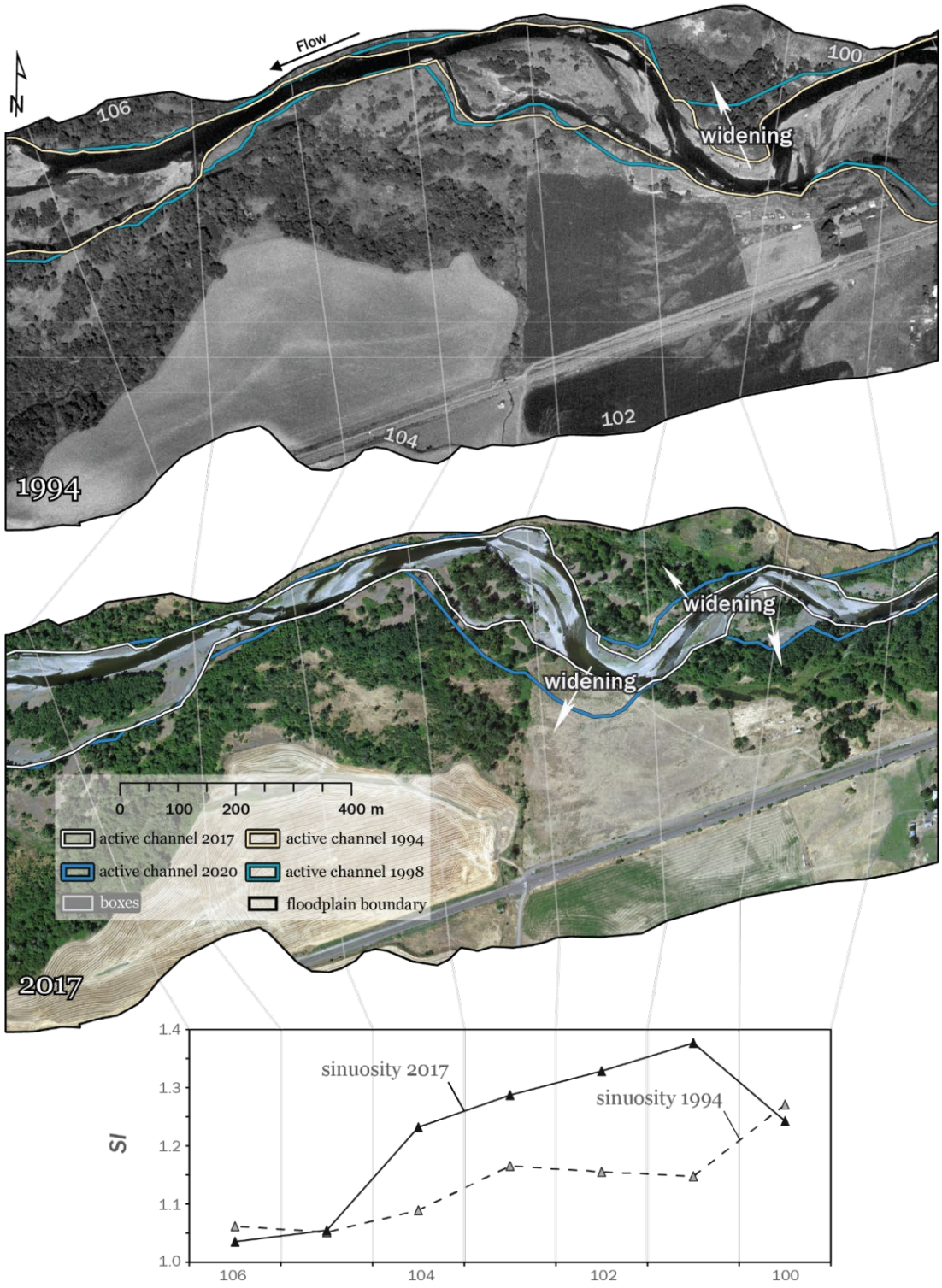

Figure 24. Active widening during the 1996-7 and 2020 floods (shown on 1994 and 2017 imagery with pre-flood sinuosity) in Reach 6 – boxes 100 through 106. Meanders in boxes 100 through 103 increased local sinuosity before the floods, which drove increased widening during the floods.

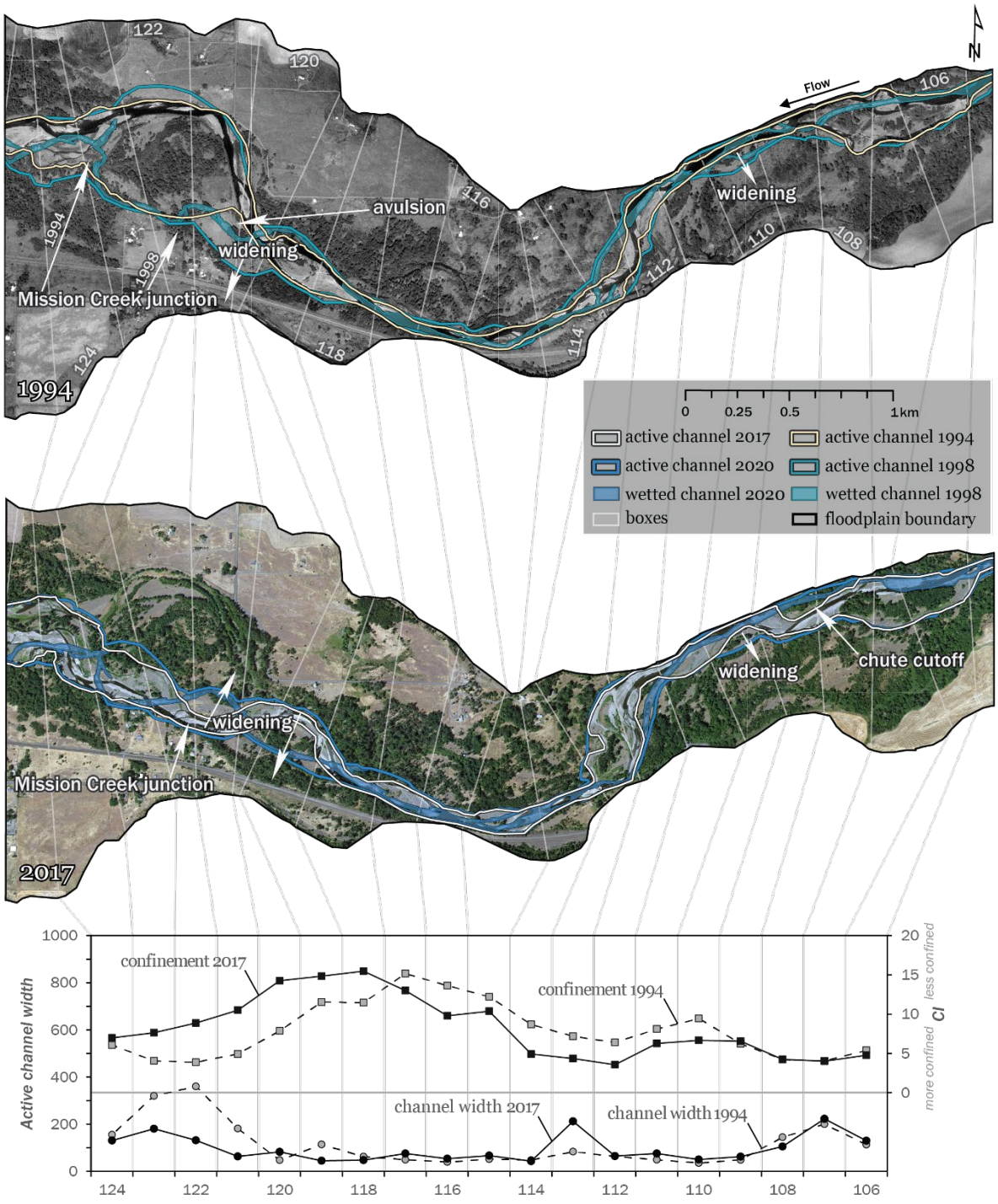

Figure 25. Active channel widening and lateral movement for the 1996-7 and 2020 floods (shown on 1994 and 2017 imagery with pre-flood confinement and channel width) in Reach 6 – boxes 106 through 114 and Reach 7 – boxes 115 through 124. A major avulsion downstream of box 120 shifted the channel during the 1996-7 floods, abandoning a major meander and capturing part of Mission Creek's channel. After this, the Mission Creek junction moved further upstream and has remained relatively stable since.

is unlikely active channel width was the main driver of the increased widening that occurred there. Above average sinuosity may better explain channel widening in those boxes.

4.2 Lateral Movement

The 1996-7 floods caused slightly less lateral movement per box than the 2020 flood, (Table 5). Regression analysis of the 1996-7 lateral movement, however, showed many similarities to the analysis of the 2020 data (Table 9, Table 11). Both SI and active channel width were positively correlated with lateral movement in 1996-7 and 2020 (Figure 11, Figure 22). CI also demonstrated a significant, positive relationship with lateral movement (lateral movement was greater where the channel was less confined) in 1996-7, a relationship which was not significant in 2020.

Although the average distance moved per box was lower in 1996-7, lateral movement varied by reach, some of which had greater lateral activity in 1996-7. The channel centerlines in Reaches 1, 2, 3, and 8 all moved similar distances in 1996-7 and 2020. Reaches 4, 7, and 9 saw larger shifts in 1996-7, while Reaches 5 and 6 saw less lateral activity. In Reaches 4 and 9, there was, on average, almost twice as much movement in 1996-7 as in 2020.

Differences in active channel width and sinuosity may have controlled where lateral activity was greatest during the two floods. The active channel was wider in 1994 than in 2017 in all reaches, which may have increased lateral movement in a few of the reaches during the earlier flood, considering the positive correlation found between active channel width and lateral movement in 1996-7 and 2020 (Table 3, Table 9, Table 11). This is can be seen in Reach 4 – boxes 62 through 64 and 73 through 76 (Figure 7, Figure 26), Reach 7 – boxes 121 through 126 (Figure 25), and in Reach 9 – boxes 149 through 154. However, sinuosity was lower in all reaches in 1994 compared to 2017 (Table 3). Because of the positive relationship between sinuosity and lateral movement, it is possible the higher sinuosity in 2017 led to greater lateral activity during the 2020 flood than the 1996-7 flood (Table 9, Table 11). Reach 5, where there was less lateral movement in the earlier flood, had a narrower active channel than almost all of the other reaches (Table 3). Perhaps sinuosity is the main driver of lateral movement in areas where the active channel is narrower.

Figure 26. (next page) Active channel widening and lateral movement (shown on 1994 and 2017 imagery with pre-flood channel width) in Reach 4 – boxes 62 through 78. Lateral activity was greatest where the active channel was widest before the flood, and because the active channel was wider before the 1996-7 floods, lateral movement was more extreme as a result of those floods.

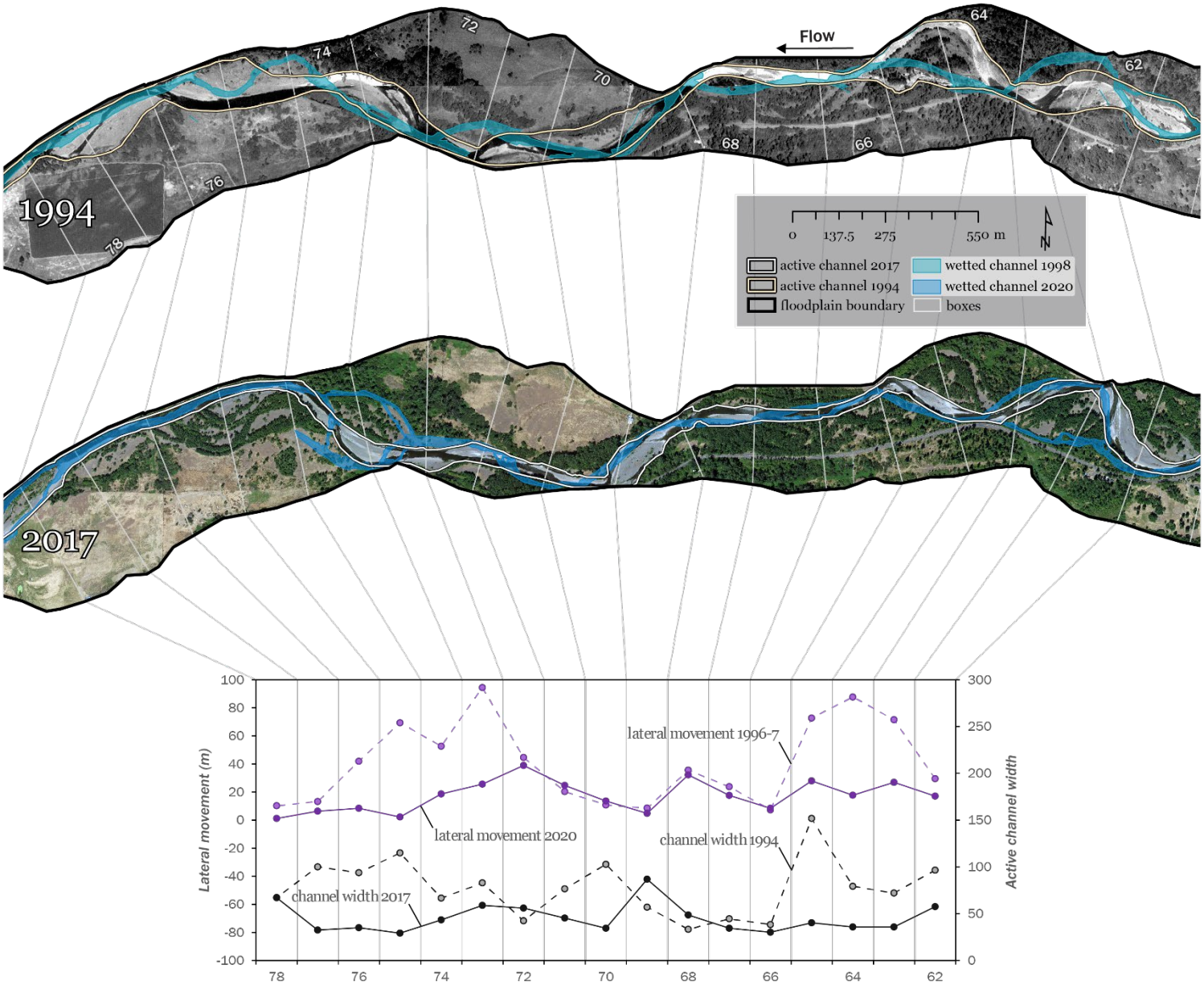
Flow
1994
2017
78
76
74
72
70
68
66
64
62
0 137.5 275 550 m
N
active channel 2017
active channel 1994
floodplain boundary
wetted channel 1998
wetted channel 2020
boxes
lateral movement 1996-7
lateral movement 2020
channel width 1994
channel width 2017
Lateral movement (m)
Active channel width
100
80
60
40
20
0
-20
-40
-60
-80
-100
300
250
200
150
100
50
0
78
76
74
72
70
68
66
64
62

Despite a similar number of occurrences of both avulsions and extensions between them, the channel centerline was moved much further in 1996-7 than in 2020 by those types of lateral movement (Table 6). However, there were far fewer instances of straightening or translation in 1996-7 and the magnitude of channel movement caused by both was much less than in 2020.

4.2.1 Sinuosity Change

After the 1996-7 floods, the channel was more sinuous than it had been in 1994. The difference in the total distance attributed to each lateral movement type reflected this increase in sinuosity (Table 5, Table 6). The greatest increases in sinuosity occurred in Reach 1, where channel extension was the major driver in lateral activity, and in Reach 7, where a major avulsion completely cut off a large meander bend but introduced several smaller meanders which increased local sinuosity (Figure 25).

None of the control variables exerted significant control on sinuosity change in either 1996-7 or 2020. However, while the control variables all had negative relationships with sinuosity change in 2020, in 1996-7, SI, CI, and active channel width all had positive relationships with sinuosity change at the reach level (Table 9, Table 11). There appeared to be very little connection between the distance the channel migrated and the change in sinuosity in 1996-7.

Reaches 2 and 6 were the only reaches where sinuosity decreased, and in Reach 6, sinuosity decreased more than it did in 2020. After Reach 7, which was consistently the most sinuous reach, both before and after the floods, Reaches 2, 4, and 6 were the next most sinuous (Table 3). Despite the positive relationship between sinuosity and sinuosity change, this higher sinuosity may have played a part in the box level loss in sinuosity in Reaches 2 and 6, and limited sinuosity increase in Reach 4, which had the second-smallest increase in sinuosity behind Reach 8 (Table 5).

One of the few areas where sinuosity was greater in 1994 than in 2017 was Reach 2 – boxes 29 through 32, and sinuosity decreased there more than any surrounding areas (Figure 27). Similarly, peaks in sinuosity in Reach 6 – boxes 100 through 102 and 112 through 114 coincide with decreases in sinuosity as a result of flooding. Reaches 2 and 6 had smaller shifts from extensions than most other reaches, including reaches in 2020 (Table 6), and Reach 6 had the largest change due to straightening seen from any of the reaches, both of which may have contributed to the decrease in sinuosity there (Table 5).

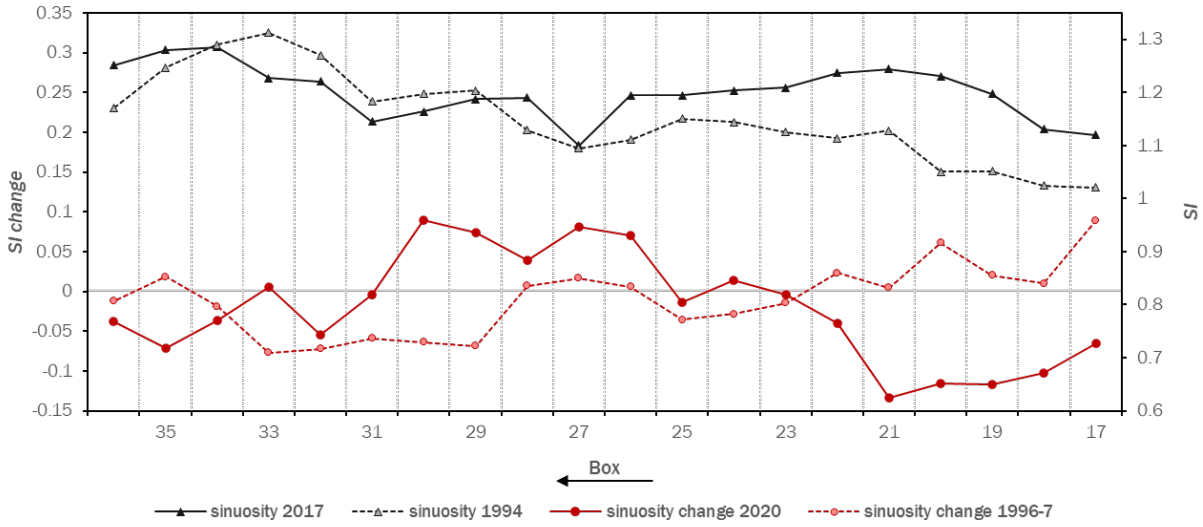

Figure 27. Comparison of pre-flood sinuosity and sinuosity change for the 1996-7 and 2020 floods in Reach 2 – boxes 17 through 36. The dark gray horizontal line indicates no change in sinuosity.

4.3 Bar Area Change

Analysis of bar accretion from 1994 to 1998 excluded boxes that had no bars in 1994 (36 in total), as was done in analysis of the more recent flood (see grayed out boxes in Figure 21). In addition, boxes with more than 4,000% change in bar area were also excluded and considered outliers, largely because the initial bar area had been extremely small (see blacked out boxes in Figure 21). Bar area change was not significantly correlated with any of the control variables in 1996-7 (Table 11). Like these relationships in 2020, SI had a positive relationship with bar accretion and CI had a negative relationship with bar accretion. In contrast to the negative relationship between these variables in 2020, active channel width had a positive relationship with bar area change in 1996-7.

As a result of the 1996-7 floods, bar area more than tripled, as was seen in 2020 (Table 5). Reach 2 was one of the two reaches that underwent the greatest increase in bar area in both 1996-7 and 2020, although in 2020 Reach 2 was second to Reach 5, while in 1996-7 it was the reach with the greatest increase in bar area. Five out of the nine reaches had larger increases in bar area after the 1996-7 floods than the 2020 flood. Reach 8 was the only reach that lost bar area after flooding, which only happened in the 1996-7 floods.

Similar to the downstream trend in bar area change in 2020, there was a general trend of bar accretion decreasing from the upstream to downstream ends of the site, except for Reach 2,

where bar formation surpassed that of Reach 1, and Reach 8, which often behaved differently because it had been channelized (Table 5). Once again, the two reaches with the least bar area before the flood, excluding Reach 8, saw some of the greatest increases in bar area. Reach 2, which had extensive bars in 1994, however, surpassed either in bar accretion.

The main difference in bar area change in 1996-7 was that there were more boxes with extreme change, and that change was larger than was seen in 2020 (Figure 5, Figure 21). Bar area was more evenly distributed in 2017, in comparison to 1994, which may explain why there was greater uniformity in bar accretion in 2020 (Table 3).

Although there were some areas that had a great deal of bar accretion after both floods (e.g. Reach 5 – boxes 81 or 85, where bar area increased over 600%), there were more boxes that differed in their level of response in bar area than there were for active channel widening or lateral migration (Figure 5, Figure 21). In Reach 2, for example, bar formation from the 1996-7 floods was greatest in boxes 17, 19, 21, and 28, where bar area increased, on average, 1876%. After the 2020 flood, in contrast, bar area in those same boxes only increased 43%. The four boxes in Reach 2 where bar accretion was greatest in 2020 were 24, 29, 31, and 35, where bar area increased an average of 619%. Meanwhile, bar area only increased 3% in those boxes from 1994 to 1998.

CHAPTER V

DISCUSSION

1. Overview

The purpose of this discussion is to explain the results of the study by drawing connections to river processes and relating the findings with similar studies and other flood effects literature. It is divided into two main sections. The first, 2. Drivers of Change, addresses the first two research questions by summarizing how causal variables were related to planimetric changes during flooding, and the second, 3. Historical Comparison, addresses the third research question by explaining similarities and differences in flood response between the 1996-7 and 2020 floods. The final section describes limitations of this study and potential future avenues for research.

2. Drivers of Change

One goal of this research was to determine what pre-flood characteristics had the greatest influence on planimetric change on the Umatilla River during the flood events. In this section, I described the importance of four morphological control variables (SI, slope, CI, and active channel width) at the reach and subreach level as well as the influence of bedrock and tributary junctions on flood effects. Then, I explained the role three types of surface cover (bare ground, grass, and trees) played in channel change during flooding. In addition to reach and subreach analysis, vegetation controls were also investigated at the box scale. Finally, I summarized these findings.

2.1 Morphologic and Hydrologic

Geomorphic change, or work, during a flood requires the erosion and transportation of sediment by the river. The erosion and transport of individual sediment grains is controlled by shear stress, and the erosional and transport capacity of the river is controlled by stream power (of which shear stress is a component). Both are dependent on channel slope. Confinement plays a role by controlling width and depth of flow at peak flow events. Channel curvature controls bank shear stress and therefore bank erosion. New bars and other depositional features require mobilized sediment derived from bed and bank erosion as well as tributary sediment inputs. Where the channel is on bedrock, rather than alluvium, sediment entrainment is limited. Tributary junctions are therefore important in controlling sediment availability and discharge, and on the Umatilla River, they serve as major sources of sediment.

2.1.1 Sinuosity

The channel widened more and moved greater lateral distances in reaches with more sinuous channels in response to the 1996-7 and 2020 floods. Removal of herbaceous vegetation was also significantly greater in more sinuous reaches. Variations in reach-average sinuosity did not significantly influence any other response variables, although the positive relationship between sinuosity and tree loss is nearly significant.

The results, however, suggest that sinuosity may more strongly control lateral movement than channel widening. Even at the finer subreach scale, sinuosity had a positive relationship with channel widening and lateral movement, but only the relationship with lateral movement was significant. Sinuosity may also need to be sufficiently high to exert control over the response variables. Semialluvial channels, which were more sinuous than the other channel types (Table 3) exhibited the strongest relationship between sinuosity and response variables.

A correlation between sinuosity and widening has been noted in previous studies (Dean & Schmidt, 2013; Fuller, 2007; Magilligan et al., 2015). Modeling has been used and integrated into field studies to further investigate this relationship, which shows that bank shear stress along the outside of a meander bend can, in some cases, rival that expected in straight, narrow, canyon channels (Harrison et al., 2015; Miller, 1995). The greater the shear stress, the more easily the channel can erode its banks, widen, and migrate. In this way, high sinuosity is especially important for lateral migration in bedrock-constrained areas, where greater shear stress is needed to erode and shift the channel. Although bedrock channels did not demonstrate a significant positive relationship between SI and lateral movement, this may be because those channels were the least sinuous. If sinuosity was not sufficient to allow the shear stress of the flow to overcome bank shear strength, that may have limited its control.

2.1.2 Slope

This study found channel slope exerted very little control over channel changes during the 2020 flood at the reach or subreach level, much like the conclusions reached by Nardi & Rinaldi (2015) and Beechie et al. (2006), despite its importance in controlling stream power. Bar accretion was the response variable most sensitive to changes in slope, but it was not significantly affected at the reach or subreach level when the entire data set was analyzed. Where slopes were steeper, bar area increased less. Reach-average and subreach-average slope had a very limited range at this site (Table 3), which may explain why slope was not significantly correlated with any of the response variables.

Slope values may not have varied enough or been too low at this site for a strong relationship with response variables to be observed. By controlling rates of sediment transport and deposition, slope may influence changes in channel width, bar formation, and lateral migration (Nelson & Dubé, 2016; Reid et al., 2019; Sholtes et al., 2018; Surian et al., 2016). However, slopes at this site were low and had a slightly smaller range than most studies (Nelson & Dubé, 2016; Sholtes et al., 2018; Surian et al., 2016; Table 3). Surian et al. (2016) found that multiple regressions analysis between control variables and channel widening performed better in steeper reaches (where slope > 0.04) than in non-steep reaches.

2.1.3 Confinement

Variations in channel confinement were not significantly correlated with changes in any of the response variables in 2020, but lateral movement was greater in less-confined reaches in 1996-7. Previous research of flood-driven geomorphic changes on the Umatilla from 1965 to 1975 also reported greater lateral movement in less-confined reaches (higher CI; Hughes, 2008). Reach-average and subreach-average CI values were generally high, especially before the 2020 flood, which indicated that the channel was unconfined by the valley walls throughout. Perhaps significant control of planimetric changes is only detectable when channels are more confined (lower CI), as they were in 1996-7 (Table 3). Where the channel is unconfined, flood waters may not reach across the entire floodplain, limiting the impact CI can have on stream power and geomorphic work.

It is possible that at the subreach scale, where CI varied more, the relationship between confinement and lateral movement is more complex than at the reach scale. In a comparison of several tributaries of the Manawatu River on the North Island of New Zealand, Fuller (2007) found that areas with CI greater than 38 or less than 7 saw less channel change after major flooding. There may be a similar threshold on the Umatilla River (perhaps CI between 6 and 11) where slight confinement helps to generate higher stream power to perform the geomorphic work of eroding banks and forging new channels without potential movement being too greatly restricted (Fryirs & Brierley, 2010). This is likely closely tied to the discharge threshold for channel migration found by Beechie et al. (2006), below which roots reach deep enough and are strong enough to prevent bank undercutting.

Areas where the channel transitioned from high confinement (low CI) to low confinement (high CI) tended to undergo greater widening and lateral movement, despite the lack of a linear relationship between confinement and the response variables. These were either in places where artificial constraints on the channel, often bridges (e.g. Reach 4 – boxes 61 through 68 or Reach

6 – boxes 96 through 102 in Figure 5; imagery of the former can be seen in Figure 7), or dramatic changes in valley width (e.g. Reach 7 – boxes 118 through 122 in Figure 5; imagery seen in Figure 25) created more extreme differences in CI. In previous studies, large lateral shifts and channel widening observed in areas where the channel transitions from high confinement to low confinement were attributed to drops in stream power (Dean & Schmidt, 2013; Righini et al., 2017). The decrease in stream power lowers the river's sediment transport capacity, creating depositional zones, and generating cutoffs and avulsions (Fuller, 2007; Nelson & Dubé, 2016; Righini et al., 2017). Simultaneously, without the narrow confinement of the previous reaches, the high flow is able to broaden its reach and deposit sediment across the more of the floodplain (Fryirs & Brierley, 2010; Sholtes et al., 2018).

2.1.4 Active Channel Width

Wider active channels drove increased channel widening and lateral movement during flooding at the reach level, but only lateral movement was significantly correlated with channel width at the subreach level. The scale of analysis greatly affected the relationship between active channel width and channel widening. Not only was that relationship not significant at the subreach level, but also active channel widening was less pronounced where the channel was wider. None of the other response variables were significantly controlled by active channel width.

Internal thresholds, which prevent the channel from over widening, may complicate the relationship between active channel width and widening at the subreach level. At the reach level, however, these thresholds may not operate as strongly and are clearly masked by the strong relationship between channel width and widening. For a braided river with minimal lateral confinement, like the Umatilla River, reaches with wider average active channels tend to be those that are more laterally active. On the Umatilla River, reaches with wider active channels also tended to be those with less channel confinement (high CI), which would have allowed the channel greater freedom to adjust and widen during flooding.

Because of the more frequent disturbance from even minor floods, sediment in the active channel is likely to be more readily eroded and vegetation is likely to be younger and have less root strength than on the surrounding floodplain (Beechie et al., 2006). This would facilitate lateral movement of the main channel across the active channel, and the wider that active channel, the greater potential distance that could more easily be eroded and traversed by the main channel. Channels with plentiful bedrock, however, would be more laterally constrained, even where their active channels were wider, masking this relationship. Semialluvial subreaches

were the only channel type to exhibit a significant relationship between greater lateral movement and a wider active channel width before the flood, though this relationship was nearly significant for alluvial subreaches as well. In bedrock subreaches, this relationship was not very strong.

2.1.5 Bedrock

Where bedrock was visible in the channel or where floodplain terraces directly abutted the channel bank, geomorphic work was limited. Although not measured quantitatively in this study, qualitative assessment based on visual inspection of the channel allowed identification of areas where bedrock was most and least plentiful. On average, channels in bedrock subreaches underwent less widening, bar accretion, lateral movement, and grass removal (Table 5). Because of its greater internal shear strength, bedrock is able to resist erosion and constrain channel adjustment and planform change during floods (Righini et al., 2017; Sholtes et al., 2018). Even small differences in these constraining features can have a noticeable impact. For example, Reach 9 had only slightly less visible bedrock compared to Reach 5, overall, but the channel widened 15% more in 2020.

2.1.6 Tributaries

The findings of this study echoed previous research that highlighted the role tributary junctions play in determining where major geomorphic work occurs during a flood in gravel-bedded rivers (Dean & Schmidt, 2013; Surian et al., 2016; Wicherski et al., 2017). Where tributaries meet the main channel, flow increases, giving the channel greater capacity to erode sediment and strip vegetation. Furthermore, sediment delivered to the main channel from its tributaries creates discontinuities in slope and contributes to channel widening, channel movement, and bar formation (Dean & Schmidt, 2013; Rice & Church, 1998).

In a study of channel change on the Chehalis River after major flooding and mass wasting, Nelson & Dubé (2016) found that, unsurprisingly, reaches through which the greatest sediment load passed also had the greatest increase in bar area. The intense bar accretion in Reach 5 (boxes 79 through 85 in Figure 5) may indicate an increase in sediment supplied by the Coonskin Creek basin, perhaps from a loss of vegetation there which increased erosion. This would explain why bar area increased so dramatically there in comparison to other reaches, especially Reaches 1 and 2, where Meacham and Isqúulktpe Creek, the largest tributaries in the study site, join the Umatilla River. Bar formation was not as pronounced in Reach 5 after the 1996-7 floods (Figure 21), which may support this theory. Recent restoration efforts on

Meacham Creek enhanced connectivity between the channel and floodplain and may also have increased sediment storage capacity there. This would have reduced bedload input from that tributary and lessened bar accretion in the upstream reaches, especially Reach 1.

2.2 Vegetation

Vegetation along banks and near-channel surfaces can affect channel landforms and flow regimes in ways that both reduce and enhance erosion (Corenblit et al., 2007; A. Gurnell, 2014). Banks may be protected by root systems, which increase their shear strength (Abernethy & Rutherfurd, 2001), or by the increased surface roughness of above-ground plant matter, which decreases near-surface flow velocity along with shear stress and stream power (Eaton & Giles, 2009; Huang & Nanson, 1997). Trees may be downed in large floods and large woody debris accumulations can slow flow velocity and encourage deposition in the channel, or else they may redirect flow and create flow turbulence which increase erosion, especially in nearby unvegetated areas (Bennett et al., 2002; Marshall et al., 2024; Wohl & Scott, 2017). Aggradation within the channel may trigger an avulsion, which can increase both lateral movement and active channel widening (Nardi & Rinaldi, 2015).

Because of the shallower rooting depth of grasses, surfaces covered in herbaceous vegetation are generally more readily eroded than those with tree cover. Studies of have shown that vegetation effects on a channel like those above can even control planform and geometry, although these effects are most strongly felt in small streams where shear stress does not regularly surpass the shear strength of the bank, strengthened by root systems (Beechie et al., 2006; Corenblit et al., 2007; Eaton & Giles, 2009). A flood as large as was seen on the Umatilla River in February of 2020, therefore, likely overwhelmed any additional erosional resistance offered by vegetation, especially grasses and other herbaceous cover. However, surface cover still impacted changes that occurred during the 2020 flood on the Umatilla River.

Reach-scale changes during the 2020 flood were controlled less by vegetation than they were by morphological variables. Furthermore, several of the response variables exhibited positive relationships with all three cover types. This may mean vegetation was less important than other controls, and the relationships detected were mostly related to other factors and not the surface cover itself.

In reaches where grass made up a larger proportion of surface cover, active channel widening and lateral movement were both greater. Subreaches with more grass cover underwent significantly greater channel widening, increases in bar area, lateral movement, and grass loss.

Herbaceous vegetation offered little protection from erosion. Therefore, the channel was able to widen and shift laterally more in areas dominated by grasses. The increased erosive potential in these areas also provided ample sediment for building bars.

Tree cover was only important in subreaches with bedrock channels, where greater proportions of tree surface cover lead to more widening, lateral movement, and tree removal. On the Umatilla River, tree cover often drove the formation of secondary channels, increasing active channel width and lateral migration and forming vegetated islands between the multiple channels (e.g. Figure 7). In the case of Figure 7, it appears that downed trees partially obstructed the main channel, which was also constrained by point bar accretion, leading to the formation of a secondary channel through the woody vegetation.

2.3 Summary

Results of this study suggest that shear stress and stream power and the resulting erosive geomorphic work (such as channel widening and lateral movement), are controlled more by sinuosity than other morphological factors on the Umatilla River, and that it tended to be greater where the channel was more sinuous. This may be due to the limited range of slopes or the lack of highly confined channels, which did not provide the variation necessary to significantly alter stream power or control planimetric changes. Due to their role as sediment sources, tributaries controlled bar accretion more than other morphological factors. Greater bedrock influence generally reduced the severity of flood effects and limited change. The role of vegetation in geomorphic change was unclear and may not have been very strong, though vegetation seemed to have increased channel change as opposed to protecting against it.

3. Historical Comparison

The 2020 flood caused well-above-average flow at all gages on the Umatilla River and is anomalous even among other historical floods, considered to be a 200 to 500-year event. Before that, the 1996 flood, considered to be between a 20 and 70-year event, was the largest flood on record at the Gibbon gage (Figure 2) and within the top 10 recorded floods at the Pendleton and Umatilla gages. Both floods caused considerable damage to the communities around the river, and news coverage of the 2020 flood often compared it with the 1996 flood. The results of this study show they had similar effects on wetted width, bar area, and lateral movement, but patterns in active channel widening and changes to sinuosity differed. Additionally, although the 1996-7 floods performed less geomorphic work overall, especially in terms of active channel

widening, that flood did result in greater extremes in lateral movement and bar formation, perhaps due to the lower but longer sustained peak discharge of the 1996 flood.

It is possible changes in active channel width and sinuosity were affected by internal thresholds maintained by the river pattern and the geometry and geology of the valley, which prevent the river from becoming overly straight or wide, such as interactions between flow and the many bars and vegetated islands. The river began wider and less sinuous before the 1996-7 floods compared to before the 2020 flood, widened much less in 1996-7 compared with 2020, and increased in sinuosity in 1996-7 while decreasing in sinuosity in 2020. If the river was already near the upper threshold for its active channel width, the lower discharge in 1996-7 may not have been sufficient to widen the river much more. After the early February flood in 1996, the river experienced several instances of elevated discharge (Figure 3), which, although not sufficient to raise the river above flood stage, may have increased erosion, particularly at meander bends, thus increasing sinuosity between 1994 and 1998.

3.1 Persistent Patterns in Change

Because active channel widening was often a factor of channel avulsion or secondary channel generation and less dependent on bank erosion on the Umatilla River, lateral migration and active channel widening often occurred in tandem. Furthermore, many areas where active channel widening and lateral movement were greatest in 2020 were the same areas that had undergone a great deal of change in 1996-7. In Reach 6, for example, change in either variable peaked nearly simultaneously (Figure 28). The main exception to this was between boxes 98 and 100, where both response variables saw much less change in 1996-7 than 2020. Because the channel directly abutted the valley wall in those boxes in 1994, but not in 2017, movement and widening were constrained in 1996-7. Hughes (2008) also found that reaches where the active channel widened the most tended to undergo a great deal of lateral movement.

Reaches 6 and 7 are the most morphodynamically active reaches in this site, as evidenced by channel widening and migration during the floods studied here (Figure 5, Figure 21) as well as in previous research by Hughes (2008). The dramatic increase in valley width, beginning in Reach 6 and continuing through Reach 8 (Figure 4), coupled with a lower valley gradient (Table 3) and far fewer lateral constraints from bedrock (Figure 4) have allowed the braided channel to persist, which means a large area of the floodplain has remained activated and connected with the channel. Previously abandoned channels are often rewetted in major floods, or else flood-driven avulsions may shift the thalweg so that it follows that path once more or shifts to secondary channels formed during the flood (e.g. Figure 7).

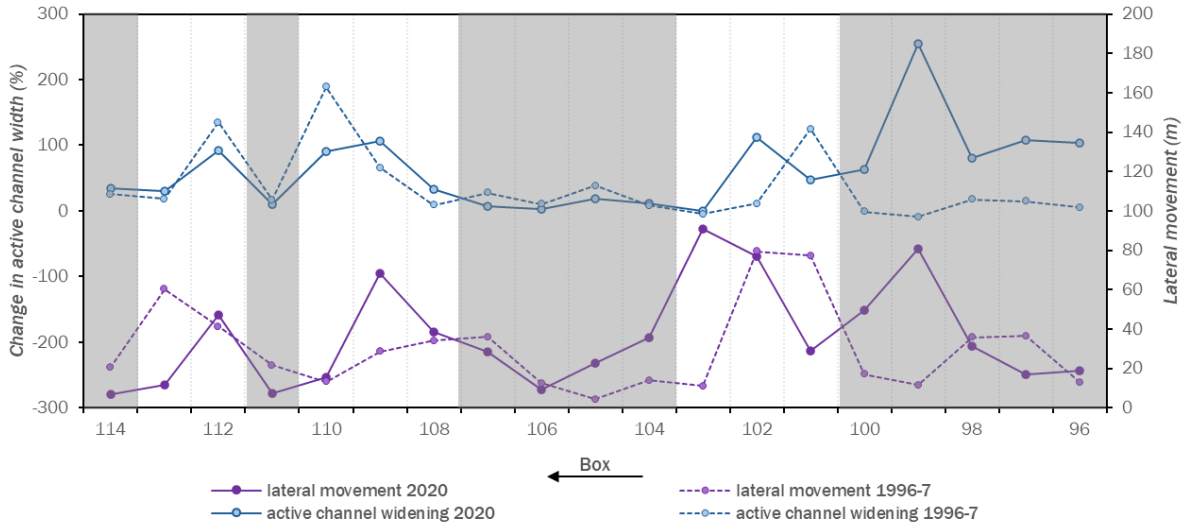

Figure 28. Lateral movement and active channel widening for each box in Reach 6 for the 1996-7 and 2020 floods. Boxes that have not been grayed out show where both channel widening and lateral movement peak in similar areas in 1996-7 and 2020. Imagery of most of Reach 6 can be seen in Figures 24 and 25.

The floodplain cycles into and out of the active channel frequently, increasing connectivity between the channel and floodplain and creating complexity (A. M. Gurnell et al., 2001; Nanson & Knighton, 1996; O'Connor et al., 2003). Near-channel floodplain is annexed by new channels or shifts in channel location and becomes vegetated islands within the active channel. Later the channel may shift again, and that island becomes a part of the larger floodplain, once more. Alternatively, eroded sediment is built into bars which may become stabilized islands once they become vegetated. This increased complexity is beneficial to anadromous salmon, which are important both ecologically and culturally, and other aquatic biota (Marshall et al., 2024; Ward et al., 2001; Wohl, 2016). However, it poses significant risk to human life and property.

That risk can be mitigated when historical analysis is used to determine where the river has undergone the most change during previous floods and measures are taken to prevent further development or focus protection there (Arnaud-Fassetta et al., 2005). This research also underscores the importance of observing multiple response variables when studying flood effects. Many studies focus on channel widening, because that variable tends to undergo the most change, but including other response variables, such as lateral movement, may help to identify additional areas at risk. Washington and Oregon have both begun efforts to map historic channel movements in order to identify high risk areas which might not be identified by traditional FEMA maps.

4. Limitations and Future Directions

Remote sensing was well-suited to this research because it provided recent and historical data for planimetric and vegetative characteristics over a large area. However, because this study was limited to analysis via aerial imagery without a field work component, measurements and classification based on digitization were not verified on the ground. In addition, without channel bed slope data collected in the field, stream power, the main driver of channel change during flooding, could not be calculated.

Also, this study made use of aerial imagery that had already been collected, and so the resolution and dates of the flights could not be controlled. Because of the two years between the 1996 flood and post-flood imagery , it is possible some of the changes observed reflect changes unrelated to the flood. Conversely, some changes may be masked by recovery of the channel. Both floods occurred around two years after the pre-flood imagery, so it is possible pre-flood conditions differed slightly from those recorded here. However, in both cases, it should be noted that channel change tends to occur at a much slower pace outside of major disturbances, like the floods, so changes, especially geomorphic changes, are assumed to be negligible. The range of some control variables was also narrow at this site, which may have prevented them from exerting control over the response variables or otherwise limited the strength of their relationships.

Further study of flood effects on the Umatilla River would benefit from the inclusion of field work in addition to aerial imagery analysis so that stream power or total energy could be incorporated into the analysis. This would provide further insight into flood effects and facilitate comparison of geomorphic effectiveness with other rivers. Including tributaries into future studies would provide a wider range of values, which may clarify causal relationships.

CHAPTER VI

CONCLUSION

In February of 2020, an atmospheric river event brought heavy rain, which, on top of snowmelt, resulted in record-breaking discharge at all three gages on the Umatilla River. Aerial imagery captured shortly before and after the flood was collected and digitized. This allowed the changes wrought by this flood to be mapped to determine the geomorphic effectiveness of the flood, compare it with previous flooding on the same river, and analyze causal variables via regression analysis. Most of the changes observed reflect the results of other studies of geomorphic flood effects on the Umatilla River and on similar rivers as well (channel widening, bar accretion, lateral movement, sinuosity loss, vegetation removal), and though not many of the relationships analyzed proved significant, those that did generally support theories of flood effect controls.

The research questions and hypotheses posed by this study were as follows:

1. What effects did the 2020 flood have on the geomorphology (active channel width, lateral movement, sinuosity, bar accretion) and vegetation of the Umatilla River?

a. Hypothesis 1 – *The active channel will widen and bar area will increase.*
b. Hypothesis 2 – *Sinuosity will decrease, and lateral migration will be dominated by movement that decreases sinuosity (cutoffs, straightening, avulsions).*
c. Hypothesis 3 – *More herbaceous vegetation than woody vegetation will be removed.*

All three of these hypotheses were supported by the results.

2. What role did surface cover type, active channel width, channel slope, channel confinement, or sinuosity before the flood play in changes to active channel width, bar formation, lateral movement, sinuosity, and vegetation cover?

a. Hypothesis 1 – *Increases in channel width are likely to be related to high sinuosity, low confinement, low active channel widths, and greater proportion of grass surface cover.*
b. Hypothesis 2 – *Lateral activity is likely to be related to increased sinuosity, low confinement, high active channel widths, and greater proportion of grass cover*
c. Hypothesis 3 – *Increases in bar area are likely to be related to low slopes and a greater proportion of grass cover.*

d. Hypothesis 4 – *Greater losses of grass and trees are likely to be related to high sinuosity, high confinement, and lower proportion of bare surface cover.*
e. Hypothesis 5 – *Increases in sinuosity are likely to be related to low sinuosity and high slopes.*

None of these hypotheses were fully supported by the results because most of the causal variables failed to exert significant control over the response variables.

3. How do changes caused by the 2020 flood compare to changes from the 1996-7 floods?

a. Hypothesis 1 – *Due to its greater discharge, the 2020 flood was the more geomorphically effective flood.*
b. Hypothesis 2 – *Highly geomorphically dynamic areas in 1996-7 will be similarly active in 2020.*

Both of these hypotheses were supported by the results.

Active channel widening and lateral movement were the most sensitive to the control variables at the reach level both in 2020 and in 1996-7. Sinuosity played a particularly important role in controlling change in these variables; where sinuosity was greater before flooding, the channel widened more and moved greater distances. Because slope and confinement had limited ranges at this site, variations in stream power, and therefore erosive power, were largely dependent on variations in sinuosity. Increased sinuosity was also correlated with greater stripping of grass and scrub from surfaces in the active channel. In 2020, the reach-average and subreach-average width of the channel before the flood was also significantly and positively correlated with lateral migration. Wider active channels often contained secondary or abandoned channels where the channel could more easily shift during flooding, which increased the likelihood of large lateral movement.

Vegetation did little to prevent erosion during this catastrophic flood, and conflicting relationships between cover types calls into question the significant relationships that were detected. Active channel widening and lateral migration were consistently, across scales, greater where grasses made up a larger proportion of the surface cover, and box level analysis also indicated widening and lateral movement increased where trees dominated. At the subreach and box level, bar accretion and grass loss were also greatest where grass was more widespread.

Bar accretion was most dependent on sediment availability, which was controlled by tributary transport. However, steep slopes prevented bar building around some tributaries, which created a disconnect between aggradation and tributary junctions.

Differences in control variables did not adequately explain patterns of tree loss or sinuosity change at the reach or subreach scale in 2020, nor did they have significant explanatory power for changes in bar area or sinuosity in 1996-7.

Although the effects of the 1996-7 floods and the 2020 flood were very similar, observed differences support theories of intrinsic controls on channel processes and the importance of flood duration. The 2020 flood had a higher discharge and was therefore more geomorphically effective. However, despite its lower discharge, the greater time spent at or near its peak discharge in 1996 as well as the extended period of above-average discharge in the months that followed made its overall effectiveness much more like the 2020 flood than it would have otherwise been.

Understanding how a river responds to flooding provides valuable insight for river managers. This research highlights the importance of identifying highly dynamic parts of the floodplain, such as Reaches 6, 7, and 9, which are likely to be active during future floods and should, therefore, be areas where development is discouraged. While channelization efforts do reduce the local damage from floods, as was seen in Reach 8, they also severely hinder fluvial processes of scour, erosion, channel formation and abandonment, and bar/island development that drive habitat patchiness, floodplain connectivity, and overall ecological health of the basin in a braided river like the Umatilla.

Climate change is likely to increase flooding in this region, so better understanding flood effects, and therefore flood risk, is becoming increasingly important. Climate models for the region are not completely in agreement, but many predict drier summers and wetter winters in the coming decades. In addition, extreme weather events are expected to become more frequent, although warmer temperatures will also limit the chances of rain-on-snow events, which are responsible for many of the most disastrous floods in the basin. Identifying characteristics of channels that are likely to undergo the greatest shifts during future floods, such as particularly sinuous reaches or reaches downstream of confinement, may help managers choose where to allocate resources for flood mitigation measures and provide further support for efforts already underway to map flood risk based on channel processes and historic movement.

APPENDIX

BOX-LEVEL DATA

Measurements of floodplain dimensions and centerline length before and after flooding.

Box number	*Floodplain area (m^2)*	*Floodplain length (m)*	*Centerline length in 2017 (m)*	*Centerline length in 2020 (m)*	*Centerline length in 1994 (m)*	*Centerline length in 1998 (m)*
2	77080.9	188.8	275.8	196.2	204.8	259.0
3	77710.1	201.0	292.2	228.6	259.2	237.3
4	72449.5	195.1	198.7	206.9	187.7	196.6
5	77591.7	189.2	134.7	135.8	132.7	133.9
6	80796.0	198.1	191.8	192.8	191.4	198.4
7	86644.1	198.8	245.9	247.4	248.8	249.2
8	82360.1	195.9	256.0	190.8	181.4	206.3
9	85117.4	195.3	188.7	187.5	191.1	196.4
10	85760.4	202.3	234.7	249.2	227.6	228.3
11	92499.5	218.2	171.7	173.0	157.5	188.5
12	78408.9	197.6	275.0	308.1	237.9	273.4
13	85140.7	204.3	302.5	334.3	278.2	316.7
14	89813.1	199.4	281.0	377.7	329.0	368.8
15	95440.8	195.4	141.5	141.1	133.8	150.0
16	94668.2	199.8	169.3	170.1	171.9	170.8
17	93981.2	222.9	324.0	312.2	309.7	309.5
18	115801.7	200.3	261.4	221.6	219.4	219.1
19	130047.2	199.9	171.9	136.0	139.3	145.0
20	117224.6	208.8	277.7	241.6	241.4	249.2
21	94324.5	204.0	293.9	287.7	263.6	270.7
22	89662.1	199.9	227.2	238.3	203.4	237.1
23	104882.3	202.8	262.8	217.3	288.7	233.6
24	109831.5	194.7	276.5	299.9	201.8	215.0
25	110231.6	202.8	214.3	231.0	233.1	221.2
26	100580.5	203.1	236.1	240.5	230.6	223.5
27	86979.9	199.2	196.0	187.2	195.2	198.6
28	79606.9	200.8	266.8	292.5	243.9	257.5
29	79806.0	200.7	213.1	263.2	206.8	216.7
30	81311.6	195.8	259.6	217.5	215.4	220.3
31	94064.0	202.4	226.9	265.7	317.3	222.7
32	83941.2	193.0	160.5	170.1	175.8	163.2
33	91230.7	209.8	254.4	187.7	266.3	297.8
34	90678.6	195.5	270.3	223.7	223.1	245.5
35	78967.1	199.9	159.0	212.5	152.6	141.5
36	65108.4	199.9	217.2	212.9	220.6	210.0
37	61733.6	197.0	270.7	274.5	277.0	271.0
38	69403.4	204.0	211.9	211.6	211.0	212.2
39	52650.5	195.7	202.2	209.4	201.6	194.4
40	46908.9	192.1	148.4	168.9	139.0	164.8

Measurements of floodplain dimensions and centerline length…(continued).

Box number	*Floodplain area (m^2)*	*Floodplain length (m)*	*Centerline length in 2017 (m)*	*Centerline length in 2020 (m)*	*Centerline length in 1994 (m)*	*Centerline length in 1998 (m)*
41	69765.7	193.6	232.3	194.7	185.6	198.8
42	77307.7	202.8	235.8	246.1	234.7	236.8
43	99570.3	200.6	147.2	155.4	133.2	139.8
44	158559.8	208.3	220.4	233.2	214.1	236.2
45	169779.0	198.0	455.0	492.1	300.9	334.5
46	134994.2	196.9	212.3	210.0	206.6	215.4
47	120954.9	196.4	192.9	193.6	193.8	193.0
48	121702.4	200.9	207.8	210.9	206.1	209.3
49	111042.1	205.0	206.8	206.0	209.2	207.0
50	97011.9	206.8	254.3	252.6	249.2	252.6
51	96385.7	194.9	185.4	200.7	166.7	176.9
52	93803.1	209.1	297.2	287.0	273.2	276.1
53	86949.7	204.2	257.2	261.4	242.4	241.2
54	84839.5	195.9	192.2	185.9	184.5	189.1
55	94692.7	196.0	206.1	209.7	345.3	285.5
56	102616.5	198.0	363.7	298.8	214.2	296.5
57	105675.9	201.3	292.0	250.0	421.3	437.2
58	103332.1	201.1	319.4	282.3	235.0	235.1
59	91105.7	193.7	104.2	123.7	121.5	105.3
60	92518.6	199.5	235.0	201.2	210.1	232.1
61	87215.7	200.3	222.5	250.9	216.9	225.0
62	80047.4	192.6	312.7	325.1	181.8	221.8
63	65806.8	198.5	267.8	249.7	269.6	271.1
64	78476.6	214.4	190.9	223.0	361.1	221.6
65	70378.3	197.9	268.6	242.9	207.0	219.1
66	59755.2	201.7	197.1	198.3	189.1	190.3
67	61561.5	198.9	189.6	199.6	187.9	191.1
68	51099.7	194.8	242.1	220.1	245.7	245.4
69	40684.1	201.7	196.7	205.0	247.3	274.0
70	58066.1	201.3	292.8	263.8	220.1	208.4
71	78565.4	196.6	198.1	223.7	227.5	200.9
72	83251.6	198.8	165.1	175.8	169.8	178.9
73	69743.3	197.5	169.6	197.9	271.5	186.1
74	68175.7	199.5	373.5	449.8	200.9	757.4
75	75996.8	196.3	200.8	202.1	197.4	197.1
76	76223.5	201.7	229.8	230.0	244.5	244.4
77	82570.5	203.9	235.3	231.2	232.9	230.9
78	84052.5	201.1	195.7	196.8	200.3	199.2
79	66595.1	197.6	205.1	200.4	193.3	208.8
80	38204.2	198.2	220.0	227.9	224.5	219.6

Measurements of floodplain dimensions and centerline length…(continued).

Box number	*Floodplain area (m^2)*	*Floodplain length (m)*	*Centerline length in 2017 (m)*	*Centerline length in 2020 (m)*	*Centerline length in 1994 (m)*	*Centerline length in 1998 (m)*
81	47213.6	197.3	178.2	226.3	198.6	217.1
82	49471.6	197.6	280.5	234.9	237.8	212.6
83	44101.8	199.2	281.7	223.5	234.5	240.5
84	39681.8	199.6	211.1	217.7	215.7	212.4
85	50546.9	198.3	202.3	219.7	199.6	201.9
86	75210.1	198.8	172.1	167.8	170.8	174.7
87	96242.1	198.5	116.7	122.2	117.3	132.9
88	89699.8	250.3	319.5	334.3	317.0	331.0
89	56390.6	202.4	360.1	376.5	337.8	357.5
90	75079.2	194.8	346.6	323.2	312.2	313.1
91	101461.8	192.8	224.3	224.4	224.9	225.3
92	128170.3	197.9	127.3	112.8	118.9	122.6
93	134269.8	196.9	233.7	267.2	236.2	233.1
94	123987.2	202.1	219.1	223.1	197.4	210.2
95	87973.8	198.3	224.6	258.5	215.3	223.5
96	71085.8	200.3	261.2	290.1	240.5	245.7
97	76445.5	199.3	290.9	295.0	279.9	265.2
98	101412.9	203.9	181.1	166.8	224.0	187.8
99	106056.6	192.5	111.3	77.1	80.2	74.6
100	120798.3	200.6	207.9	199.2	226.6	232.8
101	131338.4	196.3	310.2	297.6	322.6	227.8
102	138431.0	195.9	376.4	282.9	223.5	219.5
103	144858.4	202.7	217.1	303.5	209.9	242.9
104	139641.7	197.4	225.5	221.5	212.9	226.3
105	123395.9	200.4	191.7	200.8	191.9	196.6
106	123990.6	200.2	269.1	270.9	272.9	267.3
107	132641.5	203.0	100.1	94.3	109.7	90.8
108	114550.7	202.8	234.7	231.9	241.8	240.4
109	86580.6	200.4	272.3	250.5	266.3	248.2
110	83119.3	197.1	227.5	213.9	213.1	219.2
111	78573.5	199.9	201.7	208.0	201.4	198.8
112	75685.8	201.9	401.7	351.1	376.6	228.9
113	96000.6	199.6	199.1	177.4	174.4	287.7
114	109948.5	207.4	249.3	253.9	250.1	258.3
115	113292.6	197.8	315.9	299.8	293.1	300.6
116	116071.9	197.4	186.7	175.3	174.7	176.7
117	150023.1	198.3	181.8	178.6	178.5	180.6
118	186746.9	197.8	323.2	249.3	264.4	270.3
119	170018.8	192.2	235.4	221.3	224.1	218.5
120	199857.0	266.6	143.7	111.9	272.9	152.0

Measurements of floodplain dimensions and centerline length…(continued).

Box number	*Floodplain area (m^2)*	*Floodplain length (m)*	*Centerline length in 2017 (m)*	*Centerline length in 2020 (m)*	*Centerline length in 1994 (m)*	*Centerline length in 1998 (m)*
121	217801.9	205.3	168.4	259.9	397.9	224.5
122	222791.2	203.8	176.9	161.3	249.4	217.9
123	229304.0	194.6	251.4	416.1	194.1	466.6
124	248257.9	223.0	339.9	175.3	172.3	156.9
125	289806.0	204.7	150.6	192.6	131.8	182.9
126	303821.7	208.2	298.0	283.8	239.5	265.3
127	310503.4	198.0	312.3	241.5	306.5	305.1
128	332100.1	233.8	202.9	193.6	209.2	273.3
129	335565.8	197.6	423.5	533.5	227.5	223.7
130	327026.7	198.8	178.5	180.6	317.2	301.5
131	332999.8	223.8	277.3	265.7	426.6	499.5
132	316728.7	197.0	218.1	215.3	215.9	216.5
133	327081.5	198.7	154.1	152.5	153.5	153.2
134	320479.8	194.8	229.1	228.0	227.2	229.4
135	322787.6	216.2	191.3	190.4	189.8	189.6
136	322460.7	200.5	230.7	238.5	228.0	230.9
137	304529.4	191.0	177.1	187.0	179.7	182.7
138	287923.2	195.5	226.2	200.8	202.9	202.5
139	293611.7	199.3	203.0	201.1	197.1	198.9
140	276092.7	199.4	201.2	198.8	199.2	197.1
141	248411.6	198.6	221.6	217.4	210.6	215.6
142	193180.6	199.4	194.0	192.5	186.1	189.3
143	212469.4	214.2	213.2	213.8	199.6	202.3
144	273170.6	197.9	195.6	195.6	192.6	193.4
145	275532.8	192.9	192.2	190.3	197.6	189.8
146	256734.6	207.3	202.4	215.3	211.0	220.6
147	232124.9	193.2	211.7	202.6	196.9	197.5
148	196568.9	193.7	218.4	208.0	194.8	190.9
149	199604.4	205.8	274.8	298.2	234.5	281.4
150	183314.3	201.0	294.8	279.6	222.2	240.7
151	158623.2	190.8	223.4	220.6	192.4	197.4
152	148674.5	198.2	196.7	195.2	222.5	191.2
153	134393.1	208.3	178.8	185.1	230.2	240.7
154	90366.9	195.8	362.7	247.6	206.9	213.7
155	97483.6	206.4	247.6	240.8	222.8	236.8
156	96164.4	197.3	215.4	227.4	212.6	223.6
157	97073.3	189.3	164.4	166.0	152.5	157.4

Measurements of active channel area before and after flooding.

Box number	*Active channel area in 2017 (m^2)*	*Active channel area in 2020 (m^2)*	*Active channel area in 1994 (m^2)*	*Active channel area in 1998 (m^2)*
2	23462.1	37174.2	33397.8	34856.3
3	14755.2	22625.7	23240.5	23299.7
4	8720.5	10401.2	11992.3	13171.6
5	4905.7	4704.6	5137.8	5476.3
6	6123.9	5671.3	9870.9	12804.9
7	8324.4	8108.7	25070.3	15673.5
8	8988.5	10414.2	10794.2	10084.8
9	5106.4	7599.4	14852.5	14396.4
10	9093.6	10576.6	30000.5	30990.7
11	9007.4	9263.0	13178.8	17047.1
12	14908.8	18206.9	17283.3	19105.6
13	20608.5	25614.9	18667.7	23927.8
14	45502.4	45362.2	41832.4	46796.9
15	7613.7	14086.5	27465.3	9413.4
16	5169.2	7425.5	23335.5	22334.6
17	12437.2	13904.6	25167.7	28803.4
18	13319.7	16821.8	18083.8	18251.8
19	10131.4	22008.2	12574.1	14290.2
20	8991.1	12529.7	19582.3	21612.3
21	8994.3	10175.1	28792.8	27586.0
22	11025.2	15288.8	26480.0	28409.5
23	10300.0	16465.6	37563.1	40725.6
24	20459.1	29842.6	22868.7	25218.4
25	16943.9	25952.9	14442.3	14826.0
26	5640.7	8805.5	8065.5	8008.1
27	6195.6	6776.1	6250.4	7334.0
28	10350.4	13106.0	15318.7	15103.7
29	11268.1	16763.8	12130.6	18400.5
30	13436.0	26381.4	15354.1	16920.1
31	8409.5	17446.0	17147.8	21200.5
32	5346.5	7444.2	8138.4	8401.0
33	19922.7	22372.8	14260.3	14910.8
34	18232.3	21560.8	11096.9	8373.9
35	9555.7	12851.6	8569.1	8490.2
36	8337.6	11535.9	13314.8	10921.3
37	9040.6	8828.2	23402.8	27234.6
38	8624.9	8745.6	15040.9	17172.9
39	10387.6	12385.6	13474.8	12610.4
40	8852.5	10175.4	6536.2	8207.6
41	11596.3	15757.7	18557.4	16930.8
42	6923.0	13869.7	9129.4	8340.5

Measurements of active channel area before and after flooding (continued).

Box number	*Active channel area in 2017 (m^2)*	*Active channel area in 2020 (m^2)*	*Active channel area in 1994 (m^2)*	*Active channel area in 1998 (m^2)*
43	5392.9	6042.6	4846.1	5077.1
44	13262.5	20567.8	8768.8	17278.8
45	22320.0	30222.3	14881.8	14061.1
46	7646.7	7783.7	20711.4	9129.6
47	5580.1	5540.6	9364.3	9106.4
48	6425.8	8026.1	8217.5	10724.3
49	4486.2	6723.0	17502.8	17121.2
50	7397.2	7587.3	22981.3	21137.1
51	6528.1	7712.6	9673.2	11345.0
52	10178.1	10925.8	25627.3	25294.6
53	15126.3	15552.7	10779.8	12432.4
54	16590.8	18674.2	11165.5	14237.5
55	48480.1	44575.9	31341.6	36034.8
56	19955.6	23364.9	18080.1	18674.9
57	17604.1	19184.2	15370.0	24329.0
58	19938.2	20596.1	9181.3	5311.0
59	3948.0	4765.5	5169.9	3600.6
60	7283.5	7750.5	8552.0	10804.5
61	8189.5	14411.0	17499.3	19452.6
62	17972.6	30830.6	17539.9	17608.9
63	9558.9	36110.2	19405.8	26821.4
64	6814.6	11646.4	28634.4	29922.5
65	10788.5	15922.0	31402.3	32517.9
66	5935.6	6392.1	7250.6	12971.6
67	6522.6	8261.0	8365.0	10434.7
68	11759.3	13144.8	8191.8	16568.5
69	17052.0	17105.3	14052.1	15202.5
70	10054.4	12099.4	22592.1	21798.8
71	8957.1	11155.7	17390.6	19917.0
72	9235.5	13174.2	7180.1	11961.7
73	9986.4	30346.1	22523.2	27431.2
74	16201.7	38864.2	13388.3	28928.0
75	5862.7	9300.2	22664.7	29937.8
76	8028.9	7817.4	22904.1	29548.6
77	7634.7	7467.9	23261.1	21713.7
78	13108.3	13065.6	13445.4	14646.9
79	15845.9	20179.2	9048.2	8819.6
80	11802.5	12044.1	18421.4	16200.6
81	15319.6	16953.2	16221.0	14823.7
82	29423.7	32995.0	21008.6	29010.5
83	12510.4	13651.2	8835.8	13503.3

Measurements of active channel area before and after flooding (continued).

Box number	*Active channel area in 2017 (m^2)*	*Active channel area in 2020 (m^2)*	*Active channel area in 1994 (m^2)*	*Active channel area in 1998 (m^2)*
84	6096.2	8772.4	9092.2	8214.6
85	5599.9	8074.8	8578.7	7619.6
86	4855.5	7363.9	7192.2	7090.4
87	3933.1	5936.9	6507.6	6801.8
88	15335.9	25253.6	18312.0	21331.7
89	19677.6	20361.9	15500.7	16934.7
90	13973.2	16839.8	10915.5	9647.6
91	6180.7	6382.1	6230.4	5800.3
92	6356.1	6733.6	7082.4	6036.4
93	9965.3	13850.9	26041.5	25515.6
94	15418.0	25046.9	23118.8	24504.9
95	10747.5	17824.8	14082.5	19628.2
96	8660.4	19567.5	33288.7	35930.7
97	12006.2	25390.4	39361.4	42727.3
98	5542.2	9204.9	40785.7	40145.4
99	3591.6	8813.9	39131.8	33173.1
100	13498.2	21108.0	36187.2	36781.1
101	19080.5	26879.8	21141.7	33574.3
102	22349.1	35659.9	35060.5	38333.7
103	26555.6	37007.6	23656.4	25975.6
104	10842.3	11854.1	7454.9	8590.6
105	8358.0	10367.4	7109.9	10075.7
106	34945.3	36144.6	30738.7	33169.5
107	22314.8	22435.2	21920.4	23187.1
108	24606.1	32284.6	34985.1	37868.2
109	16839.3	31869.7	12777.6	19704.2
110	11378.9	20334.2	7444.7	22105.2
111	15188.0	17325.7	9850.1	11356.1
112	25884.3	43577.4	23620.8	33709.6
113	42193.5	48949.8	14558.1	28474.4
114	10648.1	14592.5	11757.6	15240.5
115	21142.1	21411.2	15197.5	19146.0
116	9964.6	10472.4	6942.3	9338.9
117	13690.5	16624.7	8787.5	9608.1
118	15382.7	23159.9	16393.5	20440.5
119	10443.3	38960.1	25591.1	36816.8
120	11786.0	19919.5	12933.4	26971.3
121	10555.6	28665.5	72099.5	95111.1
122	23301.8	32122.0	89831.6	105860.2
123	45462.6	56153.4	62109.1	68227.4
124	44410.2	48444.3	26751.2	36715.1

Measurements of active channel area before and after flooding (continued).

Box number	*Active channel area in 2017 (m^2)*	*Active channel area in 2020 (m^2)*	*Active channel area in 1994 (m^2)*	*Active channel area in 1998 (m^2)*
125	33082.0	34712.3	18109.8	28435.3
126	40501.6	41882.6	25951.3	26640.3
127	20017.4	24206.6	21513.0	14728.3
128	8635.2	20362.7	13825.4	14958.7
129	32092.8	55022.9	11490.8	15066.7
130	9671.7	15863.9	24827.4	44367.3
131	14436.7	22865.7	18016.8	26826.4
132	9532.4	11001.1	8036.7	7373.5
133	7342.6	7278.0	6466.6	6110.5
134	8196.5	8611.7	8420.2	7546.2
135	7484.0	8268.5	6946.7	6169.6
136	9307.5	9827.1	10744.2	8370.0
137	10761.5	11144.9	8993.0	10385.2
138	8476.6	13922.7	7521.6	13547.2
139	8228.8	14176.5	7753.4	11802.1
140	8630.6	8741.9	8512.0	9312.3
141	10402.1	10160.7	11497.3	10526.1
142	8077.6	7975.5	8984.6	8789.1
143	10006.2	10085.6	11719.2	11409.2
144	7032.9	7216.6	6916.5	9056.7
145	7800.7	8254.8	9365.8	10575.0
146	10059.5	15660.7	14693.6	15345.2
147	15717.7	22057.6	23693.1	20141.3
148	8360.1	17072.3	27043.4	9888.6
149	9356.9	11536.2	23742.1	13018.8
150	13063.1	20490.7	34525.0	32323.4
151	6198.2	8454.4	23134.9	14649.3
152	8438.5	9658.8	16075.4	14839.7
153	15481.7	20375.2	21952.0	20623.0
154	13468.0	19273.5	9793.8	9704.3
155	11375.5	11151.1	12250.8	11044.2
156	10242.9	10549.2	13956.8	11191.2
157	5263.1	8068.8	12113.3	9972.0

Measurements of area between channel centerlines and straight-line distance between upstream and downstream points used to calculate local sinuosity.

Box number	*Lateral movement area 2020 (m^2)*	*Lateral movement area 1996-7 (m^2)*	*Straight-line distance 2017 (m)*	*Straight-line distance 2020 (m)*	*Straight-line distance 1994 (m)*	*Straight-line distance 1998 (m)*
2	21480.4	5310.1	973.6	1059.9	932.9	627.3
3	7437.7	7888.0	997.3	1123.2	1124.4	868.1
4	1915.9	3155.0	1001.3	1144.3	1096.0	1042.4
5	311.1	389.5	1025.3	1138.9	1119.7	1089.3
6	970.9	1728.2	1042.6	1125.8	1125.1	1105.2
7	2757.6	1680.6	1072.8	1123.5	1143.0	1106.4
8	6932.1	2640.1	1075.8	1126.9	1152.1	1116.6
9	1392.2	820.0	1030.1	1104.7	1129.4	1023.4
10	2054.4	2934.8	1003.2	1016.9	1118.8	1037.6
11	819.3	4159.0	1023.1	998.7	1098.8	1000.0
12	2641.3	4066.7	996.9	947.3	1020.5	992.3
13	6637.3	7081.9	984.4	833.8	1017.2	863.0
14	12066.8	33895.7	1031.8	925.9	1029.1	945.4
15	341.8	646.5	1056.2	963.0	1057.1	992.3
16	364.4	335.2	1069.2	1045.4	1100.3	1047.7
17	1148.3	530.0	1071.2	1137.0	1175.1	1080.7
18	8146.1	3067.4	1061.3	1167.3	1171.1	1159.7
19	14261.3	2391.5	1002.0	1110.4	1141.5	1119.7
20	4024.9	3483.8	974.8	1075.5	1142.0	1079.4
21	2207.3	1298.4	964.3	1080.9	1064.2	1059.8
22	2897.8	12394.2	970.3	1003.1	1077.4	1055.5
23	5323.9	28486.0	992.4	995.5	1066.1	1080.1
24	2495.6	6953.6	997.3	985.9	1048.6	1075.1
25	8320.1	8854.2	1004.3	1015.9	1043.1	1076.4
26	1229.2	1002.4	1004.9	948.9	1080.1	1074.4
27	931.7	739.4	1090.8	1015.4	1096.5	1080.1
28	4676.9	2679.3	1008.7	976.6	1062.6	1055.8
29	5730.4	5833.1	1011.0	951.4	997.3	1057.5
30	9204.6	10186.2	1030.6	956.6	1002.1	1058.5
31	8875.1	10820.2	1047.7	1051.3	1014.3	1067.8
32	1862.8	1757.2	983.1	1028.8	944.5	1001.4
33	5107.4	3901.2	977.9	973.7	914.6	971.6
34	11054.7	1962.1	933.8	960.9	930.2	944.1
35	7232.8	1521.1	937.7	992.5	962.6	948.6
36	2494.7	3760.1	959.2	989.0	1025.3	1036.1
37	1090.7	1931.4	1044.5	982.5	1050.8	1044.7
38	3449.1	1114.1	1068.9	1044.5	1066.4	1076.6
39	6314.1	2674.9	1032.0	1037.6	1091.9	1052.4
40	4347.9	4655.0	1037.1	1025.6	1095.5	1059.2

Measurements of area between channel centerlines and straight-line distance…(continued).

Box number	*Lateral movement area 2020 (m^2)*	*Lateral movement area 1996-7 (m^2)*	*Straight-line distance 2017 (m)*	*Straight-line distance 2020 (m)*	*Straight-line distance 1994 (m)*	*Straight-line distance 1998 (m)*
41	3802.9	2679.3	1062.2	1037.3	1107.4	1083.1
42	1882.2	1541.1	1014.7	1060.4	1085.9	1016.6
43	2633.7	1368.4	906.9	893.1	1089.7	1035.8
44	792.1	9215.8	904.9	876.0	1076.3	1009.5
45	7897.2	3819.1	900.6	850.8	1075.9	1007.0
46	528.0	702.8	940.6	904.0	1083.9	1031.0
47	596.1	656.5	1040.6	994.9	1078.5	1054.2
48	1218.3	1377.3	1155.9	1150.0	1148.7	1136.3
49	535.0	1657.6	1147.1	1142.1	1173.7	1161.6
50	1074.4	1910.5	1135.0	1132.2	1177.4	1166.6
51	2430.5	8468.0	1083.2	1084.1	1144.9	1140.5
52	3556.8	5516.7	1090.8	1089.3	1148.5	1138.0
53	1502.8	1515.9	1030.5	1051.5	1047.6	1049.7
54	3975.9	2353.1	992.7	1027.8	1054.8	1004.7
55	6259.4	20937.3	964.8	1040.3	946.5	963.1
56	4908.7	3752.1	869.6	996.6	832.5	799.6
57	8971.5	10354.9	858.3	984.8	880.3	782.7
58	8928.0	266.7	978.1	1016.6	922.1	932.9
59	2873.2	557.4	984.6	1055.0	935.1	908.4
60	3356.9	550.4	824.5	906.9	1010.3	871.3
61	1895.8	11858.3	888.0	863.4	1031.5	970.7
62	5538.6	6527.6	918.9	894.1	954.6	977.3
63	6726.1	19394.7	950.3	945.0	991.3	1033.5
64	3942.2	19426.5	929.6	915.9	978.3	1043.7
65	6784.4	15916.3	1120.6	1116.9	1005.8	1139.7
66	1654.1	1389.3	1108.7	1126.3	995.7	1103.9
67	3499.4	4547.5	1067.3	1115.2	1110.8	1087.5
68	7072.5	8731.4	1084.8	1121.9	1118.0	1103.6
69	978.9	2338.4	1088.9	1075.1	1111.2	1081.4
70	3568.5	2223.3	1086.6	1082.7	1028.5	1065.2
71	5528.4	4074.2	1022.7	1047.1	1014.4	1041.1
72	6840.9	7972.0	1002.2	903.1	1063.5	1085.0
73	5068.8	17559.9	1085.8	955.6	1080.9	1068.3
74	8345.7	13926.6	1050.8	946.5	1083.8	1046.8
75	446.9	13649.3	1013.9	942.1	1079.0	1025.6
76	1923.8	10235.7	1011.0	965.1	1135.5	1023.1
77	1472.7	3043.3	1148.3	1139.3	1123.5	1110.0
78	223.0	2038.1	1167.3	1147.3	1115.7	1099.9
79	1121.5	2222.6	1143.0	1144.5	1139.8	1149.5
80	1892.5	2554.8	1115.1	1138.6	1160.3	1148.6

Measurements of area between channel centerlines and straight-line distance…(continued).

Box number	*Lateral movement area 2020 (m^2)*	*Lateral movement area 1996-7 (m^2)*	*Straight-line distance 2017 (m)*	*Straight-line distance 2020 (m)*	*Straight-line distance 1994 (m)*	*Straight-line distance 1998 (m)*
81	11512.6	4895.3	1070.8	1107.5	1128.4	1122.8
82	11592.6	8166.5	1036.8	1082.3	1102.1	1099.1
83	4059.0	1673.7	1020.1	1057.8	1095.0	1089.5
84	1611.1	842.1	1072.5	1108.6	1116.1	1123.1
85	2348.5	1534.3	1107.4	1166.5	1140.0	1150.5
86	1720.2	345.7	1129.6	1107.3	1115.0	1127.0
87	2360.0	1318.1	996.2	968.4	1019.3	984.9
88	3555.3	5159.7	976.0	938.7	1007.2	955.2
89	6802.5	2956.5	1004.8	983.1	1049.9	1006.9
90	3547.9	1847.7	937.3	958.3	988.7	951.1
91	427.6	192.1	992.4	985.1	1028.2	1027.1
92	4737.1	734.7	1023.7	1039.3	1100.5	1076.5
93	5839.1	3199.7	1100.2	1047.1	1138.1	1111.1
94	2580.6	1954.9	1113.7	1041.8	1175.1	1148.3
95	3674.3	1582.3	1086.2	1015.3	1111.7	1128.0
96	5441.8	3200.7	1057.6	1015.9	1088.8	1114.8
97	4940.8	9670.7	1052.1	1047.3	1095.2	1140.8
98	5230.6	6717.3	1054.6	1075.4	1082.6	1126.5
99	6218.4	862.7	1043.9	1048.6	967.4	1116.1
100	9838.2	3950.7	965.8	1055.3	944.1	1087.7
101	8648.2	17605.8	871.5	998.7	1045.8	1095.9
102	21776.2	17450.1	903.3	949.9	1038.8	1093.9
103	27641.8	2660.1	932.2	928.0	1029.7	1098.9
104	7908.4	3144.7	974.1	1028.2	1101.6	1103.3
105	4593.0	857.5	1137.8	1056.8	1141.1	1119.7
106	2520.1	3322.4	1159.1	1122.1	1130.3	1156.8
107	2665.8	3258.5	1131.5	1160.0	1126.7	1166.3
108	8897.9	8189.4	1123.1	1161.6	1125.3	1153.9
109	17073.0	7074.8	1118.4	1140.0	1114.8	1150.0
110	3355.2	2903.8	1003.5	1090.5	1034.7	1130.6
111	1574.2	4306.5	963.8	1081.1	1059.2	1071.9
112	16481.9	9442.8	1013.4	1086.5	1062.3	1096.2
113	2036.8	17362.2	987.6	1045.7	1037.2	1071.7
114	1750.0	5312.0	876.1	990.1	980.7	983.5
115	3210.9	9480.6	1025.8	1066.3	1063.5	944.8
116	3659.5	5033.6	990.7	1101.2	1059.0	1066.8
117	10233.2	2154.3	1026.1	1143.3	1115.5	1102.8
118	6559.0	1703.5	1044.0	1139.0	1068.7	1116.6
119	29135.5	7395.0	1042.9	1103.9	1068.7	1045.9

Measurements of area between channel centerlines and straight-line distance…(continued).

Box number	*Lateral movement area 2020 (m^2)*	*Lateral movement area 1996-7 (m^2)*	*Straight-line distance 2017 (m)*	*Straight-line distance 2020 (m)*	*Straight-line distance 1994 (m)*	*Straight-line distance 1998 (m)*
120	6459.6	9641.7	1049.7	1085.6	1032.8	1048.0
121	18566.5	60771.2	1058.8	1021.6	922.2	1026.1
122	9108.3	79107.9	1045.0	986.0	959.3	952.8
123	14319.2	48542.3	1058.1	954.1	1029.4	914.1
124	13433.8	4609.2	979.4	923.3	1115.1	864.8
125	13350.9	16654.8	868.5	905.9	1104.8	808.6
126	34261.8	5680.4	871.0	1032.7	1072.4	939.6
127	6961.3	2094.5	856.2	967.4	1042.7	906.8
128	5848.4	4679.5	751.2	741.0	911.3	901.4
129	29023.3	6708.4	909.6	832.0	783.5	722.8
130	2181.9	6131.9	992.2	934.3	880.0	824.3
131	4403.8	5775.7	987.9	924.8	849.0	820.1
132	2442.6	360.4	1136.3	1123.3	950.3	930.7
133	172.6	236.8	1147.9	1168.6	1082.7	1107.5
134	715.4	667.8	1164.0	1166.3	1177.8	1166.0
135	323.8	1245.4	1167.1	1167.2	1188.7	1180.6
136	1041.5	1408.2	1161.2	1173.0	1189.8	1181.6
137	6931.5	510.7	1162.4	1171.8	1192.4	1183.4
138	1637.5	344.0	1159.1	1171.9	1192.6	1185.5
139	435.7	745.0	1150.5	1172.3	1192.8	1186.3
140	1040.8	827.1	1145.2	1175.3	1192.0	1183.6
141	1272.0	845.2	1143.4	1161.1	1191.5	1179.2
142	869.5	680.0	1146.8	1156.3	1186.5	1179.4
143	1116.3	1415.7	1150.1	1158.9	1183.8	1178.2
144	1010.4	360.4	1156.3	1154.0	1163.4	1165.9
145	787.5	3835.2	1125.8	1150.5	1162.8	1158.5
146	4116.9	6244.9	1122.6	1124.7	1158.5	1153.3
147	5812.6	11588.1	1102.1	1094.6	1152.8	1120.1
148	4693.3	3320.2	1056.5	1058.7	1148.4	1108.9
149	3037.1	3184.2	1004.8	1004.0	1141.9	1072.5
150	1523.0	21347.2	979.2	963.6	1097.1	1059.2
151	628.5	6680.9	948.7	971.7	1065.6	1013.8
152	971.5	4471.7	930.6	1036.6	1083.5	1052.0
153	6047.8	7202.2	1021.5	1107.9	1097.6	1107.3
154	6875.6	1315.1	1000.9	1093.8	1118.2	1099.4
155	2300.9	1442.7	1000.9	1104.8	1119.5	1093.3
156	760.2	3787.3	1010.7	1081.5	1113.8	1083.8
157	814.4	1253.3	1067.2	1075.0	1111.7	1086.3

Control variable values for each box before the 2020 flood.

Box number	*Bare cover (%)*	*Grass cover (%)*	*Tree cover (%)*	*SI*	*Slope (mm^{-1})*	*CI*	*Active channel width (m)*
2	28	14	46	1.233	0.0080	11.8	85.1
3	41	12	29	1.203	0.0063	6.5	50.5
4	37	18	13	1.198	0.0096	8.9	43.9
5	41	13	3	1.170	0.0061	10.6	36.4
6	10	8	10	1.151	0.0039	12.3	31.9
7	14	5	28	1.119	0.0062	12.5	33.9
8	40	3	22	1.115	0.0056	13.5	35.1
9	15	12	26	1.165	0.0038	12.7	27.1
10	23	2	25	1.196	0.0037	10.9	38.7
11	51	1	13	1.173	0.0064	8.6	52.5
12	51	7	16	1.204	0.0051	7.1	54.2
13	35	10	35	1.219	0.0078	4.4	68.1
14	36	11	40	1.163	0.0110	4.8	161.9
15	12	44	15	1.136	0.0082	5.7	53.8
16	16	10	21	1.122	0.0044	11.3	30.5
17	25	4	18	1.120	0.0048	12.3	38.4
18	46	7	24	1.131	0.0047	11.1	51.0
19	30	16	35	1.198	0.0075	12.6	58.9
20	36	6	26	1.231	0.0077	13.7	32.4
21	16	5	18	1.244	0.0040	13.2	30.6
22	20	18	26	1.237	0.0046	12.1	48.5
23	26	10	36	1.209	0.0047	9.5	39.2
24	24	26	28	1.203	0.0067	8.5	74.0
25	21	18	47	1.195	0.0078	9.1	79.1
26	7	9	31	1.194	0.0052	11.0	23.9
27	18	4	20	1.100	0.0035	14.1	31.6
28	13	4	28	1.190	0.0047	10.0	38.8
29	30	22	21	1.187	0.0042	8.4	52.9
30	30	19	28	1.164	0.0072	9.0	51.7
31	10	32	26	1.145	0.0059	10.8	37.1
32	28	4	30	1.221	0.0061	9.0	33.3
33	49	8	17	1.227	0.0066	7.4	78.3
34	15	13	45	1.285	0.0064	6.3	67.4
35	31	15	30	1.280	0.0068	7.1	60.1
36	20	8	32	1.251	0.0069	7.8	38.4
37	32	8	13	1.149	0.0057	8.7	33.4
38	41	5	9	1.123	0.0058	7.4	40.7
39	30	9	24	1.163	0.0066	5.6	51.4
40	10	31	23	1.157	0.0047	5.4	59.7
41	34	20	18	1.130	0.0061	7.1	49.9
42	12	30	26	1.183	0.0051	10.7	29.4

Control variable values for each box before the 2020 flood (continued).

Box number	*Bare cover (%)*	*Grass cover (%)*	*Tree cover (%)*	*SI*	*Slope (mm^{-1})*	*CI*	*Active channel width (m)*
43	38	5	15	1.323	0.0051	13.0	36.6
44	37	33	13	1.326	0.0056	14.5	60.2
45	45	18	16	1.332	0.0030	15.9	49.1
46	24	6	12	1.276	0.0099	18.9	36.0
47	17	7	18	1.153	0.0048	19.9	28.9
48	24	8	22	1.038	0.0055	21.6	30.9
49	2	37	6	1.046	0.0036	19.8	21.7
50	8	20	3	1.057	0.0033	17.5	29.1
51	18	4	28	1.108	0.0043	14.3	35.2
52	40	8	15	1.100	0.0060	10.7	34.3
53	47	27	4	1.165	0.0068	7.3	58.8
54	33	29	23	1.209	0.0023	3.5	86.3
55	23	19	53	1.244	0.0045	3.8	235.3
56	31	19	27	1.380	0.0073	4.4	54.9
57	41	9	18	1.398	0.0059	8.8	60.3
58	61	12	6	1.227	0.0056	9.4	62.4
59	28	8	18	1.219	0.0051	11.0	37.9
60	13	5	19	1.455	0.0050	13.0	31.0
61	32	25	18	1.351	0.0020	10.5	36.8
62	39	4	41	1.306	0.0058	9.1	57.5
63	7	18	57	1.263	0.0069	8.6	35.7
64	14	18	33	1.291	0.0037	9.4	35.7
65	38	6	33	1.071	0.0072	9.6	40.2
66	16	1	21	1.082	0.0036	9.2	30.1
67	7	3	29	1.124	0.0035	7.7	34.4
68	36	7	20	1.106	0.0045	4.6	48.6
69	60	3	7	1.102	0.0051	4.4	86.7
70	37	11	21	1.104	0.0053	5.4	34.3
71	32	3	24	1.173	0.0060	8.2	45.2
72	39	26	8	1.197	0.0041	7.3	55.9
73	21	41	26	1.105	-0.0016	7.0	58.9
74	26	34	25	1.142	0.0076	8.2	43.4
75	17	37	14	1.184	0.0040	10.3	29.2
76	0	6	4	1.187	0.0046	12.1	34.9
77	25	13	4	1.045	0.0035	8.9	32.4
78	36	38	4	1.028	0.0036	6.6	67.0
79	32	47	6	1.050	0.0043	4.8	77.3
80	49	11	11	1.076	0.0048	3.5	53.6
81	26	42	10	1.121	0.0037	2.8	86.0
82	18	29	31	1.157	0.0075	3.0	104.9
83	20	16	23	1.176	0.0093	3.8	44.4

Control variable values for each box before the 2020 flood (continued).

Box number	*Bare cover (%)*	*Grass cover (%)*	*Tree cover (%)*	*SI*	*Slope (mm^{-1})*	*CI*	*Active channel width (m)*
84	12	28	16	1.119	0.0064	6.7	28.9
85	1	18	17	1.084	0.0037	9.8	27.7
86	0	27	10	1.062	0.0022	12.5	28.2
87	0	30	9	1.205	0.0030	11.1	33.7
88	22	39	4	1.230	0.0040	8.2	48.0
89	46	12	14	1.194	0.0055	7.2	54.6
90	34	11	20	1.280	0.0056	9.7	40.3
91	0	8	13	1.209	0.0031	13.2	27.6
92	8	39	8	1.172	0.0035	15.5	49.9
93	17	19	21	1.091	0.0037	11.9	42.6
94	18	53	6	1.077	0.0040	10.8	70.4
95	27	35	12	1.105	0.0063	9.3	47.8
96	20	44	15	1.135	0.0042	9.7	33.2
97	24	36	15	1.141	0.0039	11.8	41.3
98	11	31	12	1.138	0.0062	13.7	30.6
99	12	51	11	1.150	0.0041	12.9	32.3
100	30	36	16	1.243	0.0046	11.5	64.9
101	25	40	15	1.377	0.0043	10.6	61.5
102	34	39	2	1.328	0.0048	8.6	59.4
103	18	31	39	1.287	0.0075	9.3	122.3
104	30	16	3	1.232	0.0018	9.5	48.1
105	34	26	8	1.055	0.0057	8.8	43.6
106	24	20	40	1.035	0.0033	4.8	129.8
107	31	30	31	1.061	0.0053	4.0	222.9
108	27	21	41	1.068	0.0047	4.2	104.8
109	36	33	18	1.073	0.0049	6.5	61.8
110	17	44	19	1.196	0.0055	6.7	50.0
111	45	34	8	1.245	0.0043	6.3	75.3
112	42	22	20	1.184	0.0068	3.6	64.4
113	23	56	15	1.215	0.0061	4.3	211.9
114	22	15	22	1.370	0.0037	4.9	42.7
115	41	21	14	1.170	0.0049	10.4	66.9
116	44	1	12	1.211	0.0038	9.8	53.4
117	36	19	30	1.170	0.0052	13.0	75.3
118	37	10	29	1.149	0.0041	15.5	47.6
119	15	35	40	1.151	0.0048	14.8	44.4
120	27	50	6	1.143	0.0057	14.3	82.0
121	17	42	28	1.133	0.0036	10.5	62.7
122	40	27	23	1.148	0.0020	8.9	131.7
123	30	32	26	1.134	0.0075	7.6	180.8
124	38	29	17	1.225	0.0050	7.0	130.7

Control variable values for each box before the 2020 flood (continued).

Box number	*Bare cover (%)*	*Grass cover (%)*	*Tree cover (%)*	*SI*	*Slope (mm^{-1})*	*CI*	*Active channel width (m)*
125	33	39	14	1.382	0.0087	8.2	219.6
126	27	15	41	1.378	0.0061	10.6	135.9
127	20	42	6	1.402	0.0053	18.3	64.1
128	17	55	3	1.598	0.0005	25.7	42.6
129	32	34	19	1.319	0.0065	27.6	75.8
130	20	37	18	1.209	0.0044	26.5	54.2
131	18	30	16	1.215	0.0036	31.6	52.1
132	24	2	22	1.056	0.0104	33.1	43.7
133	48	1	11	1.045	0.0070	38.5	47.7
134	6	1	15	1.031	0.0054	39.0	35.8
135	26	15	7	1.028	0.0058	41.2	39.1
136	22	6	13	1.033	0.0036	33.5	40.3
137	49	10	1	1.032	0.0057	33.7	60.8
138	19	16	19	1.035	0.0069	32.7	37.5
139	18	17	30	1.043	0.0060	35.8	40.5
140	30	3	18	1.048	0.0044	31.5	42.9
141	13	0	14	1.050	0.0054	27.4	46.9
142	20	0	14	1.046	0.0090	23.7	41.6
143	22	0	28	1.043	0.0089	26.8	46.9
144	17	0	10	1.038	0.0056	30.8	36.0
145	13	5	7	1.066	0.0048	32.1	40.6
146	26	20	7	1.069	0.0043	23.5	49.7
147	39	31	9	1.089	0.0031	21.3	74.2
148	24	27	17	1.136	0.0051	21.7	38.3
149	20	15	11	1.194	0.0024	24.8	34.1
150	29	38	8	1.225	0.0032	25.6	44.3
151	28	33	3	1.265	0.0077	21.7	27.7
152	37	22	2	1.289	0.0029	14.2	42.9
153	41	45	0	1.175	0.0002	11.1	86.6
154	20	31	14	1.199	0.0071	9.3	37.1
155	23	4	14	1.199	0.0061	10.9	45.9
156	22	2	27	1.187	0.0062	11.7	47.6
157	28	24	18	1.124	0.0041	14.4	32.0

Control variable values for each box before the 1996-7 floods.

Box number	*SI*	*CI*	*Active channel width (m)*
2	1.072	8.1	163.0
3	1.067	3.7	89.7
4	1.095	6.1	63.9
5	1.072	7.7	38.7
6	1.067	6.6	51.6
7	1.050	6.0	100.8
8	1.042	5.4	59.5
9	1.062	4.8	77.7
10	1.073	4.4	131.8
11	1.092	4.3	83.7
12	1.176	5.5	72.7
13	1.180	4.7	67.1
14	1.166	3.4	127.2
15	1.135	3.0	205.3
16	1.091	3.3	135.7
17	1.021	4.9	81.3
18	1.025	6.5	82.4
19	1.051	7.1	90.3
20	1.051	6.0	81.1
21	1.128	4.6	109.2
22	1.114	3.9	130.2
23	1.126	4.1	130.1
24	1.144	5.3	113.3
25	1.150	7.6	62.0
26	1.111	11.4	35.0
27	1.094	10.2	32.0
28	1.129	8.0	62.8
29	1.203	6.3	58.7
30	1.197	6.9	71.3
31	1.183	7.7	54.0
32	1.271	8.7	46.3
33	1.312	8.9	53.5
34	1.290	8.1	49.7
35	1.247	7.1	56.2
36	1.170	5.1	60.4
37	1.142	4.5	84.5
38	1.125	4.1	71.3
39	1.099	4.6	66.8
40	1.095	4.1	47.0
41	1.084	5.3	100.0
42	1.105	7.1	38.9
43	1.101	14.1	36.4

Control variable values for each box before the 1996-7 floods (continued).

Box number	*SI*	*CI*	*Active channel width (m)*
44	1.115	16.7	41.0
45	1.115	12.1	49.5
46	1.107	10.9	100.3
47	1.113	10.1	48.3
48	1.045	10.3	39.9
49	1.022	7.5	83.7
50	1.019	6.4	92.2
51	1.048	5.8	58.0
52	1.045	7.0	93.8
53	1.145	6.6	44.5
54	1.138	6.9	60.5
55	1.268	6.1	90.8
56	1.441	7.2	84.4
57	1.363	9.7	36.5
58	1.301	12.8	39.1
59	1.283	11.8	42.6
60	1.188	8.4	40.7
61	1.163	6.0	80.7
62	1.257	4.7	96.5
63	1.210	4.5	72.0
64	1.227	3.5	79.3
65	1.193	3.8	151.7
66	1.205	4.1	38.3
67	1.080	7.5	44.5
68	1.073	5.7	33.3
69	1.080	3.9	56.8
70	1.167	3.8	102.6
71	1.183	5.0	76.5
72	1.128	5.8	42.3
73	1.110	5.8	82.9
74	1.107	4.1	66.6
75	1.112	4.0	114.8
76	1.057	3.8	93.7
77	1.068	4.6	99.9
78	1.076	5.4	67.1
79	1.053	4.8	46.8
80	1.034	3.7	82.1
81	1.063	2.7	81.7
82	1.089	3.4	88.3
83	1.096	4.0	37.7
84	1.075	5.5	42.1
85	1.053	6.5	43.0

Control variable values for each box before the 1996-7 floods (continued).

Box number	*SI*	*CI*	*Active channel width (m)*
86	1.076	8.0	42.1
87	1.177	7.9	55.5
88	1.191	7.1	57.8
89	1.143	7.4	45.9
90	1.214	11.0	35.0
91	1.167	12.8	27.7
92	1.090	9.4	59.6
93	1.054	6.8	110.3
94	1.021	5.9	117.1
95	1.079	4.4	65.4
96	1.102	3.4	138.4
97	1.096	2.7	140.6
98	1.108	1.8	182.1
99	1.240	2.0	487.9
100	1.271	2.6	159.7
101	1.147	5.2	65.5
102	1.155	6.2	156.9
103	1.165	7.0	112.7
104	1.089	11.0	35.0
105	1.052	10.5	37.0
106	1.062	5.4	112.6
107	1.065	4.0	199.8
108	1.066	4.2	144.7
109	1.076	6.2	48.0
110	1.160	9.5	34.9
111	1.133	8.1	48.9
112	1.130	6.4	62.7
113	1.157	7.2	83.5
114	1.224	8.7	47.0
115	1.128	12.2	51.9
116	1.133	13.6	39.7
117	1.076	15.2	49.2
118	1.123	11.5	62.0
119	1.123	11.5	114.2
120	1.162	7.9	47.4
121	1.301	4.9	181.2
122	1.251	3.9	360.2
123	1.166	4.1	320.0
124	1.076	6.1	155.3
125	1.086	9.9	137.4
126	1.119	14.1	108.4
127	1.151	18.2	70.2

Control variable values for each box before the 1996-7 floods (continued).

Box number	*SI*	*CI*	*Active channel width (m)*
128	1.317	25.1	66.1
129	1.532	24.4	50.5
130	1.364	28.2	78.3
131	1.413	30.1	42.2
132	1.263	39.0	37.2
133	1.108	42.1	42.1
134	1.019	41.3	37.1
135	1.010	39.3	36.6
136	1.009	35.1	47.1
137	1.006	34.8	50.0
138	1.006	35.9	37.1
139	1.006	36.3	39.3
140	1.007	30.1	42.7
141	1.007	24.8	54.6
142	1.011	19.9	48.3
143	1.014	23.4	58.7
144	1.031	26.8	35.9
145	1.032	26.5	47.4
146	1.036	16.3	69.6
147	1.041	10.5	120.3
148	1.045	8.8	138.8
149	1.051	7.3	101.3
150	1.094	7.2	155.4
151	1.126	7.2	120.2
152	1.108	7.7	72.3
153	1.093	8.6	95.4
154	1.073	8.0	47.3
155	1.072	8.5	55.0
156	1.077	7.4	65.7
157	1.079	8.6	79.4

Measurements of wetted channel area before and after flooding.

Box number	*Wetted channel area in 2017 (m^2)*	*Wetted channel area in 2020 (m^2)*	*Wetted channel area in 1994 (m^2)*	*Wetted channel area in 1998 (m^2)*
2	3755.5	2372.5	3269.6	5140.3
3	4255.2	4807.6	6433.8	6050.9
4	3688.7	3593.3	3714.3	3349.6
5	2330.8	2045.4	4402.5	2298.6
6	5139.1	5337.9	6689.6	3324.7
7	5426.6	5074.0	6877.3	4001.6
8	3926.4	3998.9	3835.6	2882.1
9	3660.9	5295.0	5366.5	5771.7
10	5738.0	4666.8	5832.3	6134.8
11	3441.1	2873.6	3179.6	3351.1
12	4516.0	5452.3	6125.3	7613.9
13	4569.9	4938.8	8039.7	6016.6
14	5399.9	5919.8	12659.4	6952.1
15	3337.4	2503.9	4237.8	2982.0
16	3798.4	3423.2	4878.8	4367.7
17	6869.6	9510.1	8636.7	9749.2
18	3702.8	5723.7	7484.4	5438.6
19	2802.9	2794.6	5644.3	4317.9
20	4425.7	4718.9	7276.0	8848.8
21	6942.2	6870.5	7333.6	8385.9
22	5931.8	4603.9	8761.3	8062.7
23	4847.0	6548.4	9959.4	11625.2
24	5767.1	7232.5	4395.9	4625.7
25	3523.8	5548.8	6540.9	5941.4
26	4532.2	4346.6	7314.4	4944.2
27	4463.2	5948.7	5420.1	5769.1
28	8124.2	8171.6	7880.4	9749.7
29	4653.0	6414.0	4511.2	5807.6
30	4333.4	6796.7	5281.1	6843.3
31	5909.2	4923.0	8327.2	5623.7
32	3048.1	3362.5	5506.2	4049.9
33	6087.7	3700.6	9287.3	4487.1
34	4846.9	3331.4	6577.7	5282.5
35	2696.5	3432.0	6086.8	2903.4
36	5069.8	4632.6	8925.4	4186.9
37	4890.0	6157.9	7175.0	5401.0
38	4390.8	8104.5	6588.6	5453.0
39	4929.6	6194.5	5365.2	5691.2
40	3819.3	3196.5	2395.4	4210.2
41	4852.0	3408.0	4855.3	4471.6
42	4739.2	4839.3	7192.2	5091.8

Measurements of wetted channel area before and after flooding (continued).

Box number	*Wetted channel area in 2017 (m^2)*	*Wetted channel area in 2020 (m^2)*	*Wetted channel area in 1994 (m^2)*	*Wetted channel area in 1998 (m^2)*
43	2388.6	4208.9	4529.5	2726.1
44	3540.3	8051.1	5966.7	3981.2
45	6291.4	7899.0	8721.9	7795.4
46	4410.3	5250.2	6156.8	4555.7
47	3803.3	4584.2	4921.5	3528.6
48	4398.1	4592.4	7326.5	3169.0
49	4287.8	3367.3	4797.1	2785.3
50	5779.0	6904.5	6667.7	5816.9
51	4449.6	3178.7	2926.9	2859.8
52	4534.0	5197.8	7159.4	4556.6
53	3826.5	6133.8	8767.9	7873.4
54	2942.5	5473.4	4581.0	5358.6
55	2435.2	2411.9	8747.9	4390.8
56	5558.2	5005.5	7785.8	5124.1
57	6918.0	4274.9	10850.2	7002.0
58	4254.9	4179.0	6735.7	4475.5
59	2392.6	3013.1	3490.2	2110.2
60	5594.3	4367.3	6131.3	6292.4
61	3695.1	4111.3	7364.8	6603.8
62	5185.7	5049.9	6548.6	4357.2
63	6725.8	4868.3	8908.6	5870.6
64	4458.0	2717.0	9801.3	5609.3
65	3739.0	4069.5	5598.3	4159.8
66	4587.4	2941.4	5344.2	4875.3
67	5516.5	5018.5	7836.3	4191.7
68	5214.4	4012.6	7183.2	4583.4
69	5558.6	2976.0	8364.7	5957.6
70	4291.6	4409.3	6941.9	4769.9
71	4598.2	4223.9	7622.0	5893.8
72	3152.9	4093.8	5816.1	4998.4
73	3729.3	7332.0	10368.7	5918.9
74	5518.9	10309.4	5725.3	7078.4
75	3672.2	3327.7	6481.1	3029.7
76	8028.9	4388.3	7620.8	4708.7
77	4983.2	7330.8	5206.9	6734.6
78	3163.9	5807.4	6205.0	5137.6
79	3182.8	6806.5	4757.6	5044.7
80	3730.3	5653.9	6660.1	5143.4
81	3653.5	4987.4	7273.2	5405.5
82	5978.4	3485.9	7058.1	6263.3
83	6022.7	4889.0	8200.5	6227.7

Measurements of wetted channel area before and after flooding (continued).

Box number	*Wetted channel area in 2017 (m^2)*	*Wetted channel area in 2020 (m^2)*	*Wetted channel area in 1994 (m^2)*	*Wetted channel area in 1998 (m^2)*
84	3939.3	4057.3	7562.0	6924.3
85	5425.6	5733.3	7926.0	6705.0
86	4855.5	5005.6	6280.7	3792.0
87	3935.6	4388.0	3652.9	4339.7
88	9014.2	8829.2	13890.6	6832.8
89	5711.4	8635.8	10514.3	6941.7
90	6524.4	8607.5	9759.7	7932.6
91	6038.8	5731.8	6230.4	5203.4
92	3290.1	2820.6	6264.2	4299.3
93	6351.4	3795.6	9903.3	4606.9
94	4114.4	4897.4	7598.2	4119.7
95	4282.5	3709.7	5974.9	4634.9
96	4219.6	5431.5	9380.4	5413.5
97	6747.0	3947.9	6419.3	3947.7
98	4140.7	2060.2	6189.5	3354.7
99	2438.1	881.0	2546.4	1275.6
100	3927.8	2940.0	10829.0	5763.0
101	5598.4	3451.9	12479.2	4067.9
102	8865.9	7689.9	8755.1	5715.4
103	4369.2	5910.8	8476.8	5474.9
104	6496.9	3323.1	7454.9	4149.5
105	3530.6	5203.6	7109.9	5872.0
106	6033.7	11777.7	14782.5	5813.1
107	1394.0	3172.4	6032.5	1388.8
108	3641.9	3523.1	8156.0	3308.8
109	4161.3	5863.1	8613.1	5253.6
110	4163.8	4149.1	6213.4	6666.2
111	2434.1	3888.6	6819.0	4511.6
112	7182.8	6239.4	10143.7	5205.9
113	3026.5	1906.3	6020.2	6409.0
114	6131.0	6815.6	7099.7	4946.9
115	5452.4	9061.7	9614.0	7466.3
116	4410.9	5019.6	5960.0	5377.0
117	2450.4	2797.3	6511.1	4089.8
118	5777.0	7653.4	6605.5	4588.1
119	3621.3	3106.8	6521.1	3321.7
120	2452.6	1966.0	6906.1	3514.9
121	3713.6	5013.2	11034.9	3734.0
122	3264.0	2706.8	10870.8	3077.9
123	3787.9	7430.4	7593.0	9136.4
124	7941.7	3742.9	5832.4	2912.3

Measurements of wetted channel area before and after flooding (continued).

Box number	*Wetted channel area in 2017 (m^2)*	*Wetted channel area in 2020 (m^2)*	*Wetted channel area in 1994 (m^2)*	*Wetted channel area in 1998 (m^2)*
125	4975.3	3225.5	3583.5	3608.2
126	7312.0	6186.4	6066.5	3577.6
127	7294.3	6365.3	9647.2	7213.8
128	5128.6	3494.2	6784.1	4236.1
129	7769.8	8783.3	7895.2	3387.1
130	4234.1	4362.4	9015.5	5855.5
131	8699.7	5804.8	9908.6	10492.8
132	6160.5	7331.5	7996.3	5895.7
133	3233.7	2966.1	4085.5	3079.9
134	7593.9	7593.5	8420.2	7038.0
135	4929.4	5228.6	6946.7	4977.4
136	6372.6	8500.3	10744.2	6696.3
137	4713.1	7392.0	8860.6	6963.7
138	6291.1	9224.7	7194.6	6023.9
139	5163.8	5774.5	7753.4	5553.7
140	4898.8	6164.7	8077.8	7165.4
141	8281.0	9529.4	11497.3	9618.8
142	5933.0	6875.3	8273.3	7175.0
143	5607.0	6341.9	8813.2	4728.6
144	5271.0	5636.2	5319.6	4299.8
145	6354.5	7241.6	7226.9	5831.9
146	5291.2	4391.7	6561.5	5714.9
147	3765.3	4115.6	5053.2	6130.5
148	3278.2	4269.6	7136.9	6050.1
149	6831.2	6524.8	9293.2	7375.9
150	5459.4	5052.2	8205.3	4215.3
151	3540.1	3679.2	8313.5	4244.0
152	4062.4	5509.0	9407.9	3991.8
153	2849.4	5387.3	11656.3	5244.2
154	7003.6	5974.3	9127.2	7300.8
155	6992.3	8043.8	12250.8	9284.4
156	5641.0	4335.6	13334.2	5692.2
157	2561.9	2631.5	7097.7	2651.1

Measurements of bar area before and after flooding.

Box number	*Bar area in 2017 (m^2)*	*Bar area in 2020 (m^2)*	*Bar area in 1994 (m^2)*	*Bar area in 1998 (m^2)*
2	3768.1	9784.8	2184.8	2847.6
3	9597.9	13547.1	3051.3	1207.1
4	3905.6	6814.9	4833.0	7380.2
5	2574.8	2659.2	735.4	3061.9
6	984.8	333.3	3181.3	4053.0
7	2897.8	3034.7	2515.4	7718.1
8	5062.1	6415.3	0.0	3707.6
9	1445.5	1966.7	0.0	3995.5
10	3355.6	5909.8	0.0	1659.3
11	5328.5	4365.5	42.7	3060.7
12	6952.1	5732.0	3142.6	7305.2
13	8703.4	12941.7	625.0	18782.8
14	13586.8	8920.2	3340.5	2429.2
15	1083.8	1999.0	0.0	1830.4
16	1370.8	4002.3	0.0	4182.7
17	5498.1	3920.9	396.9	11593.5
18	7813.8	7485.4	4801.2	6718.8
19	2320.1	2790.5	465.4	11710.0
20	2937.7	5062.3	5372.9	2385.3
21	1969.1	3185.7	1119.8	11282.0
22	3037.3	4913.4	9993.8	7914.3
23	4155.1	4313.2	7455.1	10193.4
24	1901.7	12732.3	18472.8	8884.6
25	3446.0	10783.0	7883.0	1679.1
26	1097.7	3925.0	213.3	1411.1
27	1554.0	827.4	827.4	4276.1
28	2226.2	4933.7	845.4	12329.8
29	1439.0	6049.7	7619.5	8133.5
30	5132.4	19584.7	10073.1	14965.5
31	2500.3	12523.0	8216.4	3393.8
32	2277.7	4081.7	2632.3	6391.0
33	2907.9	9490.9	4973.1	2391.3
34	3401.2	12370.7	4519.3	3578.4
35	1295.9	5962.7	2482.3	5142.1
36	2774.2	5827.8	559.7	4151.5
37	4150.6	2550.8	0.0	3189.7
38	4234.1	641.1	0.0	3244.5
39	2801.0	5528.6	0.0	3997.5
40	564.9	4000.2	0.0	4813.4
41	6106.5	10138.7	789.4	2118.1
42	2183.7	9030.5	0.0	2351.1

Measurements of bar area before and after flooding (continued).

Box number	*Bar area in 2017 (m^2)*	*Bar area in 2020 (m^2)*	*Bar area in 1994 (m^2)*	*Bar area in 1998 (m^2)*
43	2416.9	1773.1	316.6	13273.0
44	2822.3	6580.5	2802.1	6291.9
45	12187.2	17648.8	1856.8	4135.2
46	2412.5	1261.8	567.8	5577.8
47	1776.7	956.4	1768.0	7555.4
48	2027.7	2432.3	891.0	8506.9
49	198.4	2175.3	3106.2	1927.4
50	405.7	682.8	0.0	8051.5
51	1944.6	3669.7	0.0	10176.2
52	3540.1	3530.6	0.0	4286.1
53	2845.9	6980.9	2005.2	7602.5
54	3469.8	6774.9	1420.4	8830.9
55	4928.3	10793.4	3730.5	12837.1
56	5101.4	9086.1	6612.1	17431.1
57	6047.1	12001.6	4288.2	304.4
58	3788.0	9361.2	753.8	1337.7
59	1555.4	1752.4	1679.7	4050.0
60	1689.2	3383.2	2420.6	12848.9
61	4494.5	10185.7	10134.6	14200.2
62	12786.9	15173.5	4917.1	20951.0
63	1719.8	8613.2	1686.2	2503.4
64	2355.7	5329.9	2164.4	13120.1
65	7049.5	10641.4	0.0	8096.3
66	1348.2	3419.1	0.0	5690.4
67	1006.1	3242.5	528.6	11710.6
68	6545.0	7909.7	1008.6	3486.6
69	3892.5	12008.6	14.9	2155.8
70	4943.1	7688.9	630.7	6362.6
71	4358.9	6427.5	8413.6	6402.0
72	6082.7	8414.9	1364.0	21529.6
73	6261.2	10852.0	12164.0	18237.2
74	10698.7	19041.3	6100.6	24941.9
75	2190.5	5552.8	0.0	23359.5
76	0.0	3429.0	3993.8	3168.5
77	2150.5	137.2	18054.1	4998.4
78	0.0	2934.3	7240.4	3271.1
79	587.8	8709.0	3921.4	4238.3
80	1761.4	6388.0	1666.2	8485.0
81	721.9	8554.7	3045.7	22747.7
82	2353.4	6502.4	13950.5	7275.8
83	3738.1	2886.5	635.3	1290.2

Measurements of bar area before and after flooding (continued).

Box number	*Bar area in 2017 (m^2)*	*Bar area in 2020 (m^2)*	*Bar area in 1994 (m^2)*	*Bar area in 1998 (m^2)*
84	2156.9	3815.6	1530.2	914.7
85	154.2	2341.5	275.7	3298.3
86	0.0	2358.2	911.5	2267.1
87	0.0	1283.8	2854.7	14499.5
88	6335.6	14265.9	4421.4	9867.0
89	8354.7	7694.6	4986.4	1715.3
90	4802.7	2551.8	907.3	539.3
91	141.8	265.4	0.0	1241.1
92	0.0	3919.9	818.1	12886.2
93	2938.8	10055.3	5011.2	10335.6
94	3967.3	4829.4	1693.0	3816.8
95	5245.1	8518.4	62.7	5121.3
96	4440.8	8870.5	1224.0	3273.3
97	5259.3	9952.9	4552.1	9103.8
98	1401.4	3860.1	5197.4	1361.4
99	1153.6	345.6	82.1	6591.3
100	4944.3	1278.6	2143.3	6712.6
101	3917.8	10146.7	4813.1	8065.9
102	8083.5	9413.1	3952.1	2616.9
103	3621.9	7270.0	506.7	4441.4
104	3116.8	8528.1	0.0	3769.8
105	2666.9	4755.1	0.0	13653.6
106	5553.7	3015.7	1863.3	7672.7
107	4808.1	5698.7	4873.2	9883.4
108	5517.7	7021.0	1462.8	9554.4
109	3226.6	1238.8	2618.6	8391.3
110	1863.0	4258.4	1231.3	6495.1
111	2755.9	7404.7	3031.1	19725.2
112	12009.7	31299.6	13477.1	16372.5
113	1983.9	34864.6	4563.4	10293.5
114	4273.9	7754.2	4595.7	11679.6
115	13196.2	10768.5	5583.6	3867.1
116	5295.0	5452.8	982.3	4045.2
117	8541.8	13827.4	668.9	10391.3
118	9605.8	10509.6	8983.8	11352.5
119	6281.7	7798.9	6030.3	3382.4
120	2677.9	6545.9	4231.8	4056.5
121	3638.2	9725.5	4504.4	5348.5
122	11302.4	1651.8	2121.7	13869.5
123	9602.7	15653.4	9297.5	11367.5
124	11284.5	10716.9	7484.5	17020.3

Measurements of bar area before and after flooding (continued).

Box number	*Bar area in 2017 (m^2)*	*Bar area in 2020 (m^2)*	*Bar area in 1994 (m^2)*	*Bar area in 1998 (m^2)*
125	7853.0	9237.6	12235.9	12380.6
126	8291.4	12846.4	9508.8	5557.1
127	4388.8	15186.5	4322.1	10711.0
128	2627.3	7341.2	1174.0	10146.7
129	10110.4	27820.6	3595.6	17486.5
130	2918.2	5609.9	15811.9	10168.2
131	4843.6	12000.7	8108.2	1477.8
132	3371.9	3431.1	40.4	3099.6
133	3211.2	4312.1	2059.5	270.7
134	516.9	1018.2	0.0	1192.3
135	2265.2	3051.8	0.0	1673.7
136	2934.8	1326.8	0.0	1534.3
137	3680.3	3735.5	132.4	0.0
138	2174.8	2932.1	327.1	0.0
139	3064.9	3433.0	0.0	2052.4
140	3731.7	2024.3	434.2	1113.0
141	2121.0	631.2	0.0	648.9
142	2144.6	1100.2	711.3	0.0
143	2347.1	2539.7	2906.0	0.0
144	1762.0	1580.4	1596.9	1004.7
145	1446.2	1013.2	2138.9	1904.9
146	1417.7	7563.5	8132.1	4410.5
147	5521.6	8830.5	12531.6	731.4
148	4125.9	11918.9	2582.7	3219.9
149	2525.7	4980.7	1179.1	3513.1
150	7603.7	4857.5	296.3	0.0
151	2692.2	2394.7	1024.2	2176.5
152	2097.5	3922.8	6345.9	2608.8
153	1819.2	13417.7	9849.1	1808.2
154	4149.6	8192.2	115.2	1268.5
155	3179.9	2785.9	0.0	966.8
156	2020.1	4243.7	609.5	5499.1
157	1861.9	2904.0	3123.0	7320.8

Change in response variables from the 2020 flood for each box.

Box number	*Change in active channel width (%)*	*Change in bar area (%)*	*Lateral movement (m)*	*Grass cover lost (%)*	*Tree cover lost (%)*	*Change in sinuosity*
2	123	264	109.5	87	32	-0.100
3	96	98	32.5	88	57	-0.135
4	15	145	9.3	73	96	-0.150
5	-5	45	2.3	33	9	-0.117
6	-8	-53	5.0	17	34	-0.085
7	-3	47	11.1	72	44	-0.050
8	55	78	36.3	71	72	-0.051
9	50	91	7.4	86	78	-0.079
10	10	147	8.2	48	63	-0.016
11	2	15	4.7	34	76	0.029
12	9	16	8.6	86	89	0.063
13	12	109	19.9	68	55	0.220
14	-26	-8	31.9	47	32	0.133
15	85	159	2.4	62	63	0.110
16	43	310	2.1	53	78	0.026
17	16	0	3.7	97	48	-0.065
18	49	34	36.8	84	54	-0.103
19	175	69	104.9	84	68	-0.117
20	60	142	16.7	31	72	-0.115
21	16	127	7.7	24	61	-0.134
22	32	127	12.2	66	61	-0.040
23	93	46	24.5	44	33	-0.004
24	35	839	8.3	73	29	0.014
25	42	339	36.0	50	59	-0.014
26	53	402	5.1	67	50	0.070
27	14	-25	5.0	0	69	0.082
28	16	211	16.0	15	79	0.039
29	20	490	21.8	71	3	0.074
30	134	435	42.3	97	87	0.090
31	77	602	33.4	96	78	-0.004
32	31	151	11.0	41	71	-0.054
33	52	358	27.2	45	68	0.005
34	43	410	49.4	79	69	-0.036
35	1	545	34.0	92	77	-0.071
36	41	195	11.7	100	78	-0.038
37	-4	-14	4.0	70	65	0.073
38	2	-79	16.3	53	25	0.026
39	15	177	30.2	82	75	-0.006
40	1	893	25.7	92	49	0.013
41	62	133	19.5	51	37	0.027

Change in response variables from the 2020 flood for each box (continued).

Box number	*Change in active channel width (%)*	*Change in bar area (%)*	*Lateral movement (m)*	*Grass cover lost (%)*	*Tree cover lost (%)*	*Change in sinuosity*
42	92	480	7.6	88	89	-0.051
43	6	3	16.9	67	68	0.020
44	47	227	3.4	70	49	0.044
45	25	103	16.0	64	80	0.078
46	3	-27	2.5	26	32	0.052
47	-1	-24	3.1	47	38	0.053
48	23	68	5.8	92	60	0.005
49	50	1438	2.6	72	57	0.005
50	3	136	4.3	71	24	0.003
51	9	165	12.1	51	66	-0.001
52	11	40	12.4	32	77	0.001
53	1	244	5.7	59	54	-0.023
54	16	174	21.4	75	52	-0.041
55	-10	207	29.8	71	12	-0.090
56	42	150	16.4	39	44	-0.176
57	27	178	35.9	79	75	-0.180
58	17	247	31.6	46	60	-0.046
59	2	58	23.2	30	87	-0.081
60	24	181	16.7	53	60	-0.132
61	56	218	7.6	69	71	0.038
62	65	66	17.0	90	54	0.036
63	305	602	26.9	36	25	0.007
64	46	217	17.7	85	77	0.019
65	63	112	27.9	98	89	0.004
66	7	256	8.3	3	49	-0.017
67	20	352	17.5	14	66	-0.048
68	23	70	32.1	34	71	-0.037
69	-4	333	4.8	49	23	0.014
70	34	118	13.5	83	68	0.004
71	10	107	24.7	22	81	-0.027
72	34	94	38.9	90	58	0.131
73	161	143	25.6	63	16	0.151
74	99	150	18.6	67	27	0.126
75	58	256	2.2	56	15	0.090
76	-3	-	8.4	20	2	0.057
77	0	-91	6.4	50	28	0.008
78	-1	-	1.1	25	7	0.018
79	30	1978	5.6	55	65	-0.001
80	-1	409	8.3	82	31	-0.022
81	-13	1562	50.9	84	80	-0.037

Change in response variables from the 2020 flood for each box (continued).

Box number	*Change in active channel width (%)*	*Change in bar area (%)*	*Lateral movement (m)*	*Grass cover lost (%)*	*Tree cover lost (%)*	*Change in sinuosity*
82	34	288	49.4	14	43	-0.049
83	38	8	18.2	50	15	-0.042
84	40	148	7.4	53	70	-0.036
85	33	2029	10.7	89	70	-0.055
86	56	-	10.3	81	76	0.021
87	44	-	19.3	76	46	0.035
88	57	216	10.6	75	54	0.049
89	-1	29	18.1	69	63	0.026
90	29	-24	11.0	46	74	-0.028
91	3	167	1.9	10	39	0.009
92	20	-	42.0	91	53	-0.018
93	22	389	21.9	93	59	0.055
94	60	74	11.6	47	26	0.074
95	44	132	14.2	76	79	0.077
96	103	185	18.8	80	52	0.047
97	109	170	16.8	31	74	0.005
98	80	293	31.4	81	75	-0.022
99	255	-57	80.7	15	39	-0.005
100	63	-63	49.4	30	47	-0.105
101	47	270	29.1	54	42	-0.175
102	112	66	77.0	82	76	-0.065
103	0	187	91.1	56	38	0.006
104	11	291	35.7	71	33	-0.065
105	18	155	22.9	74	55	0.081
106	3	-22	9.3	44	11	0.034
107	7	69	28.3	48	6	-0.026
108	33	82	38.4	67	38	-0.035
109	106	-45	68.2	54	61	-0.020
110	90	227	15.7	64	27	-0.095
111	11	284	7.6	68	4	-0.135
112	93	272	46.9	61	43	-0.080
113	30	2411	11.5	49	19	-0.068
114	35	159	6.9	84	61	-0.158
115	7	17	10.7	64	52	-0.045
116	12	47	20.9	0	61	-0.122
117	24	131	57.3	100	83	-0.120
118	95	56	26.3	94	85	-0.096
119	297	77	131.6	89	58	-0.064
120	117	249	57.7	81	51	-0.038
121	76	282	71.4	99	90	0.041

Change in response variables from the 2020 flood for each box (continued).

Box number	*Change in active channel width (%)*	*Change in bar area (%)*	*Lateral movement (m)*	*Grass cover lost (%)*	*Tree cover lost (%)*	*Change in sinuosity*
122	51	-79	56.5	87	78	0.069
123	-25	133	34.4	66	42	0.124
124	111	36	76.6	71	25	0.074
125	-18	68	69.3	67	37	-0.057
126	9	121	120.7	52	25	-0.216
127	56	394	28.8	88	36	-0.161
128	147	299	30.2	70	92	0.022
129	36	293	54.4	68	97	0.123
130	62	175	12.1	63	39	0.075
131	65	254	16.6	87	91	0.083
132	17	45	11.3	37	73	0.012
133	0	92	1.1	37	15	-0.018
134	6	181	3.1	1	43	-0.002
135	11	92	1.7	77	33	0.000
136	2	-35	4.4	71	45	-0.010
137	-2	45	37.1	58	18	-0.008
138	85	75	8.2	67	68	-0.011
139	74	45	2.2	26	15	-0.019
140	3	-30	5.2	37	38	-0.027
141	0	-61	5.8	0	45	-0.016
142	0	-33	4.5	34	48	-0.009
143	1	41	5.2	0	35	-0.008
144	3	16	5.2	0	18	0.002
145	7	-9	4.1	99	11	-0.023
146	46	593	19.1	66	84	-0.002
147	47	108	28.7	65	17	0.007
148	114	275	22.6	86	70	-0.002
149	14	156	10.2	76	52	0.001
150	65	-17	5.4	67	25	0.020
151	38	16	2.8	29	4	-0.030
152	15	143	5.0	59	66	-0.132
153	27	858	32.7	89	43	-0.092
154	110	156	27.8	86	60	-0.102
155	1	14	9.6	49	36	-0.113
156	-2	173	3.3	45	24	-0.078
157	52	103	4.9	53	31	-0.008

Change in response variables from the 1996-7 floods for each box.

Box number	*Change in active channel width (%)*	*Change in bar area (%)*	*Lateral movement (m)*	*Change in sinuosity*
2	-17	30	20.5	0.092
3	10	-60	33.2	0.062
4	5	53	16.0	0.047
5	6	316	2.9	0.030
6	25	27	8.7	0.019
7	-38	207	6.7	0.035
8	-18	-	12.8	0.033
9	-6	-	4.2	0.110
10	3	-	12.9	0.084
11	8	7061	22.1	0.108
12	-4	132	14.9	0.033
13	13	2905	22.4	0.211
14	0	-27	91.9	0.103
15	-69	-	4.3	0.074
16	-4	-	2.0	0.055
17	15	2821	1.7	0.089
18	1	40	14.0	0.010
19	9	2416	16.5	0.020
20	7	-56	14.0	0.061
21	-7	907	4.8	0.005
22	-8	-21	52.3	0.023
23	34	37	122.0	-0.015
24	4	-52	32.3	-0.028
25	8	-79	40.0	-0.036
26	2	562	4.5	0.006
27	15	417	3.7	0.017
28	-7	1359	10.4	0.007
29	45	7	26.9	-0.069
30	8	49	46.2	-0.064
31	76	-59	48.6	-0.059
32	11	143	10.8	-0.072
33	-6	-52	13.1	-0.077
34	-31	-21	8.0	-0.019
35	7	107	10.8	0.018
36	-14	642	17.9	-0.012
37	19	-	7.1	0.007
38	14	-	5.2	-0.011
39	-3	-	13.8	0.041
40	6	-	28.2	0.038
41	-15	168	13.5	0.024
42	-9	-	6.5	0.075

Change in response variables from the 1996-7 floods for each box (continued).

Box number	*Change in active channel width (%)*	*Change in bar area (%)*	*Lateral movement (m)*	*Change in sinuosity*
43	0	4093	9.8	0.057
44	79	125	39.0	0.074
45	-15	123	11.4	0.076
46	-58	882	3.3	0.057
47	-2	327	3.4	0.026
48	29	855	6.6	0.011
49	-1	-38	8.0	0.011
50	-9	-	7.6	0.009
51	11	-	47.9	0.004
52	-2	-	20.0	0.010
53	16	279	6.3	-0.002
54	24	522	12.4	0.057
55	39	244	73.3	-0.022
56	-25	164	12.7	0.059
57	53	-93	23.7	0.170
58	-42	77	1.1	-0.015
59	-20	141	5.3	0.038
60	14	431	2.4	0.189
61	7	40	52.7	0.073
62	-18	326	29.4	-0.029
63	37	48	71.6	-0.049
64	70	506	87.7	-0.077
65	-2	-	72.6	-0.140
66	78	-	7.3	-0.118
67	23	2115	23.8	0.023
68	103	246	35.6	0.014
69	-2	14365	8.5	0.030
70	2	909	10.7	-0.040
71	30	-24	20.3	-0.030
72	58	1478	44.6	-0.022
73	78	50	94.4	0.013
74	-43	309	52.7	0.039
75	32	-	69.2	0.058
76	29	-21	41.9	0.116
77	-6	-72	13.2	0.013
78	10	-55	10.2	0.015
79	-10	8	10.6	-0.009
80	-10	409	11.6	0.011
81	-16	647	22.5	0.005
82	55	-48	38.4	0.003
83	49	103	7.0	0.006

Change in response variables from the 1996-7 floods for each box (continued).

Box number	*Change in active channel width (%)*	*Change in bar area (%)*	*Lateral movement (m)*	*Change in sinuosity*
84	-8	-40	4.0	-0.007
85	-12	1096	7.6	-0.010
86	-4	149	2.0	-0.011
87	-8	408	9.9	0.041
88	12	123	15.6	0.065
89	3	-66	8.3	0.049
90	-12	-41	5.9	0.048
91	-7	-	0.9	0.001
92	-17	1475	6.0	0.024
93	-1	106	13.7	0.026
94	0	125	9.3	0.024
95	34	8064	7.1	-0.016
96	6	167	13.0	-0.026
97	15	100	36.5	-0.044
98	17	-74	35.8	-0.043
99	-9	7928	11.6	-0.165
100	-1	213	17.0	-0.168
101	125	68	77.3	-0.052
102	11	-34	79.5	-0.058
103	-5	777	11.0	-0.073
104	8	-	13.9	-0.002
105	38	-	4.4	0.020
106	10	312	12.4	-0.024
107	28	103	35.9	-0.036
108	9	553	34.1	-0.026
109	65	220	28.5	-0.033
110	189	428	13.2	-0.098
111	17	551	21.7	-0.014
112	135	21	41.2	-0.035
113	19	126	60.4	-0.037
114	26	154	20.6	-0.003
115	23	-31	31.5	0.142
116	33	312	28.5	-0.008
117	8	1453	11.9	0.012
118	22	26	6.3	-0.048
119	48	-44	33.8	0.024
120	274	-4	63.4	-0.017
121	134	19	270.7	-0.132
122	35	554	363.0	0.009
123	-54	22	104.0	0.147
124	51	127	29.4	0.311

Change in response variables from the 1996-7 floods for each box (continued).

Box number	*Change in active channel width (%)*	*Change in bar area (%)*	*Lateral movement (m)*	*Change in sinuosity*
125	13	1	91.0	0.398
126	-7	-42	21.4	0.158
127	-31	148	6.9	0.172
128	-17	764	17.1	0.014
129	33	386	30.0	0.129
130	88	-36	20.3	0.092
131	27	-82	11.6	0.050
132	-8	7570	1.7	0.027
133	-5	-87	1.5	-0.025
134	-11	-	2.9	0.010
135	-11	-	6.6	0.007
136	-23	-	6.1	0.007
137	14	-100	2.8	0.008
138	80	-100	1.7	0.006
139	51	-	3.7	0.006
140	11	156	4.2	0.007
141	-11	-	3.9	0.010
142	-4	-100	3.6	0.006
143	-4	-100	7.0	0.005
144	30	-37	1.9	-0.002
145	18	-11	20.2	0.004
146	0	-46	28.3	0.005
147	-15	-94	58.7	0.030
148	-63	25	17.4	0.037
149	-54	198	11.3	0.068
150	-14	-100	88.7	0.039
151	-38	112	33.8	0.058
152	7	-59	23.4	0.033
153	-10	-82	29.9	-0.010
154	-4	1001	6.2	0.018
155	-15	-	6.1	0.026
156	-24	802	16.9	0.030
157	-20	134	8.0	0.025

REFERENCES CITED

Abernethy, B., & Rutherfurd, I. D. (2001). The distribution and strength of riparian tree roots in relation to riverbank reinforcement. *Hydrological Processes*, *15*(1), 63–79. https://doi.org/10.1002/hyp.152

Arnaud-Fassetta, G., Cossart, E., & Fort, M. (2005). Hydro-geomorphic hazards and impact of man-made structures during the catastrophic flood of June 2000 in the Upper Guil catchment (Queyras, Southern French Alps). *Geomorphology*, *66*(1–4), 41–67. https://doi.org/10.1016/j.geomorph.2004.03.014

Baker, V. R. (1977). Stream-channel response to floods, with examples from central Texas. *Geological Society of America Bulletin*, *88*(8), 1057. https://doi.org/10.1130/0016-7606(1977)88<1057:SRTFWE>2.0.CO;2

Baker, V. R., & Costa, J. E. (1987). Flood power. In *Catastrophic Flooding*. Routledge.

Beechie, T. J., Liermann, M., Pollock, M. M., Baker, S., & Davies, J. (2006). Channel pattern and river-floodplain dynamics in forested mountain river systems. *Geomorphology*, *78*(1–2), 124–141. https://doi.org/10.1016/j.geomorph.2006.01.030

Bennett, S. J., Pirim, T., & Barkdoll, B. D. (2002). Using simulated emergent vegetation to alter stream flow direction within a straight experimental channel. *Geomorphology*, *44*(1), 115–126. https://doi.org/10.1016/S0169-555X(01)00148-9

Bertoldi, W., Drake, N. A., & Gurnell, A. M. (2011). Interactions between river flows and colonizing vegetation on a braided river: Exploring spatial and temporal dynamics in riparian vegetation cover using satellite data: INTERACTIONS BETWEEN RIVER FLOWS AND COLONIZING VEGETATION. *Earth Surface Processes and Landforms*, *36*(11), 1474–1486. https://doi.org/10.1002/esp.2166

Bertoldi, W., Zanoni, L., & Tubino, M. (2010). Assessment of morphological changes induced by flow and flood pulses in a gravel bed braided river: The Tagliamento River (Italy). *Geomorphology*, *114*(3), 348–360. https://doi.org/10.1016/j.geomorph.2009.07.017

Buraas, E. M., Renshaw, C. E., Magilligan, F. J., & Dade, W. B. (2014). Impact of reach geometry on stream channel sensitivity to extreme floods. *Earth Surface Processes and Landforms*, *39*(13), 1778–1789. https://doi.org/10.1002/esp.3562

Church, M. (1983). Pattern of Instability in a Wandering Gravel Bed Channel. In J. D. Collinson & J. Lewin (Eds.), *Modern and Ancient Fluvial Systems* (1st ed., pp. 169–180). Wiley. https://doi.org/10.1002/9781444303773.ch13

Corenblit, D., Tabacchi, E., Steiger, J., & Gurnell, A. M. (2007). Reciprocal interactions and adjustments between fluvial landforms and vegetation dynamics in river corridors: A review of complementary approaches. *Earth-Science Reviews*, *84*(1), 56–86. https://doi.org/10.1016/j.earscirev.2007.05.004

Costa, J. E., & O'Connor, J. E. (1995). Geomorphically effective floods. In J. E. Costa, A. J. Miller, K. W. Potter, & P. R. Wilcock (Eds.), *Geophysical Monograph Series* (Vol. 89, pp. 45–56). American Geophysical Union. https://doi.org/10.1029/GM089p0045

Dean, D. J., & Schmidt, J. C. (2013). The geomorphic effectiveness of a large flood on the Rio Grande in the Big Bend region: Insights on geomorphic controls and post-flood geomorphic response. *Geomorphology*, *201*, 183–198. https://doi.org/10.1016/j.geomorph.2013.06.020

Eaton, B. C., & Giles, T. R. (2009). Assessing the effect of vegetation-related bank strength on channel morphology and stability in gravel-bed streams using numerical models. *Earth Surface Processes and Landforms*, *34*(5), 712–724. https://doi.org/10.1002/esp.1768

Erskine, W. (1993). Erosion and deposition produced by a catastrophic flood on the Genoa River, Victoria. *Australian Journal of Soil and Water Conservation*, *6*(4), 35–43.

Erskine, W. D., & Saynor, M. J. (1996). *Effects of catastrophic floods on sediment yields in southeastern Australia*.

Fryirs, K. A. (2017). River sensitivity: A lost foundation concept in fluvial geomorphology. *Earth Surface Processes and Landforms*, *42*(1), 55–70. https://doi.org/10.1002/esp.3940

Fryirs, K., & Brierley, G. J. (2010). Antecedent controls on river character and behaviour in partly confined valley settings: Upper Hunter catchment, NSW, Australia. *Geomorphology*, *117*(1–2), 106–120. https://doi.org/10.1016/j.geomorph.2009.11.015

Fuller, I. C. (2007). Geomorphic Work during a "150-Year" Storm: Contrasting Behaviors of River Channels in a New Zealand Catchment. *Annals of the Association of American Geographers*, *97*(4), 665–676. https://doi.org/10.1111/j.1467-8306.2007.00576.x

Graf, Wi. L. (1988). *Fluvial Processes in Dryland Rivers*. Springer.

Gurnell, A. (2014). Plants as river system engineers. *Earth Surface Processes and Landforms*, *39*(1), 4–25. https://doi.org/10.1002/esp.3397

Gurnell, A. M., Petts, G. E., Hannah, D. M., Smith, B. P. G., Edwards, P. J., Kollmann, J., Ward, J. V., & Tockner, K. (2001). Riparian vegetation and island formation along the gravel-bed Fiume Tagliamento, Italy. *Earth Surface Processes and Landforms*, *26*(1), 31–62. https://doi.org/10.1002/1096-9837(200101)26:1<31::AID-ESP155>3.0.CO;2-Y

Hamlet, A. F., Elsner, M. M., Mauger, G. S., Lee, S.-Y., Tohver, I., & Norheim, R. A. (2013). An Overview of the Columbia Basin Climate Change Scenarios Project: Approach, Methods, and Summary of Key Results. *Atmosphere-Ocean*, *51*(4), 392–415. https://doi.org/10.1080/07055900.2013.819555

Harrison, L. R., Dunne, T., & Fisher, G. B. (2015). Hydraulic and geomorphic processes in an overbank flood along a meandering, gravel-bed river: Implications for chute formation: Meandering River-Floodplain Interactions. *Earth Surface Processes and Landforms*, *40*(9), 1239–1253. https://doi.org/10.1002/esp.3717

Heritage, G. L., Large, A. R. G., Moon, B. P., & Jewitt, G. (2004). Channel hydraulics and geomorphic effects of an extreme flood event on the Sabie River, South Africa. *CATENA*, *58*(2), 151–181. https://doi.org/10.1016/j.catena.2004.03.004

Hofmeister, J. (2000). *Slope failures in Oregon: GIS inventory for three 1996/97 storm events* [Special paper]. Oregon Department of Geology and Mineral Industries.

Huang, H. Q., & Nanson, G. C. (1997). Vegetation and channel variation; a case study of four small streams in southeastern Australia. *Geomorphology*, *18*(3), 237–249. https://doi.org/10.1016/S0169-555X(96)00028-1

Huckleberry, G. (1994). Contrasting channel response to floods on the middle Gila River, Arizona. *Geology*, *22*(12), 1083. https://doi.org/10.1130/0091-7613(1994)022<1083:CCRTFO>2.3.CO;2

Hughes, M. L. (2008). *CHANNEL CHANGE OF THE UPPER UMATILLA RIVER DURING AND BETWEEN FLOOD PERIODS: VARIABILITY AND ECOLOGICAL IMPLICATIONS*.

Knighton, D. (1998). *Fluvial forms and processes: A new perspective*. Arnold.

Kochel, R. C., Hayes, B. R., Muhlbauer, J., Hancock, Z., & Rockwell, D. (2016). Geomorphic response to catastrophic flooding in north-central Pennsylvania from Tropical Storm Lee (September 2011): Intersection of fluvial disequilibrium and the legacy of logging. *Geosphere*, *12*(1), 305–345. https://doi.org/10.1130/GES01180.1

Leddy, J. O., Ashworth, P. J., & Best, J. L. (1993). Mechanisms of anabranch avulsion within gravel-bed braided rivers: Observations from a scaled physical model. *Geological Society, London, Special Publications*, *75*(1), 119–127. https://doi.org/10.1144/GSL.SP.1993.075.01.07

Lisenby, P. E., Croke, J., & Fryirs, K. A. (2018). Geomorphic effectiveness: A linear concept in a non-linear world: Geomorphic Effectiveness. *Earth Surface Processes and Landforms*, *43*(1), 4–20. https://doi.org/10.1002/esp.4096

Magilligan, F. J. (1992). Thresholds and the spatial variability of flood power during extreme floods. *Geomorphology*, *5*(3), 373–390. https://doi.org/10.1016/0169-555X(92)90014-F

Magilligan, F. J., Buraas, E. M., & Renshaw, C. E. (2015). The efficacy of stream power and flow duration on geomorphic responses to catastrophic flooding. *Geomorphology*, *228*, 175–188. https://doi.org/10.1016/j.geomorph.2014.08.016

Marcinkowski, P., Grabowski, R. C., & Okruszko, T. (2017). Controls on anastomosis in lowland river systems: Towards process-based solutions to habitat conservation. *Science of The Total Environment*, *609*, 1544–1555. https://doi.org/10.1016/j.scitotenv.2017.07.183

Marshall, A., Wohl, E., Iskin, E., & Zeller, L. (2024). Interactions of Logjams, Channel Dynamics, and Geomorphic Heterogeneity Within a River Corridor. *Water Resources Research*, *60*(6), e2023WR036512. https://doi.org/10.1029/2023WR036512

McAllister, B. (1996, February 14). CLINTON VIEWS FLOOD DAMAGE IN NORTHWEST. *The Washington Post*. https://www.washingtonpost.com/archive/politics/1996/02/15/clinton-views-flood-damage-in-northwest/850bb94f-0350-4efc-b2c8-a3176a19bccb/

McDowell, P. F., Hughes, M. L., & Marcus, W. A. (2003). Geomorphic Change in Two Historical Flood Events on the Umatilla River, Oregon. *American Geophysical Union*.

Miller, A. J. (1990). Flood hydrology and geomorphic effectiveness in the central Appalachians. *Earth Surface Processes and Landforms*, *15*(2), 119–134. https://doi.org/10.1002/esp.3290150203

Miller, A. J. (1995). Valley morphology and boundary conditions influencing spatial patterns of flood flow. In J. E. Costa, A. J. Miller, K. W. Potter, & P. R. Wilcock (Eds.), *Geophysical Monograph Series* (Vol. 89, pp. 57–81). American Geophysical Union. https://doi.org/10.1029/GM089p0057

Nanson, G. C., & Knighton, A. D. (1996). ANABRANCHING RIVERS: THEIR CAUSE, CHARACTER AND CLASSIFICATION. *Earth Surface Processes and Landforms*, *21*(3), 217–239. https://doi.org/10.1002/(SICI)1096-9837(199603)21:3<217::AID-ESP611>3.0.CO;2-U

Nardi, L., & Rinaldi, M. (2015). Spatio-temporal patterns of channel changes in response to a major flood event: The case of the Magra River (central–northern Italy). *Earth Surface Processes and Landforms*, *40*(3), 326–339. https://doi.org/10.1002/esp.3636

Nelson, A., & Dubé, K. (2016). Channel response to an extreme flood and sediment pulse in a mixed bedrock and gravel-bed river. *Earth Surface Processes and Landforms*, *41*(2), 178–195. https://doi.org/10.1002/esp.3843

Newson, M. (1980). The geomorphological effectiveness of floods—A contribution stimulated by two recent events in mid-wales. *Earth Surface Processes*, *5*(1), 1–16. https://doi.org/10.1002/esp.3760050102

O'Connor, J. E., Jones, M. A., & Haluska, T. L. (2003). Flood plain and channel dynamics of the Quinault and Queets Rivers, Washington, USA. *Geomorphology*, *51*(1–3), 31–59. https://doi.org/10.1016/S0169-555X(02)00324-0

Oregon – Severe Storms, Flooding Landslides, and Mudslides – FEMA-4519-DR. (2020). [Preliminary Damage Assessment Report]. FEMA.

Osterkamp, W. R. (1998). Processes of fluvial island formation, with examples from Plum Creek, Colorado and Snake River, Idaho. *Wetlands*, *18*(4), 530–545. https://doi.org/10.1007/BF03161670

Patton, P. C. (1988). Geomorphic response of streams to floods in the glaciated terrain of southern New England. In *Flood Geomorphology*. Wiley.

Queen, L. E., Mote, P. W., Rupp, D. E., Chegwidden, O., & Nijssen, B. (2021). Ubiquitous increases in flood magnitude in the Columbia River basin under climate change. *Hydrology and Earth System Sciences*, *25*(1), 257–272. https://doi.org/10.5194/hess-25-257-2021

Reid, H. E., Williams, R. D., Brierley, G. J., Coleman, S. E., Lamb, R., Rennie, C. D., & Tancock, M. J. (2019). Geomorphological effectiveness of floods to rework gravel bars: Insight from hyperscale topography and hydraulic modelling. *Earth Surface Processes and Landforms*, *44*(2), 595–613. https://doi.org/10.1002/esp.4521

Rice, S., & Church, M. (1998). Grain size along two gravel-bed rivers: Statistical variation, spatial pattern and sedimentary links. *Earth Surface Processes and Landforms*, *23*(4), 345–363. https://doi.org/10.1002/(SICI)1096-9837(199804)23:4<345::AID-ESP850>3.0.CO;2-B

Righini, M., Surian, N., Wohl, E., Marchi, L., Comiti, F., Amponsah, W., & Borga, M. (2017). Geomorphic response to an extreme flood in two Mediterranean rivers (northeastern Sardinia, Italy): Analysis of controlling factors. *Geomorphology*, *290*, 184–199. https://doi.org/10.1016/j.geomorph.2017.04.014

Rinaldi, M., Amponsah, W., Benvenuti, M., Borga, M., Comiti, F., Lucía, A., Marchi, L., Nardi, L., Righini, M., & Surian, N. (2016). An integrated approach for investigating geomorphic response to extreme events: Methodological framework and application to the October 2011 flood in the Magra River catchment, Italy. *Earth Surface Processes and Landforms*, *41*(6), 835–846. https://doi.org/10.1002/esp.3902

Sholtes, J. S., Yochum, S. E., Scott, J. A., & Bledsoe, B. P. (2018). Longitudinal variability of geomorphic response to floods: Geomorphic response to floods. *Earth Surface Processes and Landforms*, *43*(15), 3099–3113. https://doi.org/10.1002/esp.4472

Sloan, J., Miller, J. R., & Lancaster, N. (2001). Response and recovery of the Eel River, California, and its tributaries to floods in 1955, 1964, and 1997. *Geomorphology*, *36*(3–4), 129–154. https://doi.org/10.1016/S0169-555X(00)00037-4

Smith, B. (2013). *The role of vegetation in catastrophic floods: A spatial analysis*.

Surian, N., Mao, L., Giacomin, M., & Ziliani, L. (2009). Morphological effects of different channel-forming discharges in a gravel-bed river. *Earth Surface Processes and Landforms*, *34*(8), 1093–1107. https://doi.org/10.1002/esp.1798

Surian, N., Righini, M., Lucía, A., Nardi, L., Amponsah, W., Benvenuti, M., Borga, M., Cavalli, M., Comiti, F., Marchi, L., Rinaldi, M., & Viero, A. (2016). Channel response to extreme floods: Insights on controlling factors from six mountain rivers in northern Apennines, Italy. *Geomorphology*, *272*, 78–91. https://doi.org/10.1016/j.geomorph.2016.02.002

Tamminga, A. D., Eaton, B. C., & Hugenholtz, C. H. (2015). UAS-based remote sensing of fluvial change following an extreme flood event. *Earth Surface Processes and Landforms*, *40*(11), 1464–1476. https://doi.org/10.1002/esp.3728

Thompson, C., & Croke, J. (2013). Geomorphic effects, flood power, and channel competence of a catastrophic flood in confined and unconfined reaches of the upper Lockyer valley, southeast Queensland, Australia. *Geomorphology*, *197*, 156–169. https://doi.org/10.1016/j.geomorph.2013.05.006

Vocal Ferencevic, M., & Ashmore, P. (2012). CREATING AND EVALUATING DIGITAL ELEVATION MODEL-BASED STREAM-POWER MAP AS A STREAM ASSESSMENT TOOL. *River Research and Applications*, *28*(9), 1394–1416. https://doi.org/10.1002/rra.1523

Ward, J. V., Tockner, K., Uehlinger, U., & Malard, F. (2001). Understanding natural patterns and processes in river corridors as the basis for effective river restoration. *Regulated Rivers: Research & Management*, *17*(4–5), 311–323. https://doi.org/10.1002/rrr.646

Wicherski, W., Dethier, D. P., & Ouimet, W. B. (2017). Erosion and channel changes due to extreme flooding in the Fourmile Creek catchment, Colorado. *Geomorphology*, *294*, 87–98. https://doi.org/10.1016/j.geomorph.2017.03.030

Wittwer, A. (2022, January 5). Northeastern Oregon sees $22 million in reimbursements for 2020 floods. *The Observer*. https://www.lagrandeobserver.com/news/local/northeastern-oregon-sees-22-million-in-reimbursements-for-2020-floods/article_7f5dfdfe-68f2-11ec-ad50-df148bb6f19d.html

Wohl, E. (2016). *Messy rivers are healthy rivers: The implications of physical complexity for river ecosystems* [Online post]. Global Water Forum.

Wohl, E. E. (2000). Geomorphic Effects of Floods. In E. E. Wohl (Ed.), *Inland Flood Hazards* (1st ed., pp. 167–193). Cambridge University Press. https://doi.org/10.1017/CBO9780511529412.007

Wohl, E., & Scott, D. N. (2017). Wood and sediment storage and dynamics in river corridors. *Earth Surface Processes and Landforms*, *42*(1), 5–23. https://doi.org/10.1002/esp.3909

Wolman, M. G., & Gerson, R. (1978). Relative scales of time and effectiveness of climate in watershed geomorphology. *Earth Surface Processes*, *3*(2), 189–208. https://doi.org/10.1002/esp.3290030207

Wolman, M. G., & Miller, J. P. (1960). Magnitude and Frequency of Forces in Geomorphic Processes. *The Journal of Geology*, *68*(1), 54–74. https://doi.org/10.1086/626637

Yochum, S. E., Sholtes, J. S., Scott, J. A., & Bledsoe, B. P. (2017). Stream power framework for predicting geomorphic change: The 2013 Colorado Front Range flood. *Geomorphology*, *292*, 178–192. https://doi.org/10.1016/j.geomorph.2017.03.004